THE ROLE OF VESSEL COLLAPSE ON THE FLOW OF AQUEOUS HUMOR

by

JOHN LUIGI BATTAGLIOLI

B.Sc., Union College
(1979)

SUBMITTED IN PARTIAL FULFILLMENT
OF THE REQUIREMENTS FOR THE
DEGREE OF

MASTER OF SCIENCE

at the

MASSACHUSETTS INSTITUTE OF TECHNOLOGY

June, 1981

Signature of Author Signature redacted
Department of Mechanical Engineering
February 28, 1981

Certified by Signature redacted
Thesis Supervisor

Accepted by Signature redacted
Chairman, Department Committee on Graduate Studies

THE ROLE OF VESSEL COLLAPSE ON THE FLOW OF AQUEOUS HUMOR

by

John Luigi Battaglioli

Submitted to the Department of Mechanical Engineering on February 28, 1981 in partial fulfillment of the requirements for the Degree of Master of Science.

ABSTRACT

An improved understanding of the structural and fluid mechanical aspects of the aqueous outflow system is essential in the study of glaucoma and its causes. In this study, we explore the role of aqueous vein collapse in determining the overall resistance to the flow of aqueous humor, at normal and elevated intraocular pressures.

Experiments conducted on scleral samples, to obtain additional information required in the structural analysis of the aqueous veins, showed; (i) that the radial compressive modulus of the sclera is a factor of 100 less than its circumferential tensile modulus, and (ii) that Poisson's ratio for scleral tissue is between 0.46 and 0.50.

Through complimentary theoretical and experimental studies, the relationship between the cross-sectional area of a circumferentially oriented vessel and intraocular pressure was found to be nearly linear and only weakly dependent on the radial position of the vessel. This information was then incorporated into a simple model of the aqueous outflow system in order to predict the relationship between intraocular pressure and the rate of aqueous outflow. Using this model, we were able to show that the resistance of the aqueous veins is not significant at low intraocular pressures, but can become important when the vessels begin to collapse at intraocular pressures between 35 and 60 mm Hg.

Thesis Supervisor: Roger Kamm
Title: Assistant Professor of Mechanical Engineering

ACKNOWLEDGEMENTS

To Professor Roger Kamm goes my special thanks, for without his patient guidance this work would not have been possible. I thank Professor Ascher Shapiro for his help and interest in this project. I am also indebted to the staff of the Howe Laboratory of the Massachusetts Eye and Ear Infirmary. Through our monthly meetings, they provided me with a wealth of information.

To Mr. Dick Fenner, our resident designer, goes my most sincere appreciation. Dick provided invaluable assistance in the design and construction of the apparatus, as well as broadening my understanding of Mechanical Engineering. More importantly, he was a good friend. I am also grateful to Sandy Williams for her perserverence in typing my thesis.

I thank my wife for enduring the long hours of work required to conduct this research. To my parents, who have continually provided me with moral and financial support, goes my deepest thanks. They are truly the finest of parents.

Finally, I am indebted to the National Institute of Health (Grant No. 1 R01 EY 03141-01), which provided the financial support of this project.

TABLE OF CONTENTS

CHAPTER 1

INTRODUCTION

A pressure drop of about 7 mm Hg is generally sufficient to drive the aqueous humor from the anterior chamber of the eye to the episcleral veins, at which point the aqueous humor mixes with venous blood. In glaucoma, this pressure difference can rise to more than 20 mm Hg due to pathological changes occuring somewhere in the complex outflow network. The present study has two objectives:

1) to identify the important sites of resistance in normal eyes and,

2) to determine what changes might result in elevated resistance and, consequently increased intraocular pressure.

More specifically, since there are many aspects to the aqueous outflow network, this report will deal exclusively with the aqueous veins and their significance to the resistance of the outflow system. In this report, the term aqueous vein refers to the segment of the outflow system from Schlemm's canal to the surface of the eye, consistent with the terminology used by Ascher (1949). This is, however, contrary to more recent usage in which these same vessels are termed "collector channels".

The potential for the collapse of the aqueous veins will be considered with the aim of establishing under what conditions vessel collapse will significantly affect the total outflow resistance. To

provide a backdrop for the analysis of the flow through the aqueous veins, we provide the following general information on the entire outflow system.

1.1 Aqueous Outflow System

The flow of aqueous humor enters the posterior chamber of the eye from the ciliary epithelium by a combination of secretion and ultrafiltration at a rate of about 2 μℓ/min [Bill (1975)]. The aqueous humor then proceeds from the posterior chamber to the anterior chamber via the pupil (Figure 1), and from there exits by two distinct routes. The first, which accommodates approximately 20 percent of the flow rate, and is illustrated in Figure 2, leads from the anterior chamber into the tissue spaces within the ciliary muscle, into the suprachoroid, and from there into the sclera [Bill (1975, 1975b)]. This route has been termed the uveal-scleral pathway.

The remainder of the aqueous humor passes through the trabecular meshwork, which is generally subdivided into 3 parts (Figure 3). The aqueous humor first encounters the uveal meshwork, a forward extension of the ciliary muscle [Bill (1975b)]. The openings within the uveal meshwork are large and overlap extensively. The aqueous humor then passes through the corneo-scleral meshwork, which consists of perforated sheets of connective tissue extending between the scleral spur and the cornea [Bill (1975b)]. The openings within the corneo-scleral meshwork are smaller than those in the uveal meshwork and overlaping of the openings is rare. Finally, the aqueous humor passes through the juxtacanalicular meshwork, which consists of loose connective tissue and endothelial cells

[Bill (1975b)]. The pathways for flow within the juxtacanalicular meshwork are very narrow and irregular, thus the flow must follow a somewhat tortuous path.

The interior of Schlemm's canal is separated from the meshwork by a single layer of endothelial cells. Several theories have been proposed to explain the transport of aqueous across the endothelium. These have been summarized by Tripathi (1971) and include the following;

- Micropinocytosis,
- Intercellular gaps or openings,
- Intracellular channels,
- Endothelial vacuolation.

Due to the small size of the outflow channels within the trabecular meshwork and endothelial lining, these sites are often named as the location of greatest flow resistance. This view has been supported by Grant (1958), who showed that in enucleated human eyes approximately 75 percent of the resistance within the aqueous outflow system was found on the anterior side of Schlemm's canal. It has also been suggested that the collapse of Schlemm's canal could cause a significant portion of the outflow resistance [Moses (1977)].

Upon entering Schlemm's canal, the aqueous flows circumferentially until reaching one of the approximately 30 collector channels, which in turn merge with aqueous veins. The canal is

thought to be a nearly continuous channel of roughly elliptical cross-section running circumferentially around the eye at the limbus. Its inner wall is the outermost margin of the trabecular meshwork and is therefore highly distensible. Its outer wall is the sclera which, as compared to the meshwork, is rigid. Running between the inner and outer walls are a network of supporting members termed septae which presumably act to maintain patency of the canal lumen.

Casting studies of the aqueous outflow system conducted by Grant (1965) showed that aqueous veins originate either directly from Schlemm's canal, or from a series of channels in close proximity to Schlemm's canal and having many interconnections with it. The aqueous veins then pass through the sclera and emerge on the outer surface of the eye to connect with the episcleral veins. Infrequently, Grant (1965) observed that an aqueous vein possessed a very fine branch connecting with the ciliary muscle. According to Ascher (1947), there are three basic classifications of aqueous veins. The largest aqueous veins, which account for about 20 percent of the total, originate in the scleral emissarium. The smallest, which comprise about 30 percent of the total, originate near the limbal meshwork. The remaining aqueous veins, about 50 percent, originate near the corneal limbus and possess a semi-circular or U-shaped arch. These vessels are larger in diameter than those originating near the limbal meshwork, but smaller than those originating in the scleral emissarium. According to Ascher (1949), aqueous veins range in diameter from 0.01 mm to 0.1 mm with most

having a diameter of approximately 0.05 mm.

In the past there has been some experimental evidence to suggest that a significant portion of the resistance of the outflow system can be attributed to the aqueous veins. Perkins (1955) showed, by measuring pressures in rhesus monkey's within Schlemm's canal and the anterior chamber simultaneously, that the pressure within Schlemm's canal was only 10 percent less than intraocular pressure. Sears (1966) showed using similar techniques that in living monkey eyes, the majority of the outflow resistance lies beyond the inner wall of Schlemm's canal. These results seem to implicate either Schlemm's canal or the aqueous veins as the major site of resistance. However, these results contradict the findings of Grant (1958) which, as mentioned previously, showed that the majority of the outflow resistance lies on the anterior side of Schlemm's canal.

By a simple calculation, one can show that for the aqueous veins to be the site of greatest resistance, they must be in a highly collapsed state. If collapse does indeed occur, it is likely to be due to the stresses exerted on the aqueous veins by the surrounding scleral tissue.

The sclera is comprised of dense connective tissue with a collagen framework supported by a matrix consisting of mucopolysaccharides, sugars, proteins, and protein-polysaccharide complexes [Curtain (1969)]. The relative percentage of collagen

to matrix is of considerable importance with respect to the material properties of the tissue.

Many researchers have performed unaxial tensile tests on strips of sclera [Curtain (1969), Glouster (1957), and Yamada (1973)], all of which exhibited a non-linear relationship between stress and strain such that the tissue becomes less compliant with increasing stress. Through the combination of experimentation and a finite element model of the eye, Woo (1972) obtained an exponential relationship between stress and strain for the sclera of the form

$$\sigma = 1.8 \times 10^5 (e^{41.8\varepsilon} - 1) \text{ dynes/cm}^2 . \qquad (1)$$

Representative values for the tensile modulus of sclera lie in the range of 1×10^7 to 9×10^7 dynes/cm^2.

1.2 Thesis Overview

The studies reported here have two main components, one is an analysis of the structural properties of the sclera and aqueous veins with the objective of, given values of intraocular pressure and internal pressure, determining the vessel cross-sectional area. With this information, we can proceed to the second step, which is the development of a flow model to determine the pressure drop across the aqueous veins.

The structural model requires more information on the material properties of the sclera than was available from the literature. Thus, experiments were designed to yield the needed information concerning the compressive modulus of scleral tissue. These experiments and their results are reported in Chapter 2. These results enabled us to move on

to the experimental and analytical study of aqueous vein collapse as presented in Chapter 3. The results of this study, presented in Chapter 4, provided us with a relationship between cross-sectional area of the veins and intraocular pressure. These results were then incorporated into a fluid mechanical model of the aqueous veins, which is presented along with the results of this model in Chapter 5.

CHAPTER 2

EXPERIMENTS TO MEASURE THE COMPRESSIVE MODULUS OF SCLERAL TISSUE

2.1 Methods

If the eye is idealized as a sphere, the stresses found in the sclera are tensile in the two tangential directions and compressive in the radial direction. As discussed previously, the tensile properties with respect to the tangential directions have been studied by many investigators. However, the compressive properties in the radial direction, or with respect to its thickness, have not previously been investigated. Since this information was vital to our analysis of aqueous vein collapse, we designed and constructed a testing system capable of determining the radial compressive modulus of the sclera.

The apparatus used for these compression tests needed to satisfy several very stringent design constraints. The test system had to be capable of applying, and precisely measuring, compressive stresses on the order of 100 dynes/cm^2, of measuring displacements on the order of microns, and of determining the magnitude of sample volume changes. Also, it was necessary that the sample be submerged in an isotonic solution and maintained within 1°F of normal body temperature during the test.

2.2 Experimental Apparatus

The compressive testing system was comprised of 6 major components:

1) air piston,
2) optical displacement probe,

3) sample container and isotonic solution,
4) compressed air supply and manometer,
5) heating elements and thermometer
6) plexiglass enclosure

Compressive stresses were applied using an airpot damper (Figure 4) consisting of a graphite piston within a pyrex cylinder. This choice was based on the extremely low friction force (less than 500 dynes) opposing the motion of the piston, which allowed the precise application of very small magnitude compressive stresses. To provide greater control over the compressive stress applied to the sample, the piston's bore was chosen as small as possible (0.627" diameter).

An aluminum rod attached to the piston supported a plexiglass dish containing the sample submerged in an isotonic solution (Figure 4). The dish was mounted to the aluminum rod via a low friction ball joint to ensure that the compressive stress was applied perpendicular to the surface of the sample.

The pressure in the airpot cylinder was regulated and measured using a water manometer, to an accuracy of $\pm$ 50 dynes/cm^2. Vertical motion of the piston caused the sample to be compressed against the top of the enclosure, where this surface as well as the dish were lubricated to reduce end effects.

To measure strains as small as 1 percent, since the sample thickness was approximately 1000 microns, the device used must be capable of discerning motions on the order of ten microns. This requirement was met by the use of an optical displacement probe (Figure 4), which not only

had excellent resolution ($\pm$ 0.5 μm) but also allowed the measurement to be made without making contact with the moving surface. Use of the device required that a reflective surface be attached to the dish containing the sample. The output voltage of the probe was calibrated to distance as discussed in Section 2.4.

During the test, the samples were maintained at normal body temperature by means of a small heating element placed inside the plexiglass enclosure surrounding the apparatus. Temperatures within the enclosure were monitored and controlled to within 1°F. A photograph of the completed testing system is shown in Figure 5.

2.3 Poisson's Ratio Experiments

To determine Poisson's ratio (ν) for the sclera, we photographed the surface of the sample under high magnification during the compression tests. The photographs were then enlarged, to increase the accuracy of the measurements, and the cross-sectional area of the sample was measured using a planimeter. Through a simple analysis, one can show that

$$\ln {}^{A_s}/_{A_{so}} = (1 + \nu\varepsilon_c)^2 \quad ,$$

where A_{so} is the original cross-sectional area of the sample, A_s is the cross-sectional area of the sample after application of the compressive load, and ε_c is the applied compressive strain. From this expression and the measurements of the sample's cross-sectional area at known levels of applied strain, one can easily determine Poisson's ratio.

2.4 Calibration and Use of the Optical Probe

Although extremely sensitive, the optical probe has a non-linear response curve and had to be calibrated prior to use in the experiments. The probe's output is a voltage proportional to the amount of light reflected back from the moving surface. To calibrate the probe, it was mounted in a cylindrical section of plexiglass and attached to a micrometer via three spring loaded bolts to allow the precise alignment of the probe with respect to the moving surface.

The probe was brought into contact with, and aligned perpendicular to, the reflective surface, giving a zero voltage output. Using the micrometer, the probe was then moved away from the surface until its voltage output reached a maximum (approximately 0.3 mm from the reflective surface). The maximum output of the probe was set at one volt by adjusting the gain, and the probe was then brought back into contact with the reflective surface and realigned so its output was again zero volts. This procedure was repeated until the output of the probe in contact with the reflective surface was zero volts and its maximum output was one volt.

To obtain a calibration curve, the probe was brought into contact with the reflective surface and then moved away in 10 micron increments recording the voltage output of the probe at each step. The results are shown in Figure 6. A linear regression was performed on the data within the linear region of output (from 0.15 volts to 0.55 volts) yielding a calibration constant of 9.3 mV per micron of displacement. During the experiments, we always operated within this linear region.

2.5 Preparation of Scleral Samples

In the first series of tests, we measured the compressive properties of cattle eyes (obtained from Joseph T. Trelagan Company). These eyes were obtained immediately upon enucleation, placed in an isotonic solution, and stored at 4°C until used. All experiments were conducted within 48 hours of enucleation.

For the second series of tests three pairs of human eyes were obtained from the Howe Laboratory of the Massachusetts Eye and Ear Infirmary. The ages of the three donors were 93, 74, and 63 years. The experiments were conducted on the human tissue within 72 hours of enucleation.

To prepare the eyes, the epithelium covering the cornea and sclera was removed from the surface of the eye using a scapel. Also, for the cattle eyes, the stubs of the rectus muscles were removed. Next, the globe was bisected at the equator to allow the removal of the lens, iris, and choroid. Cylindrical samples were taken from the region of the sclera immediately adjacent to the cornea using a trephine of 9 mm diameter and immediately placed in an isotonic solution and stored at 4°C until used. Once the samples were excised from the eye, they were used within 3 hours.

2.6 Test Procedures and Control Experiment

The accuracy of the scleral test system was determined by measuring the compressive modulus of very thin sections of a compliant material of known modulus. The material chosen was a silastic rubber sheet, the compressive modulus of which was obtained from the manufacturer. The results of these tests are discussed later.

The first step in conducting each test was to measure the original thickness of the sample using a spring loaded thickness gage with an accuracy of ± 10 μm. Then, the sample was placed into the dish containing a buffered saline solution attached to the piston. At this point, the piston was raised to bring the sample into contact with the upper surface of the enclosure by supplying a pressure of approximately 15, 500 dynes/cm^2 to the airpot cylinder. However, the majority of the pressure was required to overcome the weight of the piston-rod-dish assembly (14,600 dynes/cm^2) and the friction force (250 dynes/cm^2) leaving a net compressive stress of 2000 dynes/cm^2 (650 dynes/cm^2 x Ap/As). The initial compression served to eliminate the difficulty in determining the exact position of contact between the sample and the upper surface, but it also causes a deformation which cannot be determined. This point was used as a reference ($\varepsilon = 0$) from which all subsequent strains were measured.

After allowing approximately 30 minutes for the sample to stabilize, the probe was brought into contact with the reflective surface and the alignment adjusted as discussed previously. The probe was then positioned at the upper limit of the linear region (0.35 volts) so that when the piston compressed the sample, the reflective surface moved towards the probe and into the region of linearity. The stress acting on the sample was computed from the airpot cylinder pressure and the surface areas of the piston and

sample, while the strain induced in the tissue was determined by

$$\varepsilon_c = \ln \frac{t}{t_o}$$

where t_o is the original thickness of the sample and t is the thickness of the sample after deformation. Although experiments were usually conducted only for increasing loads, decreasing loads were also applied to one sample in order to check for hysteresis.

2.7 Results

In order to verify the accuracy of the test system, we experimentally determined the compressive modulus of a 0.5 mm thick section of silastic rubber. The results of this experiment, shown in Figure 7, yield a value of the modulus of

$$E = 5.169 \times 10^6 \pm 9 \text{ dynes/cm}^2 ,$$

as determined by linear regression. This was in excellent agreement with the value obtained from the manufacturer,

$$E = 5.52 \times 10^6 \text{ dynes/cm}^2 .$$

The error range associated with the experimentally determined compressive modulus is due to uncertainties in the measurements of pressure within the airpot, original thickness of the sample, and displacement of the reflective surface.

2.7.1 Experiments on Cattle Sclera

The first tests were conducted on cattle eyes primarily for the purpose of perfecting our experimental techniques. Samples of cattle

sclera were taken from two pairs of eyes, the results of which pointed out some interesting aspects of scleral tissue (Figures 8-11). First, it was observed that cattle sclera creeps with a variety of time constants, the fastest on the order of tens of seconds and the slowest on the order of minutes. Therefore, we waited 30 minutes between increments of pressure to allow the sample to stabilize. Also, we observed that under compressive loads the relationship between stress and strain is somewhat non-linear, such that the tissue becomes less compliant with increasing loads. This result is in agreement with data obtained from tensile tests on human sclera conducted by Glouster (1957) and Curtain (1969).

A linear regression of the data produced values for the linear compressive modulus shown in Table 1. These data fall in the range

$$1.21 \times 10^5 \pm 15\% \leq E_{cc} \leq 1.88 \times 10^5 \pm 14\% \text{ dynes/cm}^2 \quad ,$$

for compressive stresses between 2000 dynes/cm^2 and 26,000 dynes/cm^2. The linear regression fitted the data well, as evidenced by the correlation coefficients (between 0.975 and 0.985) shown in Table 1.

2.7.2 Experiments on Human Sclera

The human sclera, behaved in a manner very similar to cattle sclera (Figures 12-19). As with the cattle sclera, human sclera creeps with a variety of time constants, the fastest on the order of tens of seconds and the slowest on the order of minutes (Figure 20). The relationship between stress and strain was also found to be somewhat nonlinear, such that the tissue becomes less compliant with increasing loads. In addition, after removing the load, the sample returned to its original

thickness signifying that the material experienced no permanent set. However, the sample did exhibit some hysteresis as the load was removed (Figure 12).

The analysis of aqueous vein collapse required a linear compressive modulus for human sclera. Thus, one was obtained by means of a linear regression of the data, the results of which are shown in Table 2. Results obtained for compressive stresses from 2000 dynes/cm^2 to 40,000 dynes/cm^2 show that the linear compressive modulus of human sclera is within the following range:

$$2.7 \times 10^5 \pm 13\% \leq E_{cs} \leq 4.12 \times 10^5 \pm 11\% \text{ dynes/cm}^2 \quad .$$

The linear regression fitted the data well, as evidenced by the correlation coefficients (between 0.982 and 0.993) shown in Table 2.

2.7.3 Poisson's Ratio Experiments

The experiments to determine Poisson's ratio were conducted on six samples of human sclera for compressive stresses between 2000 dynes/cm^2 and 40,000 dynes/cm^2, the results of which are shown in Table 2. These results show that Poisson's ratio for the sclera is between

$$0.46 \pm 6\% < \nu < 0.50 \pm 6\% \quad .$$

The errors associated with the value of Poisson's ratio are due to uncertainties in the measurement of both cross-sectional area of the sample and the applied strain.

Since Poisson's ratio for sclera is very nearly 0.5, the volume of the sample is approximately constant during the test. This finding served

to answer a serious question concerning the possibility that the results were influenced by loss of fluid from the sample. We are therefore confident that the surprisingly low values for the compressive modulus are real and not due to an artifact associated with fluid loss from the sample. It should be noted, however, that fluid could have been displaced from the sample during the initial compression.

CHAPTER 3

ANALYTICAL AND EXPERIMENTAL STUDY OF AQUEOUS VEIN COLLAPSE

As mentioned in Chapter 1, if aqueous vein collapse does occur, it will come as a result of the stresses exerted on the vessel by the surrounding scleral tissue. In this chapter, we first determine the stresses acting on a particular vessel, then determine the amount of collapse that occurs as a result of this stress level. We analyzed aqueous vein collapse by two separate methods:

1) a simple analytical model valid for small deformations and,
2) a large scale experimental model from which the results for large deformations were obtained.

The experimental model also provided a verification of the analytical model for small deformations.

3.1 Analytical Model

The analytical determination of vessel collapse requires both the radial compressive modulus, obtained in the experiments of Chapter 2, and the tangential tensile modulus. To obtain a single value to be used as the tangential tensile modulus, we applied a linear regression to the data of Glouster (1957), Curtain (1969), and Woo (1972), the results of which are given in Table 3.

From these results, the linear tensile modulus of the sclera was

considered to lie between

$$2.0 \times 10^7 \leq E_{ts} \leq 1.2 \times 10^8 \text{ dynes/cm}^2 \quad ,$$

where the majority of information suggested that it was nearer the lower limit of the range. This result was approximately a factor of 100 greater than the compressive radial modulus of the sclera, which was previously shown to lie in the range

$$2.7 \times 10^5 \leq E_{cs} \leq 4.12 \times 10^5 \text{ dynes/cm}^2 \quad .$$

For the purpose of this analysis, we assumed values for the radial compressive modulus and tangential tensile modulus of

$$E_{cs} = 3.3 \times 10^5 \text{ dynes/cm}^2 \quad ,$$

$$E_{ts} = 3.3 \times 10^7 \text{ dynes/cm}^2 \quad .$$

To simplify the analysis, we made the following assumptions concerning an aqueous vein and its interaction with the sclera:

1) the wall of the aqueous vein possesses the same material properties as the sclera,
2) the aqueous vein is attached uniformly to the sclera everywhere along its surface, and
3) since the ratio of vessel diameter to the thickness of the sclera is small (approximately 1/20), the vessel behaves as though it were surrounded by an infinite medium.

With these assumptions, we modeled an aqueous vein as a hole of circular cross-section extending through an infinite three-dimensional medium.

The path an aqueous vein follows through the sclera determines the orientation and magnitude of the stresses acting on it. If the aqueous vein follows a purely radial path through the sclera, the stresses exerted on it would tend to enlarge its area rather than cause collapse. An aqueous vein running in a circumferential direction is the most apt to collapse, and it is this particular orientation that is the subject of our analysis. Intermediate orientations would require a much more difficult analysis and were therefore not considered. It can be said, however, that a vessel with intermediate orientation will be less collapsed than a circumferentially running vessel and is therefore not considered.

3.1.1 Magnitude of the Stresses Imposed on the Sclera

In order to determine the magnitude of the stresses imposed on the sclera by intraocular pressure, we modeled the eye as a spherical pressure vessel with an outside radius of 1.2 cm and an inside radius of 1.1 cm. One might question this assumption, particularly in the limbal region where the aqueous veins are found, due to the change in curvature between the sclera and cornea locally. This proves to be a relatively small effect, however, according to a finite element model of the eye [Woo (1972b)], which found the strains within the limbal region only 25 percent greater than the strains within other nearby regions of the sclera.

According to Timoshenko (1934), for spherical shells with intraocular pressure (IOP) inside and zero pressure outside, the tangential

stress as a function of radial position is

$$\sigma_{t_1} = \sigma_{t_2} = \frac{IOP \left(1 + \frac{r_b^3}{2r^3}\right)}{\frac{r_b^3}{r_a^3} - 1}$$

and the radial stress as a function of radial position is

$$\sigma_d = \frac{IOP \left(1 - \frac{r_b^3}{2r^3}\right)}{\frac{r_b^3}{r_a^3} - 1}$$

where r_b is the outside radius and r_a the inside radius of the spherical shell. Therefore, from the dimensions given above, the tangential stress was found to range between 5.5 IOP at the inner surface and 5.0 IOP at the outer surface, while the radial stress was found to range between -IOP at the inner surface and zero at the outer surface.

Consistent with our stated assumptions, the stresses from the spherical model of the eye were considered to act at an infinite distance from the hole. To simplify the analysis, the average stress in the tangential directions was used, since the tangential stress varied only slightly between the inner and outer surfaces, whereas the radial stress is a relatively strong function of the location of the vessel within the sclera.

3.1.2 Model Development

To simplify the analysis of a circumferentially oriented aqueous vein, the stresses within the plane of the hole were analyzed separately from the stresses acting parallel to its axis (Figure 21). In the plane of the hole, the stress distribution was determined for the condition of plane strain ($\varepsilon_z = 0$), and the strains induced by the stresses acting parallel to the axis of the hole were then superimposed on this result.

In order to account for the difference between the compressive and tensile moduli of the sclera, we initially analyzed the structure as if it was an isotropic material. Then, the results of this analysis were used to determine the angular position (θ_1), with respect to a cylindrical coordinate system with origin at the center of the circumferentially oriented aqueous vein, measured from an axis pointed circumferentially, at which the inner wall of the vessel underwent no deformation. A radial plane with angle θ_1 is assumed to approximately denote the boundary between a region of predominantly tensile stress and a region of predominantly compressive stress. In the model, the large elastic modulus is used in the tensile region while the small elastic modulus is used in the compressive region.

The complete development of the analytical model is given in Appendix A. The analysis of a circumferentially oriented aqueous vein yields

$$\frac{A}{A_0} = \frac{2}{\pi} \int_0^{\theta_1} [1 + (\frac{1 - \nu^2}{E_{ts}})(\sigma_{t_1} + \sigma_d + 2(\sigma_{t_1} - \sigma_d)\cos 2\theta) +$$

$$+ (\frac{1 + \nu}{E_{ts}})P_v - \frac{\nu}{E_{ts}}\sigma_{t_2}]^2 d\theta +$$

$$+ \frac{2}{\pi} \int_{\theta_1}^{\frac{\pi}{2}} [1 + (\frac{1 - \nu^2}{E_{cs}})(\sigma_{t_1} + \sigma_d + 2(\sigma_{t_1} - \sigma_d)\cos 2\theta) + \quad (2)$$

$$+ (\frac{1 + \nu}{E_{cs}})P_v - \frac{\nu\sigma_{t_2}}{E_{cs}}]^2 d\theta \quad ,$$

where $\frac{A}{A_0}$ is the ratio of the deformed cross-sectional area of the vessel to its original cross-sectional area, P_v is the fluid pressure within the aqueous vein, and θ_1 is the angle at which the vessel wall begins to deform inward. Using Equation (2), we can determine $\frac{A}{A_0}$ for a circumferentially oriented aqueous vein as a function of intraocular pressure (IOP), internal vessel pressure (P_v), and radial position within the sclera. The integral of Equation (2) is given in Appendix A.

The analysis, however, is restricted to small deformations. Since the analysis required that the boundary conditions be specified at the original radius of the vessel, the strains within the material from the point of the original vessel radius to the final position of the vessel wall were not taken into account. Therefore, as the deformations of the vessel became large, the analytical model ceased to be valid.

3.2 Large Scale Experimental Model

3.2.1 Dimensional Analysis

From the assumptions made in the previous section, the deformed area of the vessel can be expressed in the form:

$$A = f(\sigma_t, \sigma_d, E_{cs}, E_{ts}, \nu, P_v, A_0) \quad ,$$

which by means of dimensional analysis results in

$$\frac{A}{A_0} = f\left(\frac{\sigma_d}{E_{cs}} , \frac{P_v}{E_{cs}} , \frac{\nu\sigma_t}{E_{ts}} , \frac{E_{ts}}{E_{cs}} \right) \quad . \qquad (3)$$

Thus, to properly model the collapse of an aqueous vein, one must match these four dimensionless groups.

In the previous section, several assumptions allowed us to model the vessel-tissue structure as a circular hole extending through an infinite three-dimensional medium. According to the relationships developed in Appendix A, the effects of the hole within the medium vary as a^2/r^2 , where a is the radius of the hole and r is the radial distance from the center of the hole. Therefore, to limit the effects caused by the hole at the surface of the test section to less than one percent, the dimension of the test section measured radially from the center of the hole must be at least 10 times the radius of the hole. Also, to ensure a uniformly deformed section, the dimension of the test section parallel to the axis of the hole was made as large as possible.

3.2.2 Design and Construction of Large Scale Experiment

The experimental model consisted of 6 major parts:

1) foam block,
2) supporting structure,
3) threaded rods and plexiglass plates,
4) gearing system and thrust bearings,
5) area probe,
6) reservoir and manometer.

We found it impossible to obtain a material which would allow a perfect simulation of the sclera. A closed cell foam made from a vinyl chloride rubber was chosen which, like the sclera, has different properties in compression than it does in tension. According to the manufacturer, the tensile modulus of the foam (E_{tf}) is 2.7×10^6 dynes/cm^2, while its Poisson's ratio can be assumed to be 0.5, if the small changes in volume due to gas compressibility are neglected.

A linear regression of the data obtained by means of the scleral testing system (Figure 22) yielded a compressive modulus for the foam (E_{cf}) of $1.21 \times 10^5 \pm 15\%$ dynes/cm^2, for compressive stresses between 2,000 dynes/cm^2 and 14,000 dynes/cm^2.

The dimensional analysis suggests that to model aqueous vein collapse properly, one must match all the dimensionless groups shown in Equation (3). By properly scaling the applied loads, three of the dimensionless groups could be satisfied (P_v/E_{cs}, $\nu\sigma_t/E_{ts}$, σ_d/E_{cs}), but the fourth (E_{ts}/E_{cs}) could not. For human sclera, the ratio of its tensile modulus (E_{ts}) to its compressive modulus (E_{cs}) is approximately 100, while for the foam this ratio (E_{tf}/E_{cf}) is approximately 22.5. In order to both

ascertain the importance of this dimensionless parameter and to provide a verification of the analytical model for small strains, we conducted an analytical study of the conditions present in the experimental model. A comparison of these results is presented in Chapter 4.

The next design consideration was the size of the test section which, due to considerations already mentioned, scaled with the size of the hole. Use of the area probe, which will be discussed later, required that the hole be at least 3/8" in diameter. Therefore, to satisfy the criteria set forth previously, we chose to use an 8"×8"×12" rectangular block of foam with the axis of the hole perpendicular to the 8"×8" face. Practical constraints limited the axial length to 12".

Since the closed cell foam was only available in 1" thick sheets, a number of sheets were bonded together using a thin coat of 3M #77 spray adhesive so as not to appreciably alter the compressive or tensile properties of the laminated section.

Once the block of foam was prepared, we placed a 3/8" diameter hole through it by the following procedure:

1) A 3/16" diameter hole was bored through the block using a thin-walled stainless steel tube with a sharpened front edge (similar to a very long trephine).

2) The interior of the hole was then frozen with liquid nitrogen.

3) The final 3/8" diameter hole was bored through the block using a thin-walled stainless steel tube with a sharpened front edge.

Plexiglass sheets in contact with the block provided a rigid surface onto which the loads were applied, and were glued to those faces of the block subjected to tensile stresses using 3M #77 spray adhesive (Figure 23). The loads were applied to the block by means of three 1/2 - 20 threaded rods attached to each plate, which were in turn mounted to a supporting structure of telespar tube steel through the combination of a threaded gear and thrust bearing (Figure 24). The purpose of the gears was to allow the linkage of the three threaded rods attached to each face, which ensured a parallel planar motion of each plate, while the thrust bearings acted to prevent the binding of the gears as the loads were increased. By rotating the gears, the required degree of strain was applied to each surface of the block.

As alluded to previously, the cross-sectional area of the hole was measured by means of an area probe [McClurken (1978)], which measures area irrespective of shape by an electrical impedance technique. The electrically conducting fluid inside the hole was connected via a rigid tube to a reservoir of adjustable height, which in combination with a water manometer provided the means of applying and monitoring internal vessel pressure. The area probe itself was contained within 2 mm O.D. teflon tube which was mounted in supports that allowed its positioning anywhere within the block. A photograph of the entire test system is shown in Figure 25.

3.2.3 Test Procedure

As each test was conducted, we first established the existence of a uniformly deformed region in the center of the block, which in all

tests was at least one inch long. The first series of tests were conducted for a constant internal vessel pressure (9 mm Hg) with the radial location of the vessel at one of the four following levels:

1) outer wall of Schlemm's canal (σ_d = -IOP),
2) 0.22 mm from Schlemm's canal (σ_d = -3/4 IOP),
3) 0.46 mm from Schlemm's canal (σ_d = -1/2 IOP),
4) 0.72 mm from Schlemm's canal (σ_d = -1/4 IOP).

We conducted experiments for increasing intraocular pressures between 0 and 60 mm Hg, where at each level of intraocular pressure σ_t and σ_d were calculated as discussed previously and along with P_v are scaled according to the relationships;

$$\sigma_{t_f} = \frac{\sigma_t E_{tf}}{E_{ts}} ,$$

$$\sigma_{d_f} = \frac{\sigma_d E_{cf}}{E_{cs}} ,$$

$$P_{v_f} = P_v \frac{E_{cf}}{E_{cs}} .$$

The foam did not creep appreciably during the test, as evidenced by the fact that the cross-sectional area of the hole stabilized within 20 seconds after the load was applied. However, some hysteresis of the material was observed, as after the removal of the loads, the hole did not return to its original cross-sectional area for between 1 to 2 hours.

One additional test was conducted for a constant intraocular pressure (IOP = 16 mm Hg) and radial position within the sclera (σ_d = -1/2 IOP) while the internal vessel pressure (P_v) was varied between 0 and 50 mm Hg. This test was conducted for increasing internal pressures only, with all stresses calculated and scaled as discussed previously.

CHAPTER 4

COMPARISON OF RESULTS

The purpose of this chapter is to determine, based on the experimental and theoretical data of Chapter 3, a reasonably accurate relationship between intraocular pressure and vessel cross-sectional area for a circumferentially running aqueous vein at various positions in the sclera. This relationship will be used, in Chapter 5, to develop a pressure-flow model for the aqueous veins.

It was noted earlier that we were unable to match all the appropriate dimensionless groupings in the large scale experiments. Therefore, the experimental results could not be used directly. We were able to deduce, however, the approximate form of the relationship between intraocular pressure and vessel cross-sectional area by combining the theoretical and experimental findings in the manner described in this chapter.

4.1 Changes in Area Due to Variations in Intraocular Pressure

The results from the analytical model for both the foam and sclera, along with the experimental results for the first series of experiments (in which IOP was varied and P_v held constant), are shown in Figures 26-29. The analytical results for the foam are within 1 percent of the experimental results, in the region of low strain, for a circumferentially oriented aqueous vein 0.72 mm from Schlemm's canal, although larger discrepancies are found for those vessels located closest to Schelmm's canal.

The differences between the results could be attributed to experimental errors associated with the relatively short length of the test section, the effects of the glue, and the compressibility of the air within the foam.

An interesting and fortuitous feature of the experimental relationship between A/A_0 and intraocular pressure is the striking degree of linearity over the range of A/A_0 from 1.0 down to 0.12. In most experiments, data was obtained up to an intraocular pressure of 60 mm Hg, but in several runs we went up to an intraocular pressure of 100 mm Hg, enough for A/A_0 to reach 0.13. Since this linearity was found in all our experiments and extended all the way to vessel collapse, we assumed this to be generally true.

A comparison of the analytical results for the sclera and foam (Figures 26-29) points out the importance of E_{ts}/E_{cs} particularly at the outer margins of the sclera. Therefore, the experimental results, for which E_{ts}/E_{cs} was not properly scaled, could not be used directly as a measure of the degree of vessel collapse. However, the linearity of the experimental results suggested that a representative relationship between A/A_0 and intraocular pressure for an aqueous vein could be obtained by fitting a straight line to the theoretical results for the sclera in the region of small deformations. A line was also fitted to the theoretical results for the foam in the region of small deformations, and are shown with the previous results and the slopes of the experimental results in Table 4.

The linear relationships between A/A_0 and intraocular pressure for a circumferentially oriented aqueous vein, at the four vessel locations considered in the first series of experiments, are shown graphically in Figure 31; these will be used in the pressure-flow model of the aqueous veins presented in Chapter 5. Since the analytical results for the foam consistently underestimated the degree of collapse obtained experimentally, these linear relationships were considered to be a conservative estimate of the degree of aqueous vein collapse at a given intraocular pressure. These linear relationships also show that, according to the theoretical model of the sclera, the radial location of the circumferentially oriented aqueous vein within the sclera has little effect on the degree of vessel collapse.

4.2 The Effect of Variations in Internal Vessel Pressure

The effect of internal vessel pressure was studied both theoretically and experimentally with the results shown in Figure 30. Although each of these studies was conducted at a different initial level of collapse, each is essentially linear and has approximately the same slope. By comparing the slopes of these curves to those obtained for changes in intraocular pressure, we find that relatively large changes in internal vessel pressure were required to cause significant changes in the vessel's cross-sectional area, as suggested by the ratio of slopes:

$$\left| \frac{\frac{d\left(\frac{A}{A_0}\right)}{d\left(\frac{IOP}{E_{cs}}\right)}}{\frac{d\left(\frac{A}{A_0}\right)}{d\left(\frac{P_v}{E_{cs}}\right)}} \right| \sim 5 \quad .$$

Because of this fact, we assumed a constant internal vessel pressure (9 mm Hg) in the pressure-flow model of the aqueous veins presented in Chapter 5. This assumption will lead to some inconsistencies at highly elevated intraocular pressures (>50 mm Hg) which will be discussed later.

CHAPTER 5

PRESSURE-FLOW MODEL OF AQUEOUS OUTFLOW SYSTEM

In this chapter, we develop an approximate model capable of predicting the relationship between aqueous outflow and intraocular pressure. The model is based on changes in flow resistance due to collapse of a circumferentially oriented aqueous vein as intraocular pressure increases. The linear relationships of Chapter 4 are used to determine the extent of collapse associated with different levels of intraocular pressure. By an analysis similar to that presented in Chapter 3, we determined that the cross-sectional area of a radially oriented vessel (or segment of vessel) will increase only slightly (~3%) for intraocular pressures up to 70 mm Hg. Therefore, we considered the radially oriented vein segments to be of constant area.

5.1 Resistance to Flow of a Circumferentially Oriented Aqueous Vein

Flow in an aqueous vein is viscous dominated as evidenced by Reynolds numbers ($Re = \frac{Vd\rho}{\mu}$, where V is the velocity of the aqueous humor, d is the diameter of the vessel, and ρ and μ are density and viscosity, respectively, of the aqueous humor) ranging up to 0.02 for largest aqueous veins at a flow rate of 2$\mu\ell$/min. If we assume that the axial variations in cross-sectional area are gradual, then the flow will be locally fully-developed and the flow resistance can be determined from a Pouseuille resistance law. For area ratios ($\alpha = A/A_0$) greater than 0.36, the shape of the circumferentially oriented aqueous vein is approxi-

mated by an ellipse, the resistance of which, according to Milne-Thompson (1950), is

$$R \equiv \frac{\Delta P}{Q} = \frac{8\pi\mu L}{\alpha^3 A_0^2} \quad ,$$

where μ is the viscosity of aqueous humor (1.03-1.04 centipoise [Moses (1970)]), and ΔP is the pressure drop across a length L of the circumferentially oriented aqueous vein. For area ratios less than 0.36, the resistance was determined from an expression, derived by Flahrety (1972) for thin-walled collapsible tubes, of the form

$$R = \frac{70\mu L}{\alpha^2 A_0^2} \quad .$$

These two expressions for the resistance are, in general, functions of both intraocular pressure and internal vessel pressure through their dependence on the area ratio. However, for the purpose of this analysis, the internal vessel pressure was assumed to be constant, the implications of which will be discussed in Section 5.2.

5.2 Pressure Flow Model

From the information presented in Chapter 1, we assumed there to be 30 aqueous veins of the following size and distribution;

1) 15 aqueous veins with a diameter of 0.05
2) 9 aqueous veins with a diameter of 0.02 mm,
3) 6 aqueous veins with a diameter of 0.10 mm,

We further assumed that each vessel has a uniform unstressed area (A_0) and that no intrascleral junctions occur between vessels.

The aqueous veins were modeled as a parallel flow circuit having Schlemm's canal as the upstream node and the episcleral veins, all of which were assumed to be at the same pressure (9 mm Hg), as the downstream node with 30 parallel aqueous veins in between.

The path of the aqueous veins was idealized as a series of circumferentially and radially oriented steps beginning at the outer wall of Schlemm's canal and concluding at the surface of the sclera. The radially oriented segments, when added together, equal the scleral thickness (1 mm), while the circumferential steps were of equal length, but generally not equal in length to the radial segments. Three separate combinations of circumferentially and radially oriented steps were considered:

1) A circumferentially oriented step at the outer wall of Schlemm's canal, with additional circumferential steps 0.22 mm, 0.46 mm, and 0.72 mm from it. Between each circumferential segment is a radially oriented segment of the required length (Figure 32a).

2) Circumferentially oriented steps located 0.22 mm, 0.46 mm, and 0.72 mm from the outer wall of Schlemm's canal connecting radially oriented segments of the required length (Figure 32b).

3) Circumferentially oriented steps located 0.46 mm and 0.72 mm from the outer wall of Schlemm's canal with radially oriented segments of the required length between each circumferential segment (Figure 32c).

Several values were selected for the total vessel length in the circumferential direction ranging from 5 to 50 percent of the total vessel length.

We also considered the possibility that some aqueous veins pass through the sclera in a predominantly radial direction. To investigate

this possibility, a separate analysis was conducted assuming that one large aqueous vein runs radially through the sclera while the remaining aqueous veins conformed to the three previous descriptions of their path.

The results of this analysis will be presented in two forms, first in terms of a pressure-flow curve for the entire aqueous outflow tract via Schlemm's canal, and second, in terms of the resistance of the aqueous veins alone. In order to obtain a pressure-flow relationship for the entire outflow system, the resistance to outflow from the anterior chamber to the aqueous veins was considered to be constant. The value of this resistance was obtained by assuming an intraocular pressure of 16 mm Hg, an episcleral venous pressure of 9 mm Hg, and a flow rate of aqueous humor via the convential pathway of 2μℓ/min. This yields a value for the total outflow resistance at this intraocular pressure of 3.5 $\frac{\text{mm Hg-min}}{\mu\ell}$, from which we subtracted the resistance from the flow model for the aqueous veins at an intraocular pressure of 16 mm Hg (between 8.3×10^{-3} to 2.4×10^{-2} $\frac{\text{mm Hg-min}}{\mu\ell}$ depending on the number and length of the circumferential steps) to obtain the resistance of the remainder of the aqueous outflow system (between 3.492 to 3.476 $\frac{\text{mm Hg-min}}{\mu\ell}$).

5.3 Results

5.3.1 Pressure-Flow Relationship for the Aqueous Outflow System

Results from the pressure-flow model, determined using the three idealized paths just described, for the values of 5 and 50 percent of the total vessel length in the circumferential direction, are shown in Figures

33-35. These results exhibit a linear pressure-flow relationship up to intraocular pressures between 35 and 55 mm Hg (depending on the number and length of the circumferential steps), beyond which the pressure drop through the aqueous veins becomes significant and non-linearities in the pressure-flow relationship begin. The intraocular pressure at which the pressure drop through the aqueous veins becomes significant increases as the percentage of the total vessel length in the circumferential direction decreases.

A comparison of the results obtained for the three idealized paths of the aqueous veins, for the case of 50 percent of the total vessel length in the circumferential direction, is shown in Figure 36. This comparison demonstrates an important result of the analysis; the radial location in the sclera where the vessel begins to run circumferentially has only a slight effect on the level of intraocular pressure at which the pressure drop through the aqueous veins becomes significant (between 35 and 40 mm Hg for 50 percent of the total vessel length in the circumferential direction).

The results of this model suggest a maximum possible flow rate exists for the eye (between 10 and 15 μℓ/min), above which the pressure would increase until the eye ruptures. This result is caused in part by the neglect of the effects of changes in internal vessel pressure on cross-sectional area. As intraocular pressure reaches levels where the pressure drop through the aqueous veins becomes significant, the pressure within the vessel will increase and thus reduce the degree of collapse. Therefore,

we interpret these results as suggesting that if all aqueous veins run circumferentially for some part of their length, at elevated intraocular pressures (above 60 mm Hg) the pressure-flow relationship will exhibit strong non-linearities, but will not necessarily exhibit a flow maximum.

The results for the case of one large aqueous vein running entirely in the radial direction, while all others conform to the previous description of path, are shown in Figures 33-35. The results are shown only for the case of 50 percent of the total vessel length in the circumferential direction, which are imperceptively different from the results for 5 percent. These results show that at elevated intraocular pressures (above 60 mm Hg) all the flow will proceed through the radially oriented vessel with only a small increase in the total outflow resistance (~1%). However, if only one medium sized aqueous vein runs purely radially, at intraocular pressures above 60 mm Hg the pressure-flow relationship will be linear, after a non-linear transition region, with an increase in the total outflow resistance of 25 percent. If only one of the smallest vessels is oriented in the radial direction, at intraocular pressures above 60 mm Hg the pressure-flow relationship will be linear, after a non-linear transition region, with approximately a ten fold increase in the outflow resistance. We can conclude then that if one or more aqueous veins pass purely in the radial direction, the pressure-flow relationships will be linear at elevated intraocular pressures with the total outflow resistance remaining relatively constant or increasing by up to a factor of 10, depending on the number and size of the radially oriented aqueous veins.

5.3.2 Resistance of Aqueous Veins

One step in determining the pressure-flow curve just discussed is to compute the resistance of the aqueous veins alone. These values of resistance determined from the three idealized models previously described are shown plotted against intraocular pressure in Figures 37-42. These curves exhibit strong non-linearities such that the resistance increases more rapidly with increasing intraocular pressure. At intraocular pressures between 50 and 65 mm Hg (depending on the number and length of the circumferential steps), the resistance begins to increase dramatically (Figures 40-42); the value of intraocular pressure at which this happens increases as the percentage of the total vessel length in the circumferential direction decreases.

A comparison of the results obtained for the three idealized paths, for the case of 50 percent of the total vessel length in the circumferential direction, is shown in Figure 43. This comparison demonstrates that the radial location in the sclera where the vessels begin to run circumferentially has only a small effect on the level of intraocular pressure at which large changes in the resistance of the vessels begins (between 50 and 55 mm Hg for 50 percent of the total vessel length in the circumferential direction). Since variations in internal vessel pressure were not taken into account in the analysis, the results at elevated intraocular pressures are, however, somewhat misleading. As the resistance of the aqueous veins increase, the internal vessel pressure will increase counteracting the tendency for vessel collapse. Since the effect of internal

vessel pressure is much weaker than that of intraocular pressure, the resistance of the aqueous veins will certainly still increase, but at a more gradual rate.

The results for the case of one large aqueous vein oriented in the radial direction, while all others conform to the previous description of path, are shown in Figures 37-39. In these cases, the resistance at low intraocular pressures behaves in the same way as the results for all aqueous veins running circumferentially for some part of their length. At intraocular pressures between 40 and 60 mm Hg (depending on the number and length of the circumferential steps), the resistance for the case of one large radially oriented aqueous vein begins to asymptotically approach the value of the resistance associated with one large aqueous vein (5.27×10^{-2} $\frac{\text{mm Hg-min}}{\mu\ell}$). If some aqueous veins are oriented in a purely radial direction, the asymptotic value approached will vary from 8×10^{-3} to 33 $\frac{\text{mm Hg-min}}{\mu\ell}$, depending on the number and size of the vessels.

CHAPTER 6

CONCLUSIONS

The primary objective of this work was to determine if, and under what conditions, the collapse of aqueous veins significantly effects the total outflow resistance. It was found, however, that before the analysis of the aqueous veins could begin, we needed more information on the material properties of the sclera than was available in the literature. Through the use of a new compression testing system of our design, we determined that the compressive radial modulus of the sclera is a factor of 100 less than its tangential tensile modulus, and its Poisson's ratio is between 0.46 and 0.50.

We used the combined results from a large scale experimental study and a theoretical analysis to determine the relationship between intraocular pressure and cross-sectional area for a circumferentially oriented aqueous vein. The results from the experimental model could not be used directly as a measure of the degree of vessel collapse, because we were unable to precisely match the properties of the sclera. However, by virtue of the linearity observed in all of the experimental results, the theoretical predictions for the sclera, strictly valid only for small deformations, were extrapolated to high degrees of collapse using a linear relationship between the area ratio (A/A_0) and intraocular pressure. Internal vessel pressure was assumed constant at 9 mm Hg. These results predict nearly total vessel collapse at intraocular pressures greater

than 55 mm Hg, with the degree of collapse nearly independent of the radial location in the sclera at which the vessel begins to run circumferentially.

Using this information, we developed an approximate model capable of predicting the pressure-flow relationship for the aqueous outflow system (assuming that the resistance of other parts of the aqueous outflow system is constant). The results of this model demonstrate that the resistance, at normal intraocular pressures (16-20 mm Hg), cannot be attributed to the aqueous veins, but rather, is found in the remainder of the aqueous outflow system.

However, at higher intraocular pressures (between 35 and 55 mm Hg), if all aqueous veins run circumferentially for at least part of their length, the resistance of the aqueous veins, due to their collapse, begins to increase dramatically. The pressure-flow relationship, therefore, will become highly non-linear at these elevated pressures.

If some of the aqueous veins run in a purely radial direction, the resistance at elevated intraocular pressures (above 55 mm Hg) asymptotically approaches the value associated with the radially oriented aqueous veins by themselves (between 8×10^{-3} to 33 $\frac{\text{mm Hg-min}}{\mu\ell}$ depending on the number and size of the radially oriented vessels). The pressure-flow relationship, therefore, will become linear again at elevated intraocular pressures with an increase in the total outflow resistance of up to a factor of 10, depending on the number and size of the radially oriented vessels.

APPENDIX A

DEVELOPMENT OF ANALYTICAL MODEL

As mentioned in Chapter 3, the structure was initially assumed to be an isotropic material, for the purpose of determining the angle (θ_1) corresponding to zero radial strain. To simplify the analysis, we analyzed the stresses acting in the plane of the hole, for the conditions of plane strain ($\varepsilon_z = 0$), separately from the stresses acting parallel to its length. Then, the strains induced by the stresses acting parallel to the axis of the cylinder were superimposed on the previous result.

The equations of equilibrium for plane strain, ignoring body forces, in cylindrical coordinates are

$$\frac{\partial^2 \sigma_r}{\partial r^2} + \frac{1}{r}\frac{\partial \tau_{r\theta}}{\partial \theta} + \frac{\sigma_r - \sigma_\theta}{r} = 0 \quad ,$$

$$\frac{1}{r}\frac{\partial \sigma_\theta}{\partial \theta} + \frac{\partial \tau_{r\theta}}{\partial r} + \frac{2\tau_{r\theta}}{r} = 0 \quad .$$

The equations were solved in terms of a stress function ϕ by assuming that ϕ determines the stress components σ_r, σ_θ, and $\tau_{r\theta}$ through the relationships

$$\sigma_r = \frac{1}{r}\frac{\partial \phi}{\partial r} + \frac{1}{r^2}\frac{\partial^2 \phi}{\partial \theta^2} \quad , \qquad \text{(A-1)}$$

$$\sigma_\theta = \frac{\partial^2 \phi}{\partial r^2} \quad , \tag{A-2}$$

$$\tau_{r\theta} = \frac{1}{r^2} \frac{\partial \phi}{\partial \theta} - \frac{1}{r} \frac{\partial^2 \phi}{\partial r \partial \theta} \quad . \tag{A-3}$$

Substituting the functional relations for σ_r, σ_θ, and $\tau_{r\theta}$ in terms of the stress function ϕ into the equations of equilibrium for plane strain, results in the compatibility equation in cylindrical coordinates,

$$\left(\frac{\partial^2}{\partial r^2} + \frac{1}{r} \frac{\partial}{\partial r} + \frac{1}{r^2} \frac{\partial^2}{\partial \theta^2} \right)\left(\frac{\partial^2 \phi}{\partial r^2} + \frac{1}{r} \frac{\partial \phi}{\partial r} + \frac{1}{r^2} \frac{\partial^2 \phi}{\partial \theta^2} \right) = 0 \quad . \tag{A-4}$$

First, we considered the orientation of the stress σ_{t_1} with regard to the hole, shown in Figure A-1, along with a cylindrical coordinate system originating at the center of the hole. Then, according to Timoshenko (1934), the solution of the compatibility equation yields the general form of the stress function

$$\phi = \left(Ar^2 + Br^4 + \frac{C}{r} + D\right)\cos 2\theta \ ,$$

and the corresponding stress components from Equations (A-1), (A-2) and (A-3) are

$$\sigma_r = -\left(2A + 16 \frac{C}{r^4} + 4 \frac{D}{r^2}\right)\cos 2\theta \quad , \tag{A-5}$$

$$\sigma_\theta = \left(2A + 12Br^2 + \frac{6C}{r^4}\right)\cos 2\theta \quad , \tag{A-6}$$

$$\tau_{r\theta} = (2A + 6Br^2 - \frac{6C}{r^4} - \frac{2D}{r^2})\sin 2\theta \quad . \qquad \text{(A-7)}$$

Four boundary conditions were required to solve for the constants A, B, C, and D. As r becomes large, we require that the stress distribution reduce to

$$\sigma_{r_{r\to\infty}} = \frac{1}{2}\sigma_{t_1}(1 + \cos 2\theta) \quad ,$$

$$\tau_{r\theta_{r\to\infty}} = -\frac{1}{2}\sigma_{t_1}\sin 2\theta \quad .$$

Also, the surface of the hole must be free of normal (σ_r) and shear ($\tau_{r\theta}$) stresses. Applying these conditions, we find

$$\sigma_r = \frac{\sigma_{t_1}}{2}(1 - (\frac{a}{r})^2) + \frac{\sigma_{t_1}}{2}(1 + 3(\frac{a}{r})^4 - 4(\frac{a}{r})^2)\cos 2\theta \quad , \qquad \text{(A-8)}$$

$$\sigma_\theta = \frac{\sigma_{t_1}}{2}(1 + (\frac{a}{r})^2) - \frac{\sigma_{t_1}}{2}(1 + 3(\frac{a}{r})^4)\cos 2\theta \quad , \qquad \text{(A-9)}$$

$$\tau_{r\theta} = -\frac{\sigma_{t_1}}{2}(1 - 3(\frac{a}{r})^4 + 2(\frac{a}{r})^2)\sin 2\theta \quad , \qquad \text{(A-10)}$$

where a is the undeformed radius of the hole.

Next we considered the stress σ_d shown in Figure A-2. The stress distribution around the hole caused by this stress was determined from Equations (A-8), (A-9), and (A-10) by a simple rotation of axis, which

results in

$$\sigma_r = \frac{\sigma_d}{2}\left(1 - \left(\frac{a}{r}\right)^2\right) - \frac{\sigma_d}{2}\left(1 + 3\left(\frac{a^4}{r^4}\right) - 4\left(\frac{a}{r}\right)^2\right)\cos 2\theta \,, \qquad \text{(A-11)}$$

$$\sigma_\theta = \frac{\sigma_d}{2}\left(1 + \left(\frac{a}{r}\right)^2\right) + \frac{\sigma_d}{2}\left(1 + 3\left(\frac{a}{r}\right)^4\right)\cos 2\theta \,, \qquad \text{(A-12)}$$

$$\tau_{r\theta} = \frac{\sigma_d}{2}\left(1 - 3\left(\frac{a}{r}\right)^4 + 2\left(\frac{a}{r}\right)^2\right)\sin 2\theta \,. \qquad \text{(A-13)}$$

To analyze the effect of internal pressure, the hole and the surrounding material were modeled as a thick-walled cylinder where the outside radius (b) approaches infinity. The corresponding stresses induced in the surrounding material by an internal pressure P_v, according to Timoshenko (1934), are

$$\sigma_r = \frac{a^2 P_v}{(b^2 - a^2)} - \frac{a^2 b^2 P_v}{(b^2 - a^2) r^2} \,,$$

$$\sigma_\theta = \frac{a^2 P_v}{(b^2 - a^2)} + \frac{a^2 b^2 P_v}{(b^2 - a^2) r^2} \,.$$

As the outside radius (b) approaches infinity, the first term in each expression goes to zero, while the second term reduces to

$$\sigma_r = -\frac{a^2 P_v}{r^2} \,, \qquad \text{(A-14)}$$

$$\sigma_\theta = \frac{a^2 P_v}{r^2} \,. \qquad \text{(A-15)}$$

Since the governing equations are linear, we can superimpose the respective stress components, Equations (A-8) through (A-15), to obtain

$$\sigma_r = \left(\frac{\sigma_{t_1} + \sigma_d}{2}\right)\left(1 - \left(\frac{a}{r}\right)^2\right) + \left(\frac{\sigma_{t_1} - \sigma_d}{2}\right)\left(1 + 3\left(\frac{a}{r}\right)^4 - 4\left(\frac{a}{r}\right)^2\right)\cos 2\theta - \left(\frac{a}{r}\right)^2 P_v \quad , \tag{A-16}$$

$$\sigma_\theta = \left(\frac{\sigma_{t_1} + \sigma_d}{2}\right)\left(1 + \left(\frac{a}{r}\right)^2\right) + \left(\frac{\sigma_d - \sigma_{t_1}}{2}\right)\left(1 + 3\left(\frac{a}{r}\right)^4\right)\cos 2\theta + \left(\frac{a}{r}\right)^2 P_v \quad , \tag{A-17}$$

$$\tau_{r\theta} = \left(\frac{\sigma_d - \sigma_{t_1}}{2}\right)\left(1 - 3\left(\frac{a}{r}\right)^4 + 2\left(\frac{a}{r}\right)^2\right)\sin 2\theta \quad . \tag{A-18}$$

The strains brought about as a consequence of the above stresses were determined by Hooke's law, for an isotropic material, which specifies that

$$\varepsilon_r = \frac{1}{E}\left(\sigma_r - \nu\,\sigma_\theta - \nu\,\sigma_z'\right) \quad ,$$

$$\varepsilon_\theta = \frac{1}{E}\left(-\nu\,\sigma_r + \sigma_\theta - \nu\,\sigma_z'\right) \quad ,$$

$$\gamma_{r\theta} = \frac{1}{G}\,\tau_{r\theta} \quad .$$

The component of stress which acts parallel to the axis of the cylinder

(σ_z') is the summation of the stresses induced by the requirement of plane strain and the stress σ_{t_2}, and results in

$$\sigma_z' = \nu(\sigma_r + \sigma_\theta) + \sigma_{t_2} \quad .$$

The respective strain components become, after carrying out the indicated subsitutions

$$\varepsilon_r = \frac{1}{E}((1 - \nu^2)\sigma_r + (-\nu-\nu^2)\sigma_\theta - \nu\sigma_{t_2}) \quad ,$$

$$\varepsilon_\theta = \frac{1}{E}((-\nu-\nu^2)\sigma_r + (1-\nu^2)\sigma_\theta - \nu\sigma_{t_2}) \quad ,$$

$$\gamma_{r\theta} = \frac{1}{G}\tau_{r\theta} \quad .$$

The displacement of the surface of the hole caused by these strains was obtained by determining the radial (u) and tangential (v) displacement functions such that the relationships

$$\varepsilon_r = \frac{\partial u}{\partial r} \quad ,$$

$$\varepsilon_\theta = \frac{u}{r} + \frac{\partial v}{\partial \theta} \quad ,$$

$$\gamma_{r\theta} = \frac{1}{r}\frac{\partial u}{\partial \theta} + \frac{\partial v}{\partial r} - \frac{v}{r} \quad ,$$

are satisfied. Upon making the proper substitutions, and performing the required integrations, the radial displacement function evaluated at the surface of the hole (r=a) was found to be

$$U_{r=a} = \frac{a}{E}\left[(1-\nu^2)(\sigma_{t_1} + \sigma_d + 2(\sigma_{t_1} - \sigma_d)\cos 2\theta) + (1+\nu)P_v - \nu\sigma_{t_2}\right] . \qquad \text{(A-19)}$$

The angle at which the surface of the hole is undeformed is obtained by setting Equation (A-19) equal to zero, resulting in

$$\theta_1 = \frac{1}{2}\cos^{-1}\left(\frac{\left(\frac{\nu}{1-\nu^2}\right)\sigma_{t_2} - \left(\frac{1+\nu}{1-\nu^2}\right)P_v - (\sigma_{t_1} + \sigma_d)}{2(\sigma_{t_1} - \sigma_d)}\right) . \qquad \text{(A-20)}$$

Since the angle obtained from this expression was found to be fairly constant ($\pm$ 2°) for the conditions present in the first series of experiments conducted (Section 3.2.3), we used average value of the angle for these studies. However, when varying internal vessel pressure, the angle was calculated for each set of conditions investigated.

The isotropic model of the structure was then separated into segments; we used the tangential tensile modulus of the sclera for those portions of the vessel being enlarged (tensile stresses predominate), and the compressive radial modulus of the sclera for those portions of the vessel being compressed (compressive stresses predominate). The cross-sectional area of the vessel was determined through an integral of the form

$$\frac{A}{A_0} = \frac{2}{\pi} \int_0^{\theta_1} [1 + \frac{1}{E_{ts}}((1-\nu^2)(\sigma_{t_1} + \sigma_d + 2(\sigma_{t_1} - \sigma_d)\cos 2\theta)$$

$$+ (1+\nu)P_v - \nu \sigma_{t_2})]^2 d\theta + \frac{2}{\pi} \int_{\theta_1}^{\frac{\pi}{2}} [1$$

$$+ \frac{1}{E_{cs}} ((1-\nu^2)(\sigma_{t_1} + \sigma_d + 2(\sigma_{t_1} - \sigma_d)\cos 2\theta)$$

$$+ (1+\nu)P_v - \nu \sigma_{t_2})]^2 d\theta \quad ,$$

which results in

$$\frac{A}{A_0} = \frac{2}{\pi} [\theta_1 (1 + \frac{2(1-\nu^2)(\sigma_{t_1} + \sigma_d)}{E_{ts}} + (\frac{(1-\nu^2)(\sigma_{t_1} + \sigma_d)}{E_{ts}})^2 - \frac{\sigma_{t_2}}{E_{fs}}$$

$$- \frac{(1-\nu^2)(2\nu)(\sigma_{t_1} + \sigma_d)\sigma_{t_2}}{E_{ts}^2} - \frac{(1+\nu)(2\nu)\sigma_{t_2} P_v}{E_{ts}^2}$$

$$+ (\frac{\nu \sigma_{t_2}}{E_{ts}})^2 + (\frac{(1+\nu)P_v}{E_{ts}})^2 + \frac{2(1+\nu)P_v}{E_{ts}}$$

$$+ \frac{2(1+\nu)(1-\nu^2)(\sigma_{t_1} + \sigma_d)P_v}{E_{ts}^2} + \frac{1}{2}(\frac{2(1-\nu^2)(\sigma_{t_1} - \sigma_d)}{E_{ts}})^2))$$

$$+ \frac{1}{2}\sin 2\theta_1 \left(\frac{4(1-\nu^2)(1+\nu)(\sigma_{t_1} - \sigma_d)P_v}{E_{ts}^2} - \frac{4\nu(1-\nu^2)(\sigma_{t_1} - \sigma_d)\sigma_{t_2}}{E_{ts}^2} \right.$$

$$\left. + \frac{4(1-\nu^2)^2(\sigma_{t_1} + \sigma_d)(\sigma_{t_1} - \sigma_d)}{E_{ts}^2} + \frac{4(1-\nu^2)(\sigma_{t_1} - \sigma_d)}{E_{ts}} \right)$$

$$+ \frac{1}{8}\sin 4\theta_1 \left(\frac{2(1-\nu^2)(\sigma_{t_1} - \sigma_d)}{E_{ts}} \right)^2 \Bigg]$$

$$+ \frac{2}{\pi}\left[\left(\frac{\pi}{2} - \theta_1 \right) \left(1 + \frac{2(1-\nu^2)(\sigma_{t_1} - \sigma_d)}{E_{cs}} + \left(\frac{(1-\nu^2)(\sigma_{t_1} + \sigma_d)}{E_{cs}} \right)^2 - \frac{\sigma_{t_2}}{E_{cs}} \right.\right.$$

$$\left. - \frac{(1-\nu^2)(2\nu)(\sigma_{t_1} - \sigma_d)\sigma_{t_2}}{E_{cs}^2} - \frac{(1+\nu)(2\nu)\sigma_{t_2}P_v}{E_{cs}^2} \right.$$

$$\left. + \left(\frac{\nu\,\sigma_{t_2}}{E_{cs}} \right)^2 + \left(\frac{(1+\nu)P_v}{E_{cs}} \right)^2 + \frac{2(1+\nu)P_v}{E_{cs}} \right.$$

$$\left. + \frac{2(1+\nu)P_v}{E_{cs}} + \frac{2(1+\nu)(1-\nu^2)(\sigma_{t_1} - \sigma_d)P_v}{E_{cs}^2} \right.$$

$$\left. \left. + \frac{1}{2}\left(\frac{2(1-\nu^2)(\sigma_{t_1} - \sigma_d)}{E_{cs}} \right)^2 \right) \right)$$

$$+ \frac{1}{2}\sin 2\theta_1 \left(\frac{4\nu(1-\nu^2)(\sigma_{t_1} - \sigma_d)\sigma_{t_2}}{E_{cs}^2} - \frac{4(1-\nu^2)(1+\nu)(\sigma_{t_1} - \sigma_d)P_v}{E_{cs}^2} \right.$$

$$\left. - \frac{4(1-\nu^2)^2(\sigma_{t_1} + \sigma_d)(\sigma_{t_1} - \sigma_d)}{E_{cs}^2} - \frac{4(1-\nu^2)(\sigma_{t_1} - \sigma_d)}{E_{ts}} \right)$$

$$- \frac{1}{8}\sin 4\theta_1 \left(\frac{2(1-\nu^2)(\sigma_{t_1} - \sigma_d)}{E_{cs}} \right)^2 \Bigg] \quad .$$

This expression is used to obtain the analytical curves shown in Figures 26-30.

REFERENCES

Ascher, K.W., "Aqueous Veins and Their Significance for Pathogenesis of Glaucoma", Archives of Opthamology, 42: 66-76, 1949.

Ascher, K.W., "Aqueous Veins", Am. J. Ophthal., 25: 31-38, 1942.

Becker, B. and Constant, M., "The Facility of Aqueous Outflow", Arch. Opthal., 55: 305, 1956.

Bill, A., "Blood Circulation and Fluid Dynamics in the Eye", Physiological Reviews, 55: 383-416, 1975.

Bill, A., "The Drainage of Aqueous Humor", Investigative Opthal., 14: 1-3, 1975b.

Bill, A., "Aspects of the Regulation of the Uveal Venous Pressure in Rabbits", Ex. Eye Res., 1: 193-199, 1962.

Bill, A. and Svedbergh, B., "Scanning Electron Microscopic Studies of the Trabecular Meshwork and the Canal of Schlemm - An Attempt to Localize the Main Resistance to Outflow of Aqueous Humor in Man", Acta. Ophthal., 50: 295-320, 1972.

Bill, A., "Gross Facility, Facility of Conventional Routes and Pseudo Facility of Aqueous Humor Outflow in the Cynomolgus Monkey", Arch. Ophthal., 75: 665, 1966.

Bloom, J.N., Levene, R.Z., Thomas, G. and Kimura, R., "Fluorphotometry and the Rate of Aqueous Outflow in Man", Arch. Ophthal., 94: 435-443, 1976.

Brubaker, Richard F., Ezekiel, Shaoul, Chin, Lang, Young, Lawrence, Johnson, Steven A., and Beeler, George W., "The Stress-Strain Behavior of the Corneoscleral Envelope of the Eye I. Development of a System for Making In Vivo Measurements Using Optical Interferometry", Exp. Eye Res., 21: 37-46, 1975.

Brubaker, R.F., "Determination of Episcleral Venous Pressure in the Eye", Arch. Ophthal., 77: 110-114, 1967.

Curtin, Brian M.D., "Physiopathologic Aspects of Scleral Stress-Strain", Tr. Am. Ophthal. Soc., 67: 417-461, 1969.

Ellingsen, B.A. and Grant W.M., "The Relationship of Pressure and Aqueous Outflow in Enucleated Human Eyes", Invest. Opthal., 10: 430-437, 1971.

Flaherty, J.E., Keller, J.B., and Rubinow, S.I., "Post Buckling Behavior of Elastic Tubes and Rings with Opposite Sides in Contact," SIAM Journal of Applied Mathematics, 23(4), 1972, pp. 446-455.

Gloster, J., Perkins, E.S., and Pommier, Marie-Louise, "Extensibility of Strips of Sclera and Cornea", Brit. J. Opthal., 41: 103-110, 1957.

Grant, W.M., MD. and Jockson, V.L., MD., "Interconnections of Blood Vessels and Aqueous Vessels in Human Eyes", Archives of Opthalmology, 73: 707-720, 1965.

Grant, W.M., "Further Studies on Facility of Flow Through the Trabecular Meshwork", A.M.A. Arch. Opthal., 60: 523-533, 1958.

Grant, W.M., "Tonographic Method for Measuring the Facility and Rate of Aqueous Flow in Human Eyes", Arch. Opthal., 44: 204-214, 1950.

Greene, Peter R. and McMahon, Thomas A., "Scleral Creep vs Temperature and Pressure In Vitro", Exp. Eye Res., 29: 527-537, 1979.

Grierson, I. and Lee, W.R., "Pressure-Induced Changes in the Ultra-structure of the Endothelium Lining Schlemm's Canal", Am. J. Opthal., 80: 863-883, 1975.

Hayreh, S.S., "The Orbital Vessels of Rhesus Monkeys", Exp. Eye Res., 3: 16-30, 1964.

Inamata, H.A., Bill, A., and Smelser, G.K., "Aqueous Humor Pathways Through the Trabecular Meshwork and into Schlemm's Canal in the Cynomologus Monkey: An Electron Microscopic Study", Am. J. Opthal., 73: 760-789, 1972.

Johnstone, M.A., and Grant, W.M., "Pressure Dependent Changes in Structures of the Aqueous Outflow System of Human and Monkey Eyes", Am. J. Opthal., 75: 365-383, 1973.

Johnstone, M.A., "Pressure Dependent Changes in Configuration of the Endothelial Tubules of Schlemm's Canal", Am. J. Opthal., 78: 630-638, 1974.

Kobayashi, A.S., Woo, S.L.-Y., Lawrence, C., and Schlegel, W.A., "Analysis of the Corneo-Scleral Shell by the Method of Direct Stiffness", J. of Biomechanics, 4: 323-330, 1971.

Kobayashi, A.S., Staberg, L.G., and Schlegel, W.A., "Viscoelastic Properties of Human Cornea", Experimental Mechanics, Dec. 1973, pp. 497-503.

Levene, R. and Hyman, B., "The Effect of Intraocular Pressure on the Facility of Outflow", Exp. Eye Res., 8: 116, 1969.

Lyon, Catherine, McEwen, W.K., and Shepherd, Marvin D., "Ocular Rigidity and Decay Curves Analyzed by Two Non-Linear Systems", Investigative Ophthal., Dec. 1970, pp. 935-945.

McClurken, M.E., "Shape-Independent Area Measurement in Collapsible Tubes by an Electrical Impedance Technique", Proceedings of 31st Annual Conference on Engineering in Medicine and Biology, 1978, p. 95.

McEwen, W.K., "Application of Poiseuillels Law to Aqueous Outflow", Arch. Ophthal., 60: 290, 1958.

McEwen, W.K. and St. Helen, Roger, "Rheology of the Human Sclera", Ophthalmologica, 150: 321-346, 1965.

McEwen, W.K., Shepherd, M., and McBain, E.H., "An Electrical Model of the Human Eye. I. The Basic Model", Invest. Ophthal., 6: 155-159, 1967.

Milne-Thompson, L.M., Theoretical Hydrodynamics, MacMillan; New York, pp. 515-517, 1950.

Moses, R.A., "The Effect of Intraocular Pressure on Resistance to Outflow", Survey Ophthal., 22: 88-100, 1977.

Moses, R.A., Adler's Physiology of the Eye, 5th Edition, C.V. Mosby, St. Louis, pp. 297-310, 1970.

Nagataki, S. and Mishima, S., "Aqueous Humor Dynamics in Glaucoma-Cyclitic Crisis", Invest. Ophthal., 15: 365-370, 1976.

Nakamura, Yasuhisa, and Goulstine, David, "The Effect of Intraocular Pressure on the Vortex Vein Blood Flow", Exp. Eye Res., 15: 461-466, 1973.

Pederson, J.E. and Green, K., "Aqueous Humor Dynamics: Experimental Studies", Exp. Eye Res., 15: 277-297, 1973.

Pederson, J.E. and Green, K., "Aqueous Humor Dynamics: A Mathematical Approach to Measurement of Facility, Pseudofacility, Capilary Pressure, Active Secretion and X_c", Exp. Eye Res., 15: 265-276, 1973.

Perkins, E.S., "Pressure in the Canal of Schlemm", Brit. J. Ophthal., 39: 215-219, 1955.

Sears, M.L., "Pressure in the Canal of Schlemm and Its Relation to the Site of Resistance to Outflow of Aqueous Humor in the Eyes of Ethiopian Green Monkey's", Invest. Ophthal., 5: 610-623, 1966.

Spitznas, Manfred, Luciano, Liliana, and Reale, Enrico, "Fine Structure of Rabbit Scleral Collagen", Am. J. Ophthal., 69: 414-468, 1970.

Timoshenko, S.P., and Goodier, J.N., Theory of Elasticity, McGraw-Hill Book Co., New York, pp 65-95, 1934.

Tittel, P.G., and Richards, R.D., "Distensibility Measurement of the Rabbit Eye", Invest. Ophthal., 10: 800-809, 1971.

Tripathy, R.C., "Mechanism of the Aqueous Outflow Across the Trabecular Wall of Schlemm's Canal", Exp. Eye Res., 11: 116-121, 1971.

Tripathy, R.C., "Aqueous Outflow in Normal and Glaucomatous Eyes", Brit. J. Ophthal., 56: 157-175, 1972.

Weigelin, E., Sayegh, F., VonKlitzing, W., and Baurmann, H., "Aspects of Venous Drainage and Tissue Fluid Dynamics in the Eye", Eye, Ear, Nose and Throat Monthly, 59: 45-55, 59: 19-50, 1975.

Woo, S.L-Y, Kobayashi, A.S., Schlegel, W.A., and Lawrence, C., "Nonlinear Material Properties of Intact Cornea and Sclera", Exp. Eye Res., 14: 29-39, 1972.

Woo, S.L-Y, Kobayashi, A.S., Lawrence, C., and Schlegel, W.A., "Mathematical Model of the Corneo-Scleral Shell as Applied to Intraocular Pressure-Volume Relations and Applanation Tonometry", Annals of Biomedical Engineering, 1: 87-98, 1972b.

Yamada, H., Strength of Biological Materials, Krieger, Huntington, New York Press, pp. 238, 1973.

TABLE 1

LINEAR REGRESSION VALUES FOR THE RADIAL COMPRESSIVE MODULUS OF CATTLE SCLERA

Sample		Radial Compressive Modulus (dynes/cm^2)	Correlation Coefficient
Pair #1	1st Eye	$1.21\times10^5 \pm 15\%$	0.987
	2nd Eye	$1.83\times10^5 \pm 14\%$	0.985
Pair #2	1st Eye	$1.88\times10^5 \pm 14\%$	0.975
	2nd Eye	$1.44\times10^5 \pm 15\%$	0.985

TABLE 2

LINEAR REGRESSION VALUES FOR THE RADIAL COMPRESSIVE MODULUS OF HUMAN SCLERA

Sample	Radial Compressive Modulus (dynes/cm^2)	Correlation Coefficient	Poisson's Ratio
#1	$4.12\times10^5 \pm 11\%$	0.982	--
1st Eye			
#2	$4.00\times10^5 \pm 11\%$	0.993	$0.49 \pm 6\%$
93 year old			
#1	$3.31\times10^5 \pm 12\%$	0.991	--
2nd Eye			
#2	$3.27\times10^5 \pm 12\%$	0.988	$0.50 \pm 6\%$
1st Eye	$2.69\times10^5 \pm 13\%$	0.992	$0.48 \pm 6\%$
74 year old			
2nd Eye	$2.89\times10^5 \pm 13\%$	0.982	$0.47 \pm 6\%$
1st Eye	$3.18\times10^5 \pm 12\%$	0.989	$0.46 \pm 6\%$
63 year old			
2nd Eye	$3.24\times10^5 \pm 12\%$	0.982	$0.47 \pm 6\%$

TABLE 3

LINEAR REGRESSION VALUES FOR THE TANGENTIAL TENSILE MODULUS OF HUMAN SCLERA

Reference	Range of Tensile Stresses (dynes/cm^2)	Tangential Tensile Modulus (dynes/cm^2)	Correlation Coefficient
Glouster (1957	1.1×10^5 - 4.4×10^5	2.86×10^7	0.961
Curtain (1969)	0 - 7.3×10^5	1.97×10^7 - 1.22×10^8	0.944-0.983
Woo (1972)	0 - 7.3×10^5	1.91×10^7	0.973

TABLE 4

SLOPES OF LINEAR

RELATIONSHIPS BETWEEN A/A_0 AND IOP

Radial Location of Circumferentially Oriented Vessel	$d(A/A_0)/d(IOP/E_{cs})$ Theoretical Foam	Theoretical Sclera	Experimental
Outer wall of Schlemm's Canal (σ_d = -IOP)	-1.24	-3.43	-1.20
0.22 mm from outer wall of Schlemm's canal (σ_d = -3/4 IOP)	-1.66	-3.66	-2.15
0.46 mm from outer wall of Schlemm's canal (σ_d = -1/2 IOP)	-2.03	-3.96	-2.88
0.72 mm from outer wall of Schlemm's canal (σ_d = -1/4 IOP)	-2.48	-4.23	-3.64

LIST OF FIGURES

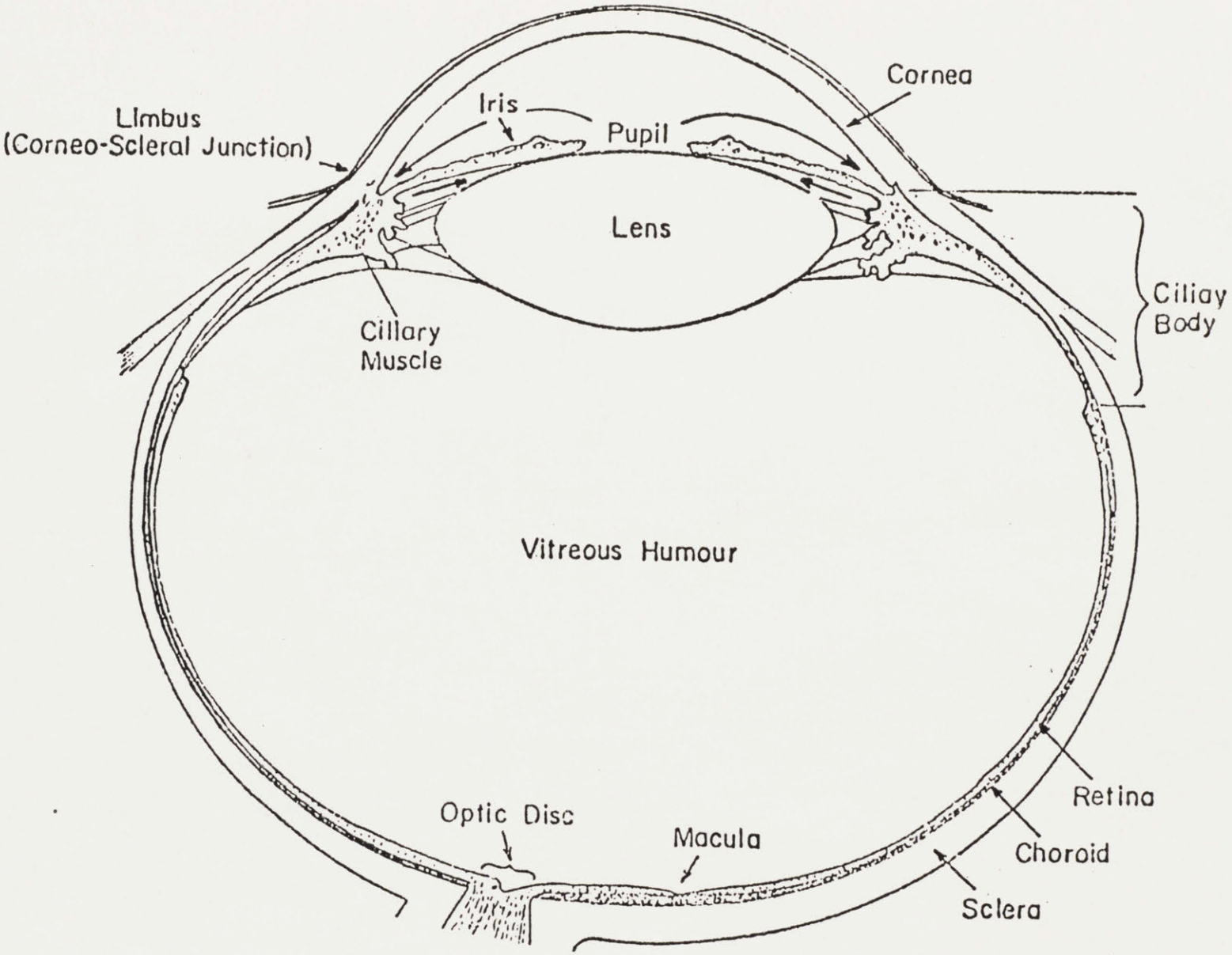
Limbus
(Corneo-Scleral Junction)
Iris
Pupil
Cornea
Lens
Ciliary
Body
Cillary
Muscle
Vitreous Humour
Optic Disc
Macula
Retina
Choroid
Sclera

Figure 1

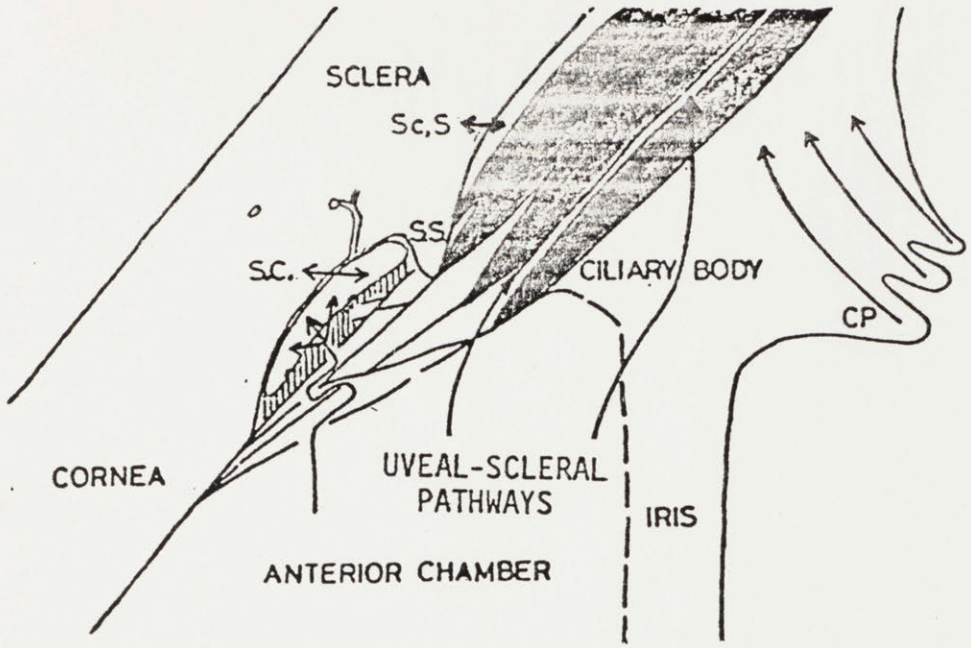

Figure 2

Figure 3

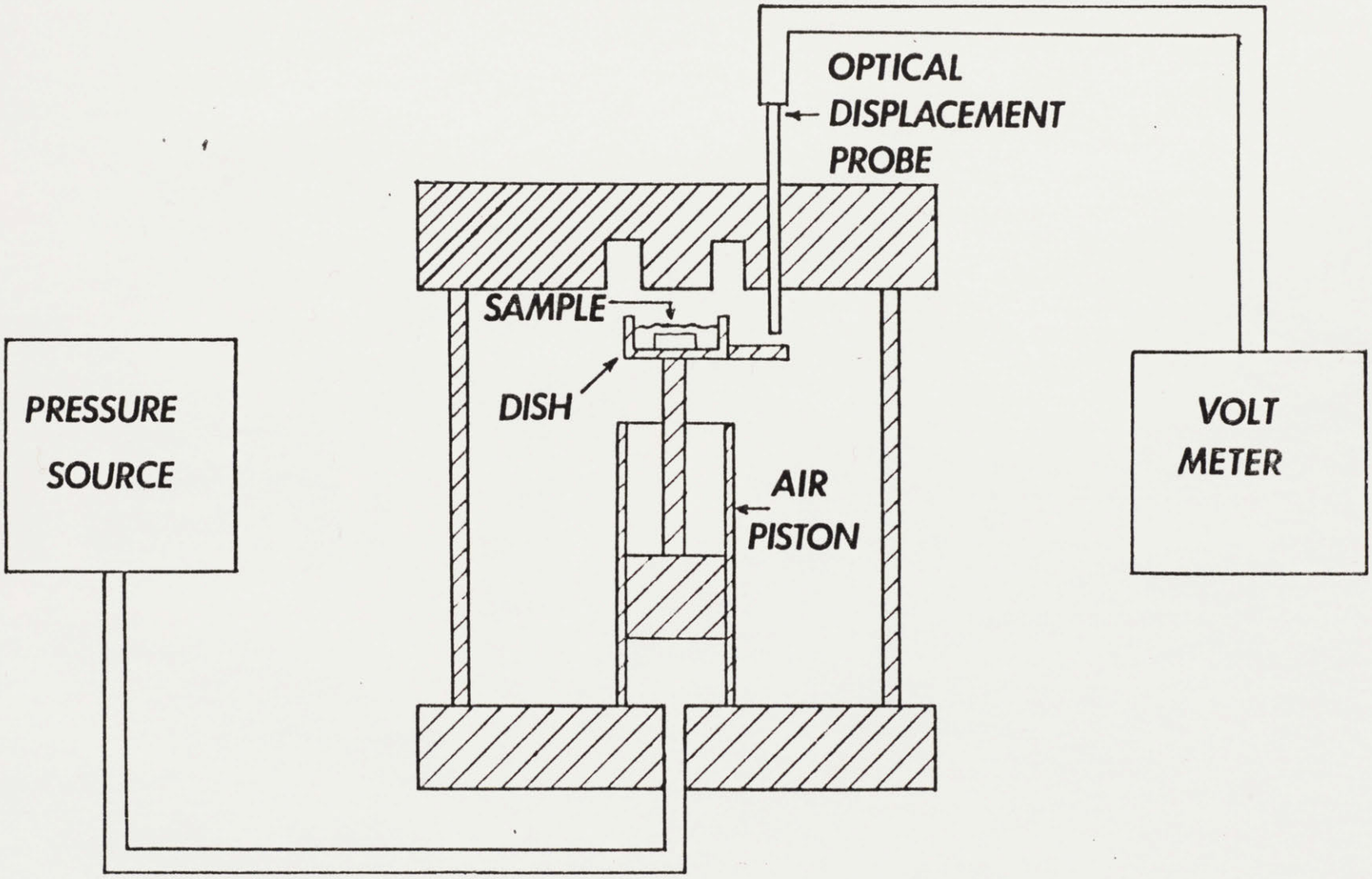
OPTICAL
DISPLACEMENT
PROBE
SAMPLE
DISH
AIR
PISTON
PRESSURE
SOURCE
VOLT
METER

Figure 4

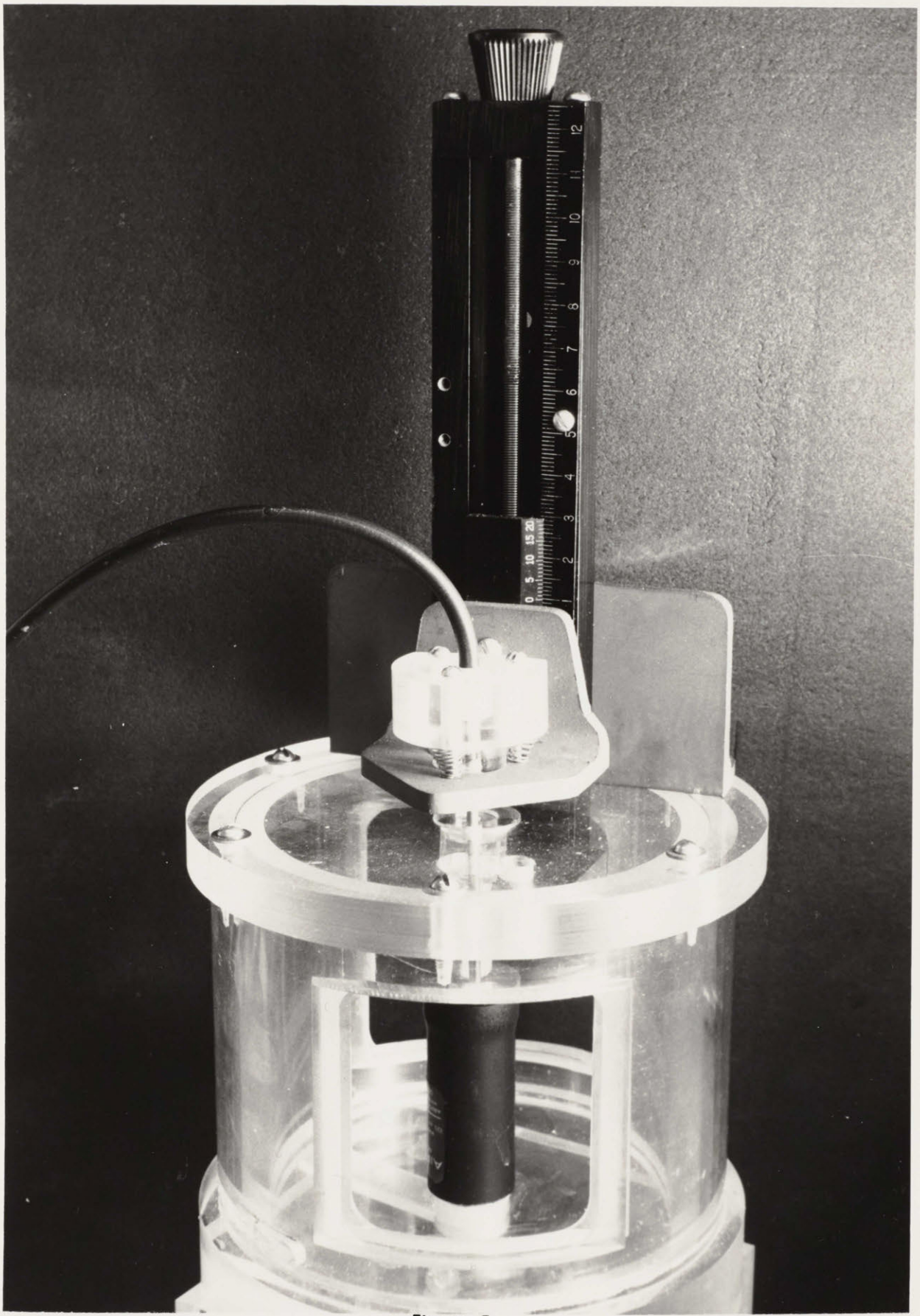

Figure 5

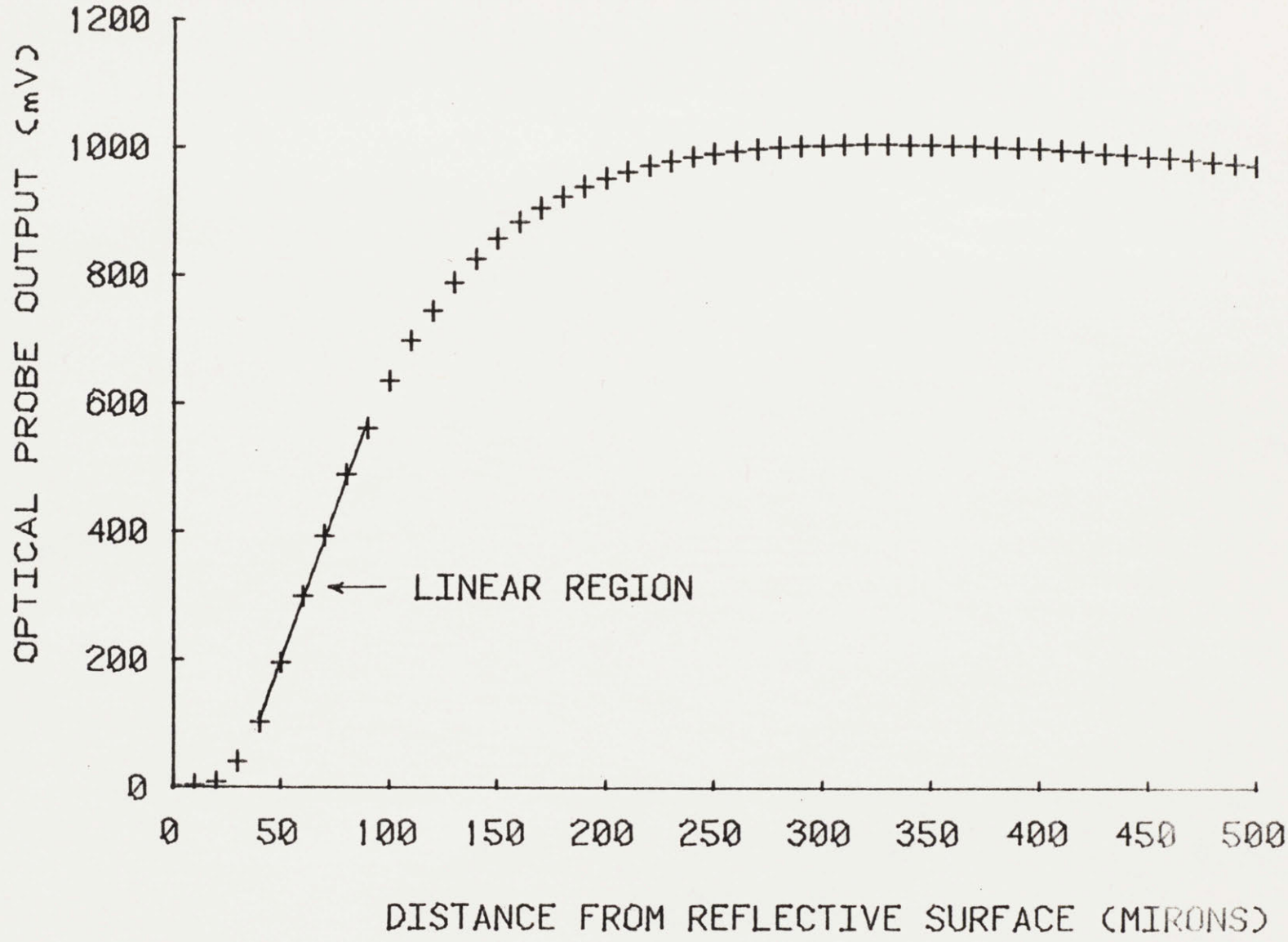
OPTICAL PROBE OUTPUT (mV)
1200
1000
800
600
400
200
0
LINEAR REGION
0
50
100
150
200
250
300
350
400
450
500
DISTANCE FROM REFLECTIVE SURFACE (MICRONS)

Figure 6

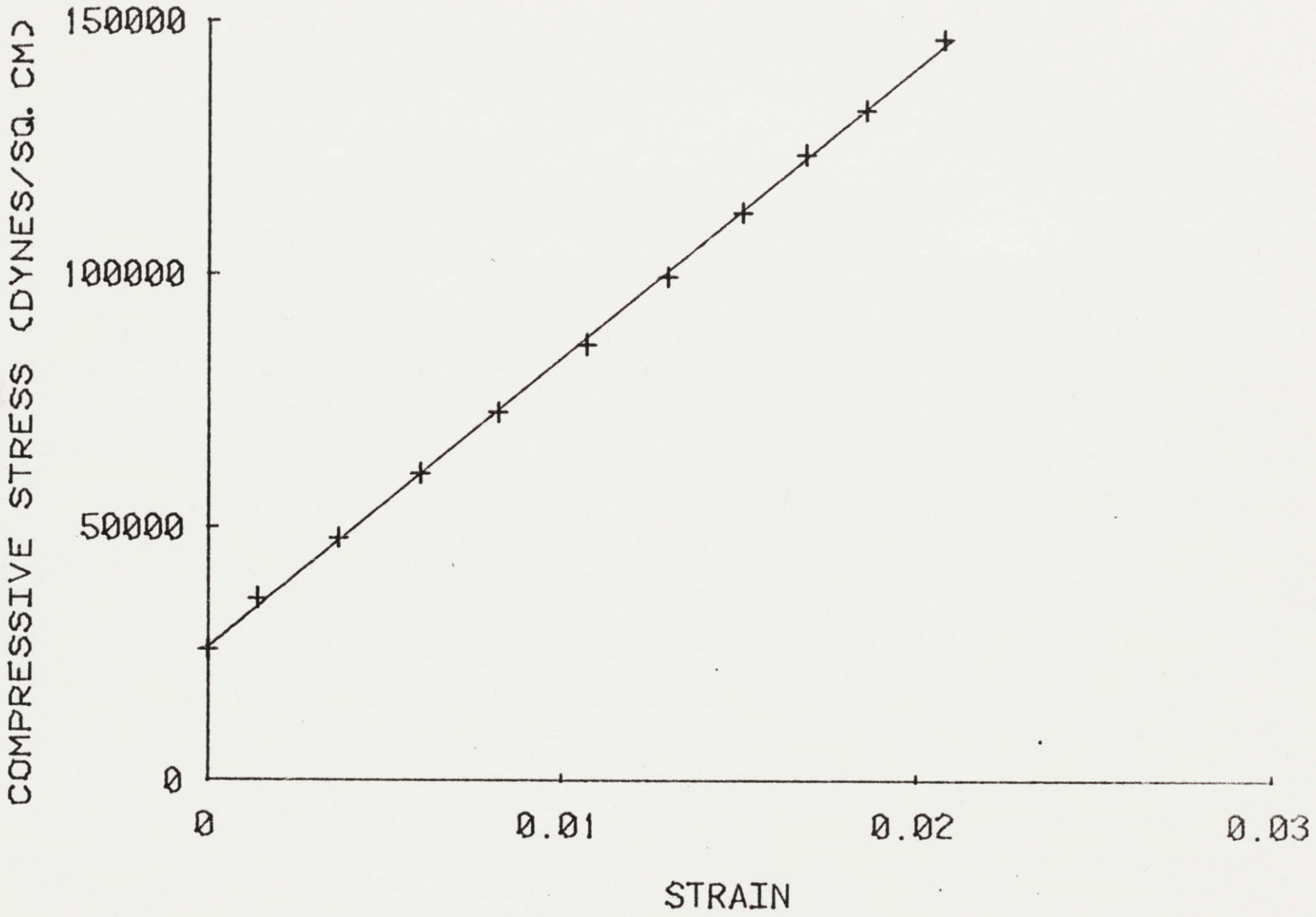
COMPRESSIVE STRESS (DYNES/SQ. CM)
150000
100000
50000
0
0
0.01
0.02
0.03
STRAIN

Figure 7

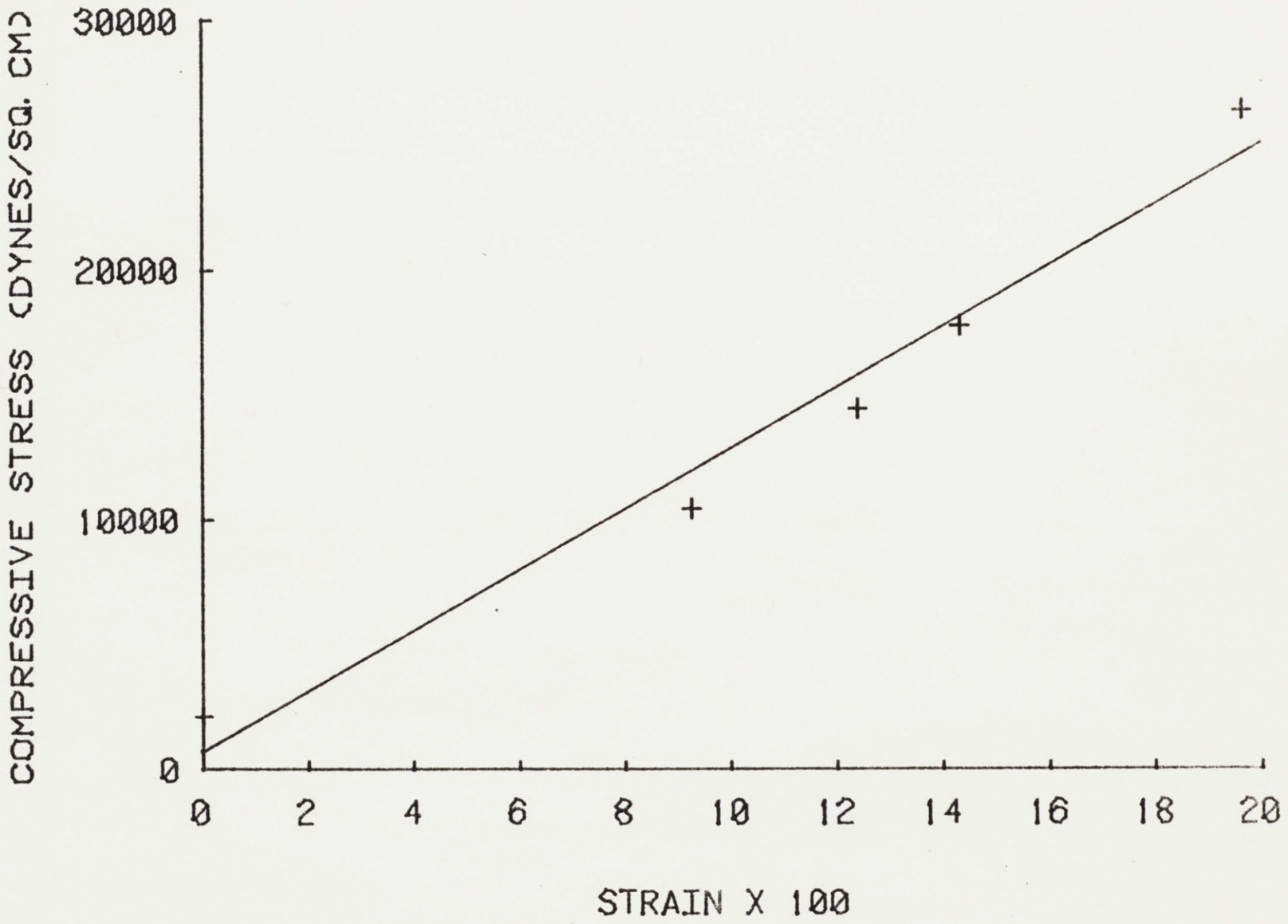
COMPRESSIVE STRESS (DYNES/SQ. CM)
30000
20000
10000
0
0
2
4
6
8
10
12
14
16
18
20
STRAIN X 100

Figure 8

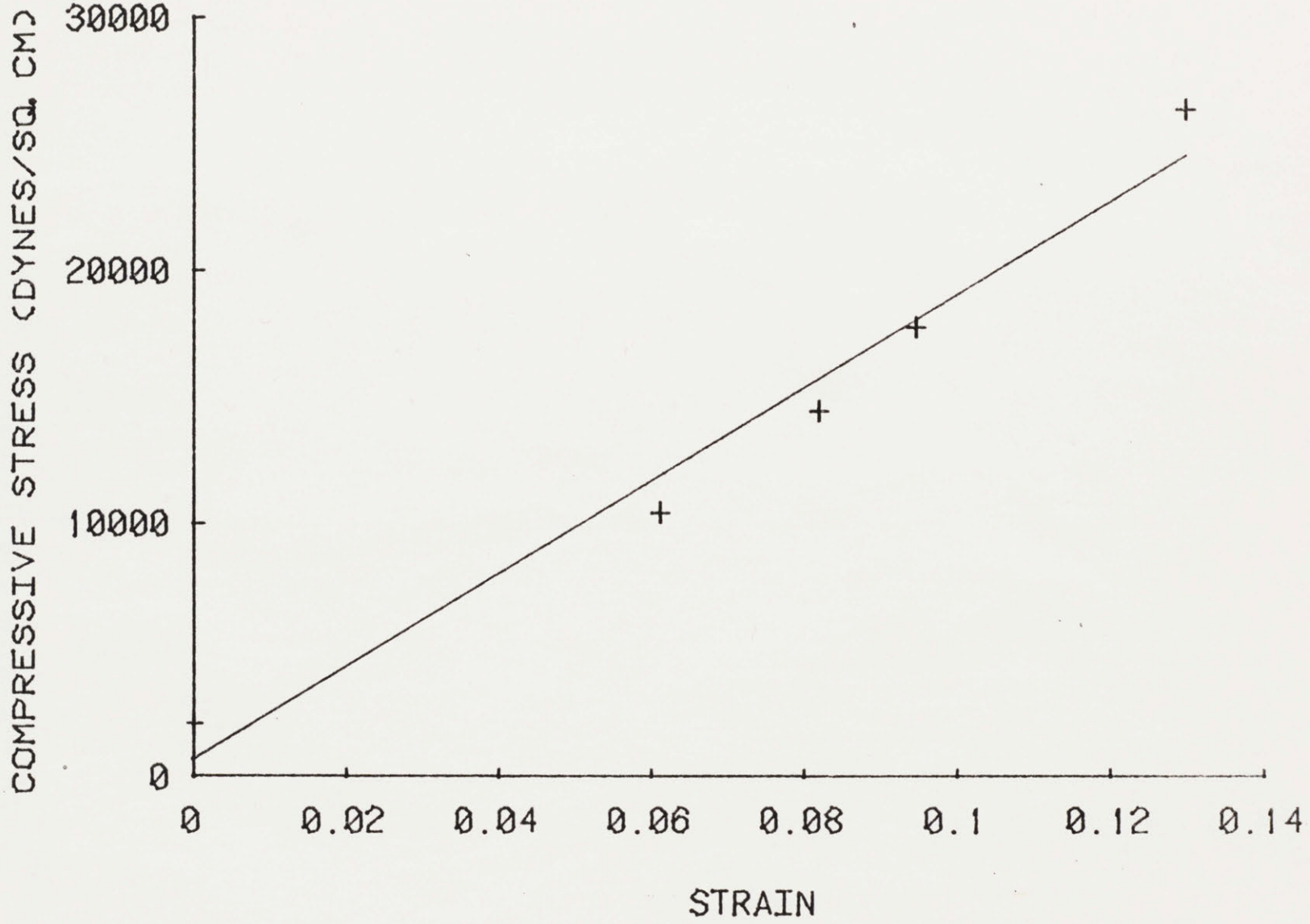
COMPRESSIVE STRESS (DYNES/SQ. CM)
30000
20000
10000
0
0
0.02
0.04
0.06
0.08
0.1
0.12
0.14
STRAIN

Figure 9

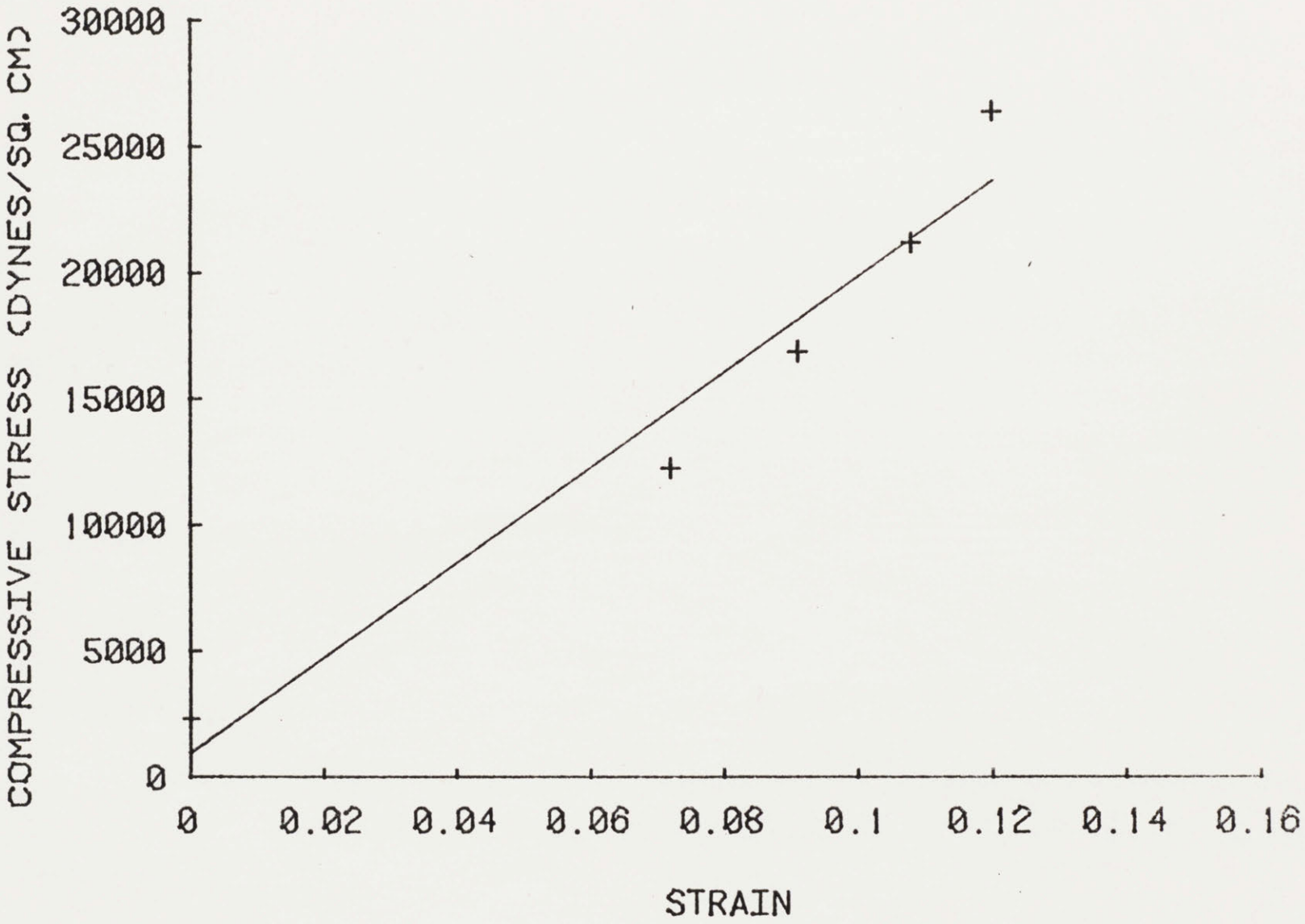
COMPRESSIVE STRESS (DYNES/SQ. CM)
30000
25000
20000
15000
10000
5000
0
0
0.02
0.04
0.06
0.08
0.1
0.12
0.14
0.16
STRAIN

Figure 10

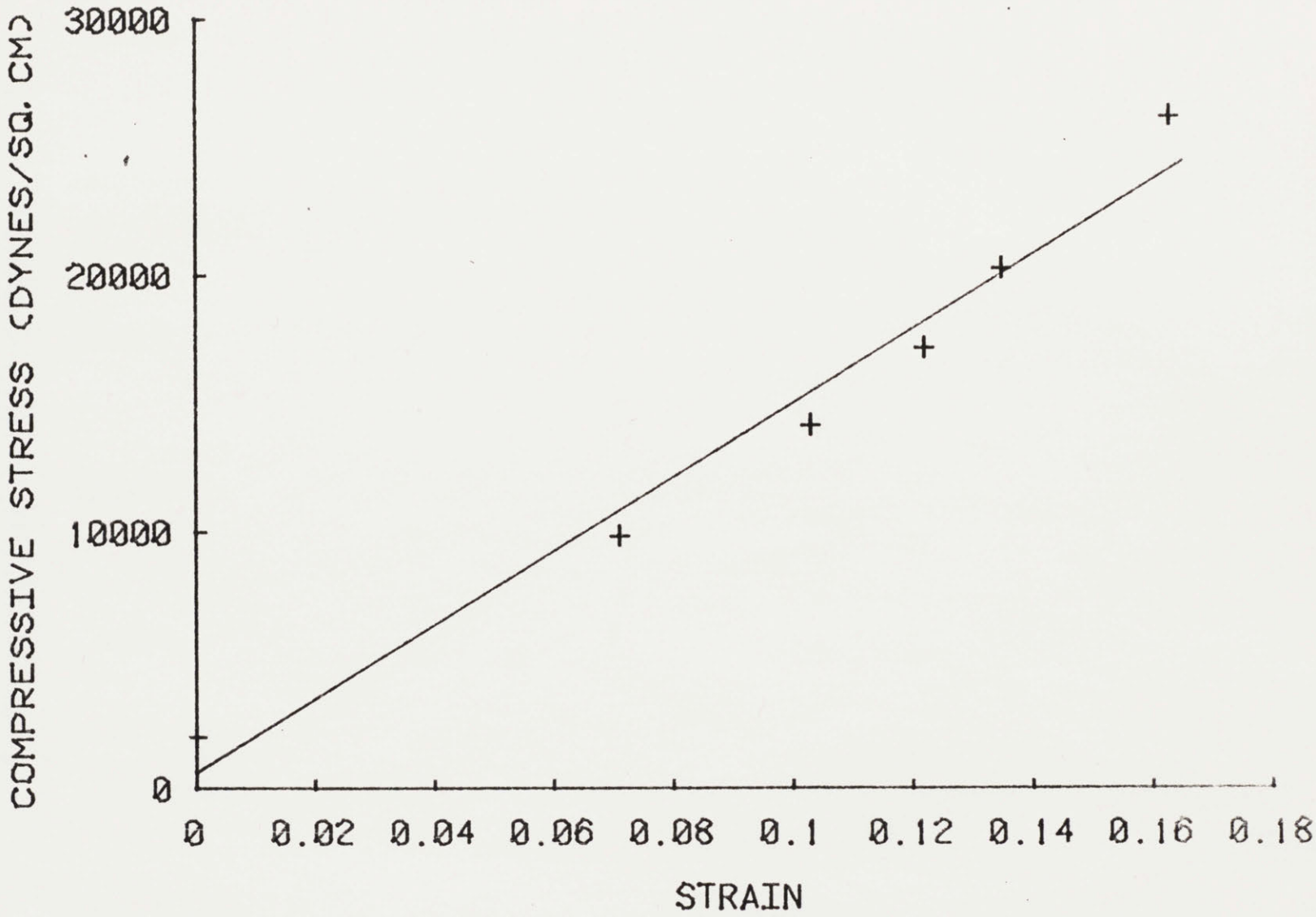
COMPRESSIVE STRESS (DYNES/SQ. CM)
30000
20000
10000
0
0
0.02
0.04
0.06
0.08
0.1
0.12
0.14
0.16
0.18
STRAIN

Figure 11

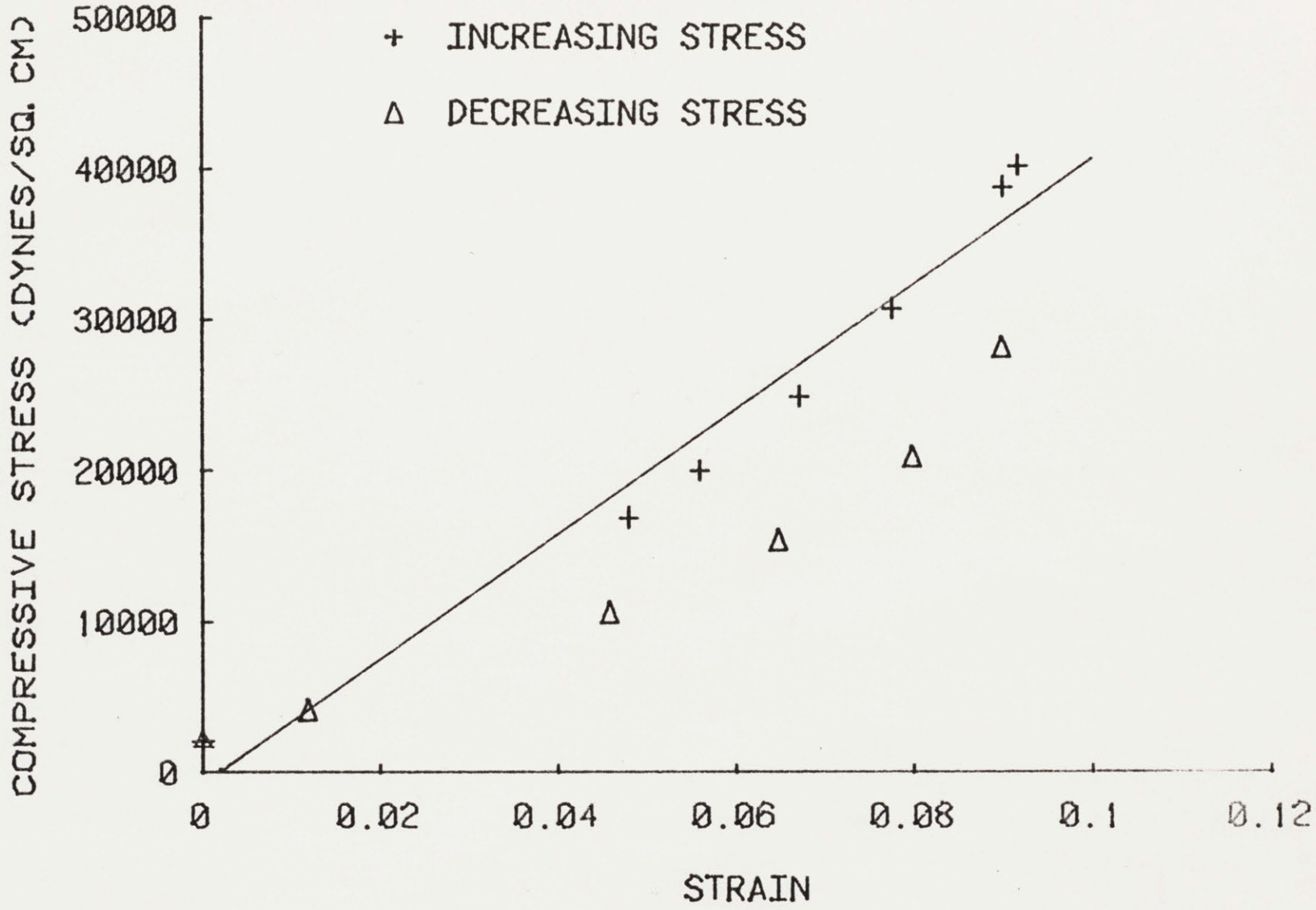
+ INCREASING STRESS
Δ DECREASING STRESS
COMPRESSIVE STRESS (DYNES/SQ. CM)
50000
40000
30000
20000
10000
0
0
0.02
0.04
0.06
0.08
0.1
0.12
STRAIN

Figure 12

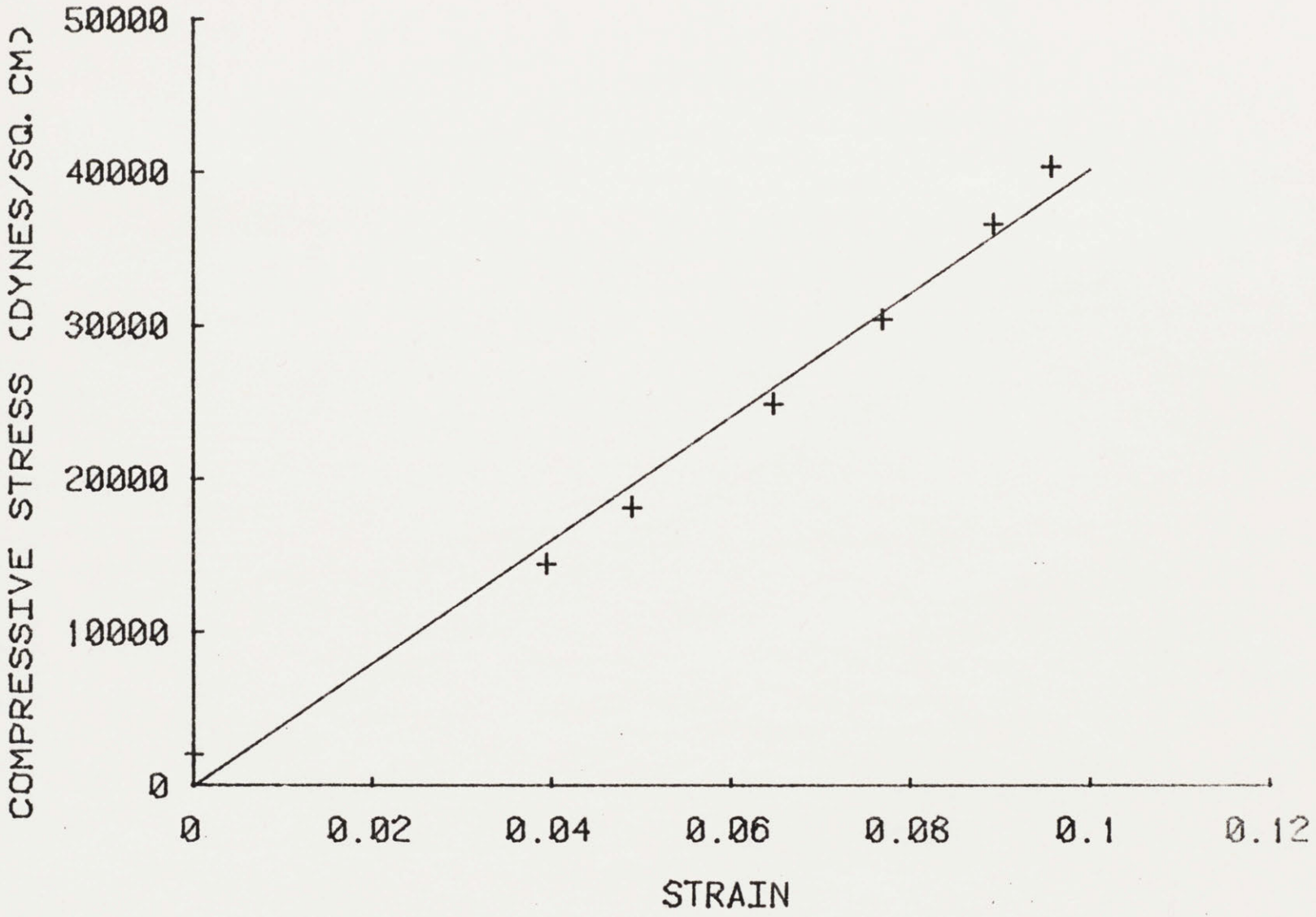
COMPRESSIVE STRESS (DYNES/SQ. CM)
50000
40000
30000
20000
10000
0
0
0.02
0.04
0.06
0.08
0.1
0.12
STRAIN

Figure 13

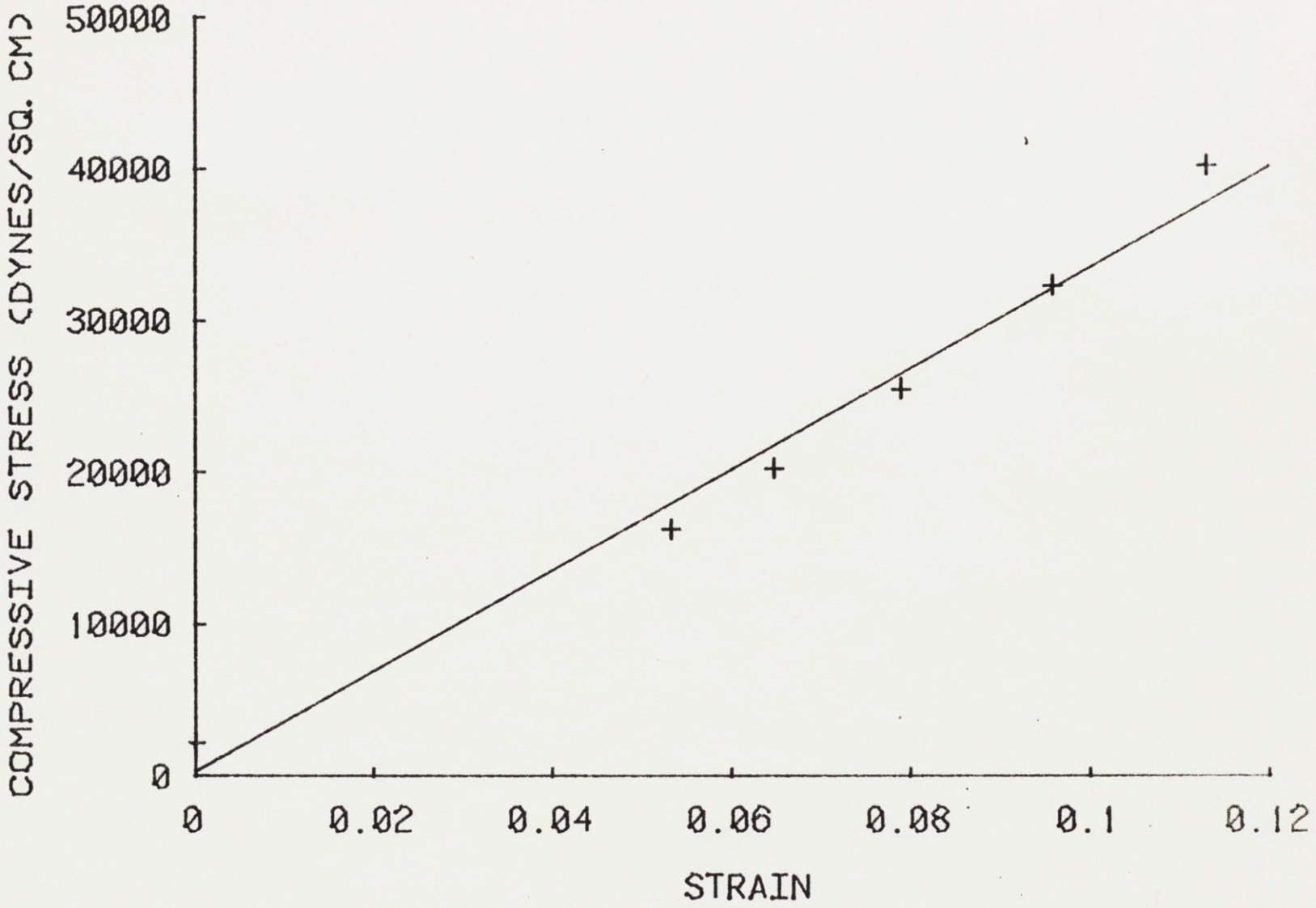
COMPRESSIVE STRESS (DYNES/SQ. CM)
50000
40000
30000
20000
10000
0
0
0.02
0.04
0.06
0.08
0.1
0.12
STRAIN

Figure 14

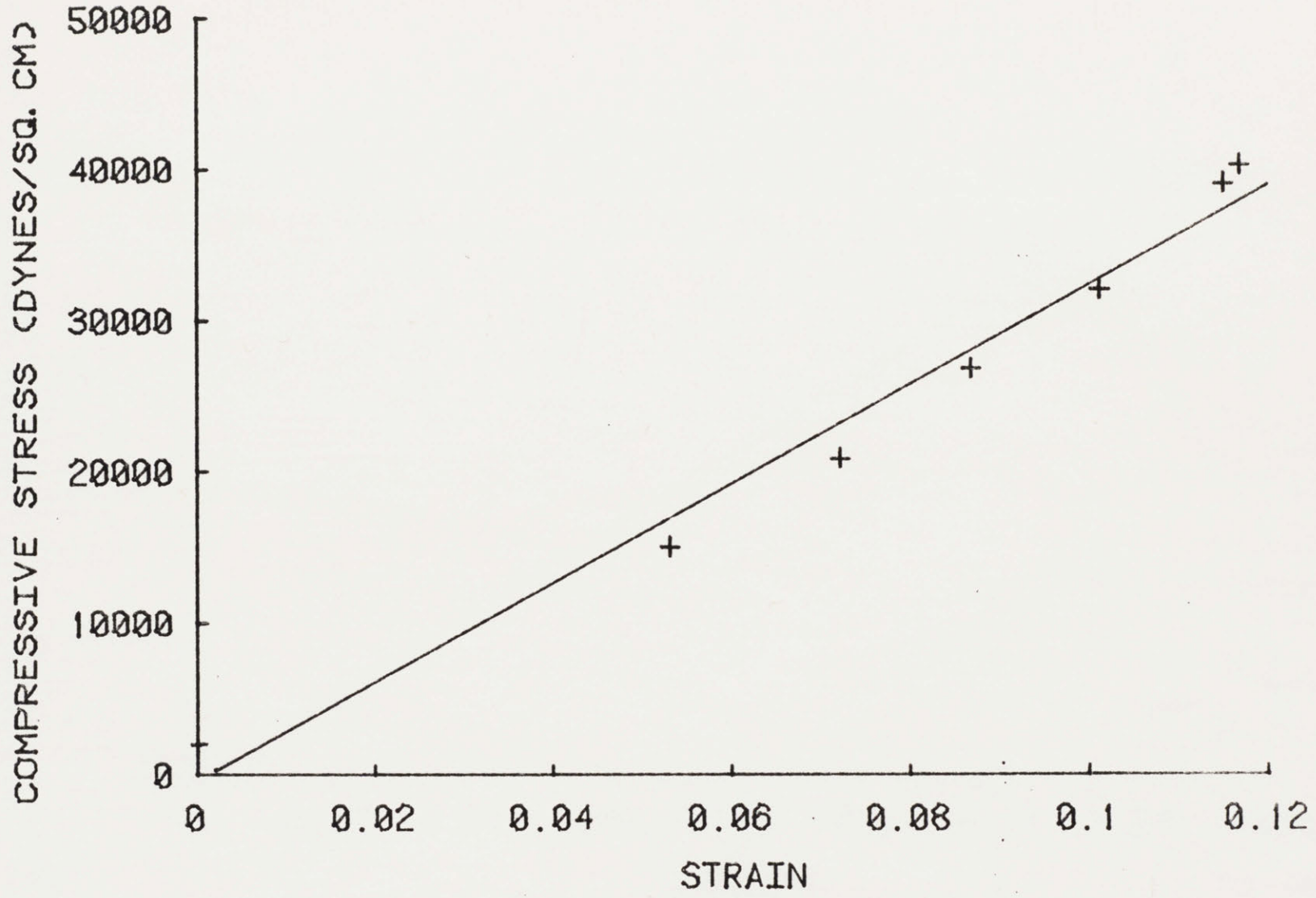
COMPRESSIVE STRESS (DYNES/SQ. CM)
50000
40000
30000
20000
10000
0
0
0.02
0.04
0.06
0.08
0.1
0.12
STRAIN

Figure 15

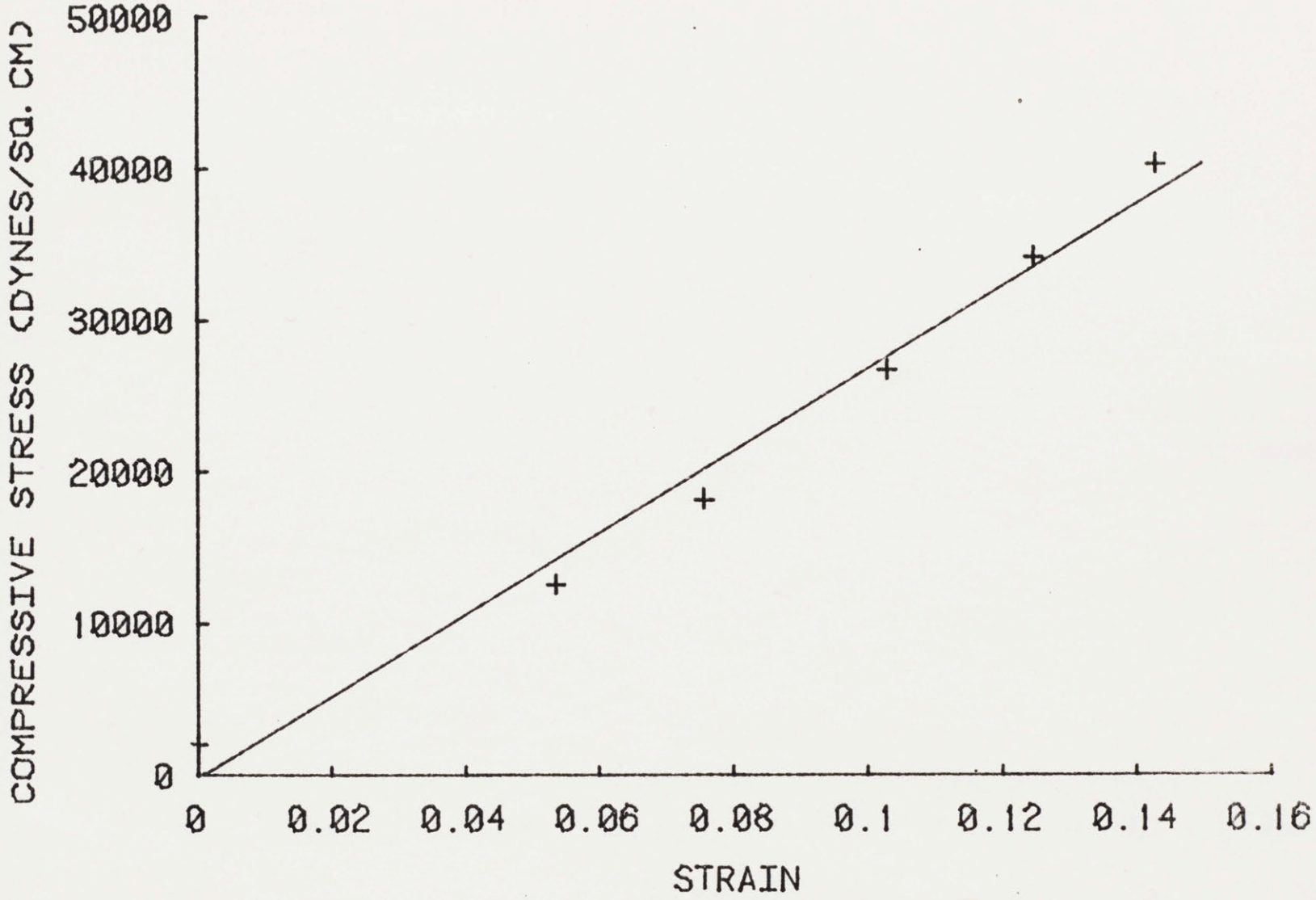
COMPRESSIVE STRESS (DYNES/SQ. CM)
50000
40000
30000
20000
10000
0
0
0.02
0.04
0.06
0.08
0.1
0.12
0.14
0.16
STRAIN

Figure 16

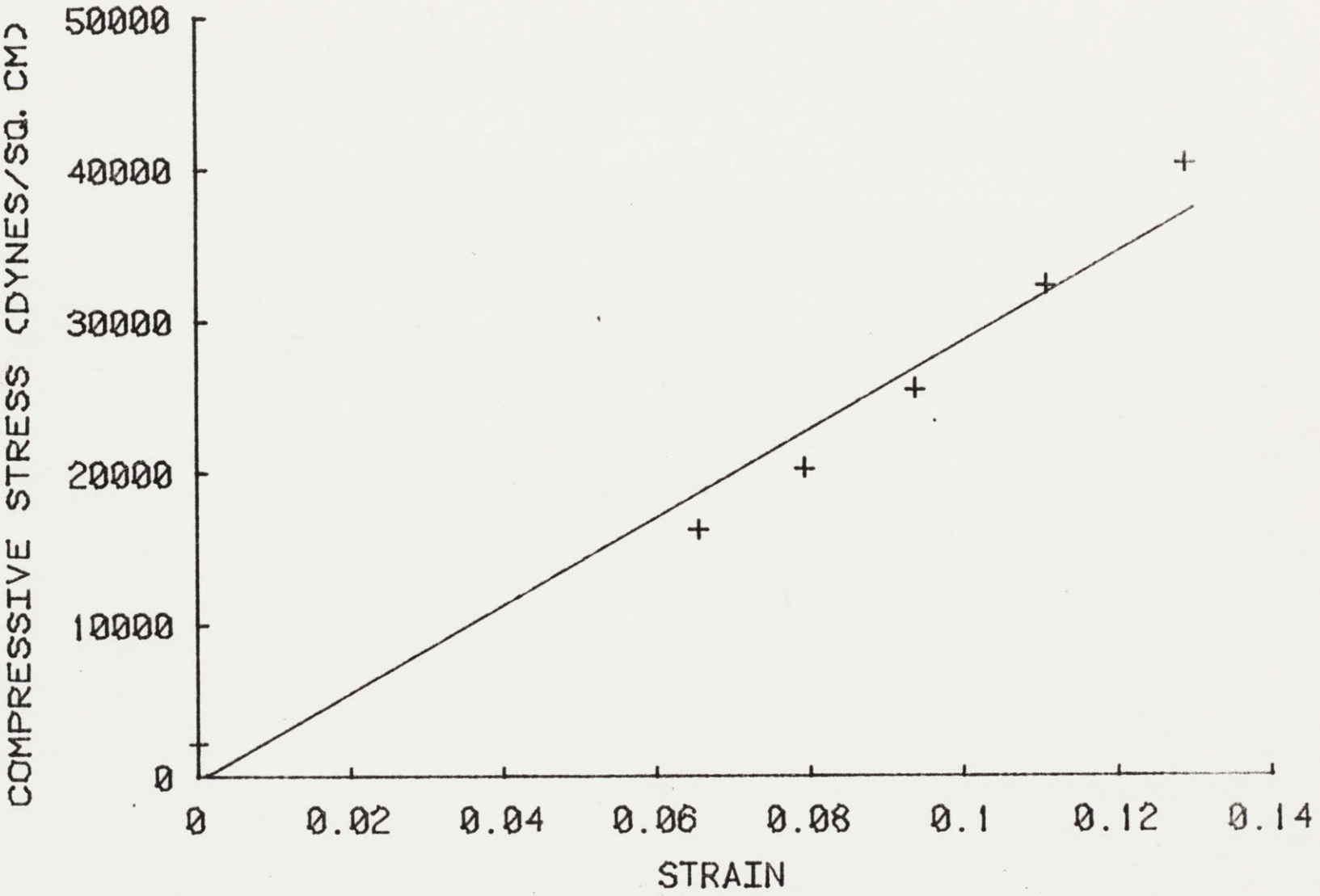
COMPRESSIVE STRESS (DYNES/SQ. CM)
50000
40000
30000
20000
10000
0
0
0.02
0.04
0.06
0.08
0.1
0.12
0.14
STRAIN

Figure 17

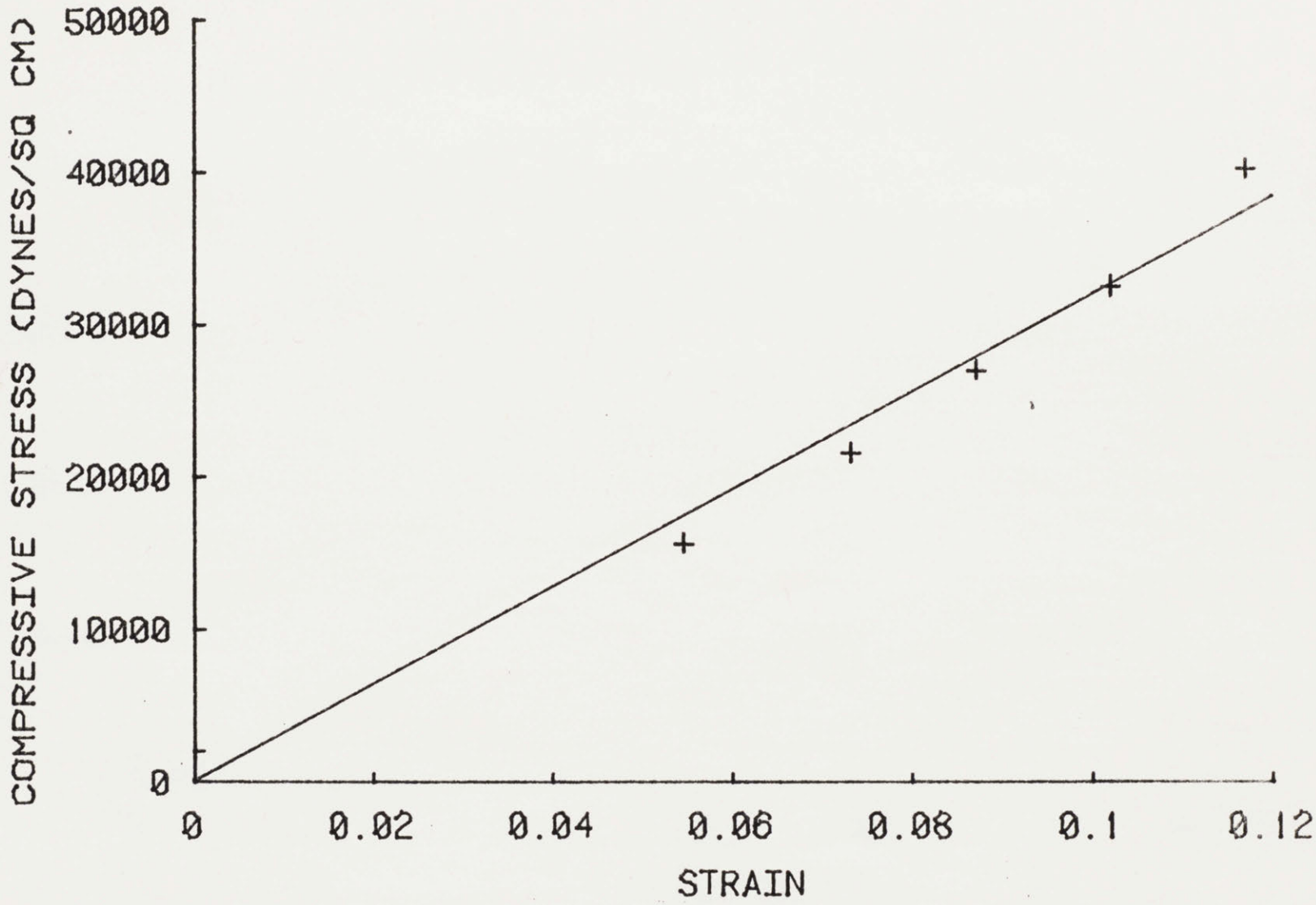
COMPRESSIVE STRESS (DYNES/SQ CM)
50000
40000
30000
20000
10000
0
0
0.02
0.04
0.06
0.08
0.1
0.12
STRAIN

Figure 18

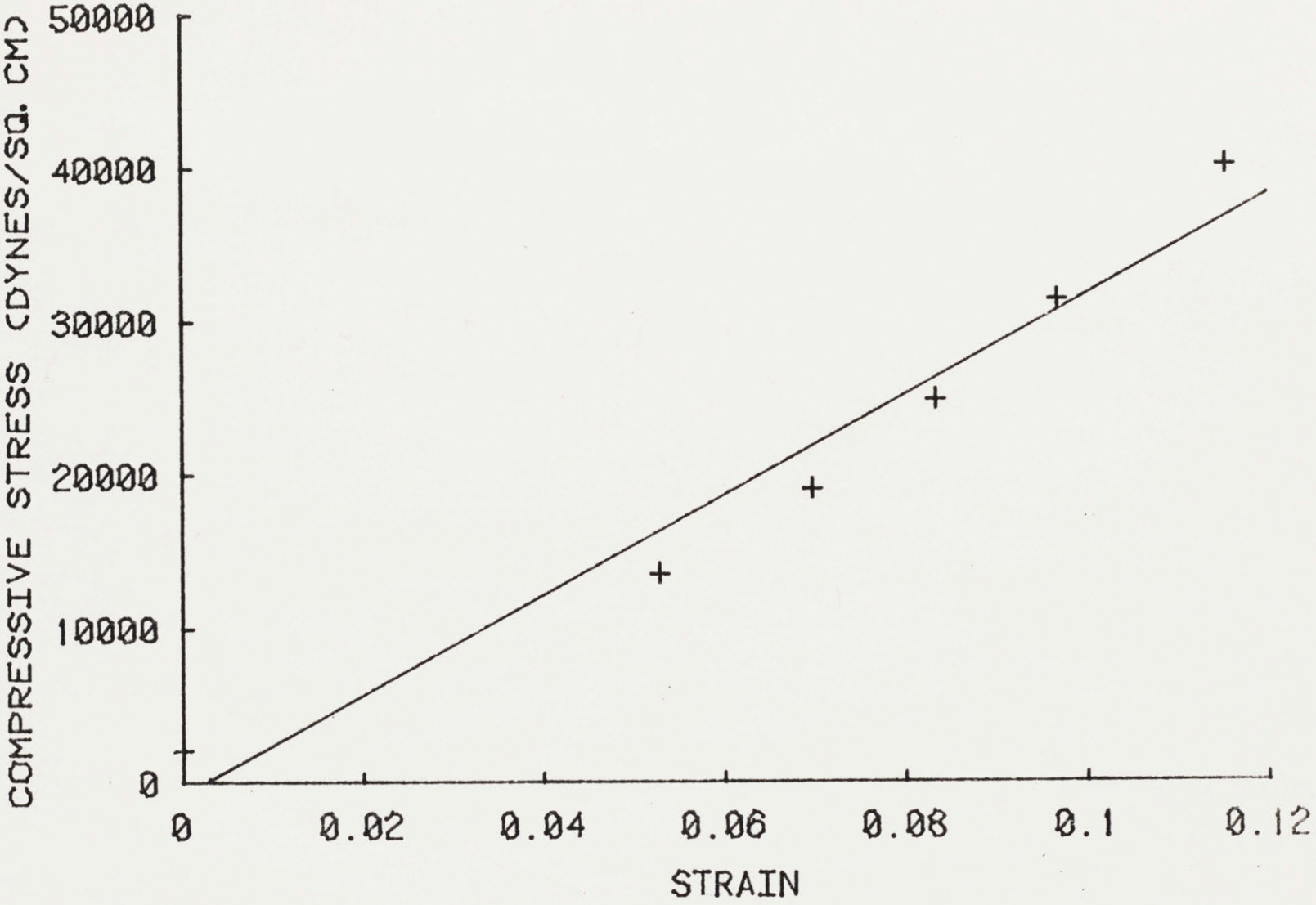
COMPRESSIVE STRESS (DYNES/SQ. CM)
50000
40000
30000
20000
10000
0
0
0.02
0.04
0.06
0.08
0.1
0.12
STRAIN

Figure 19

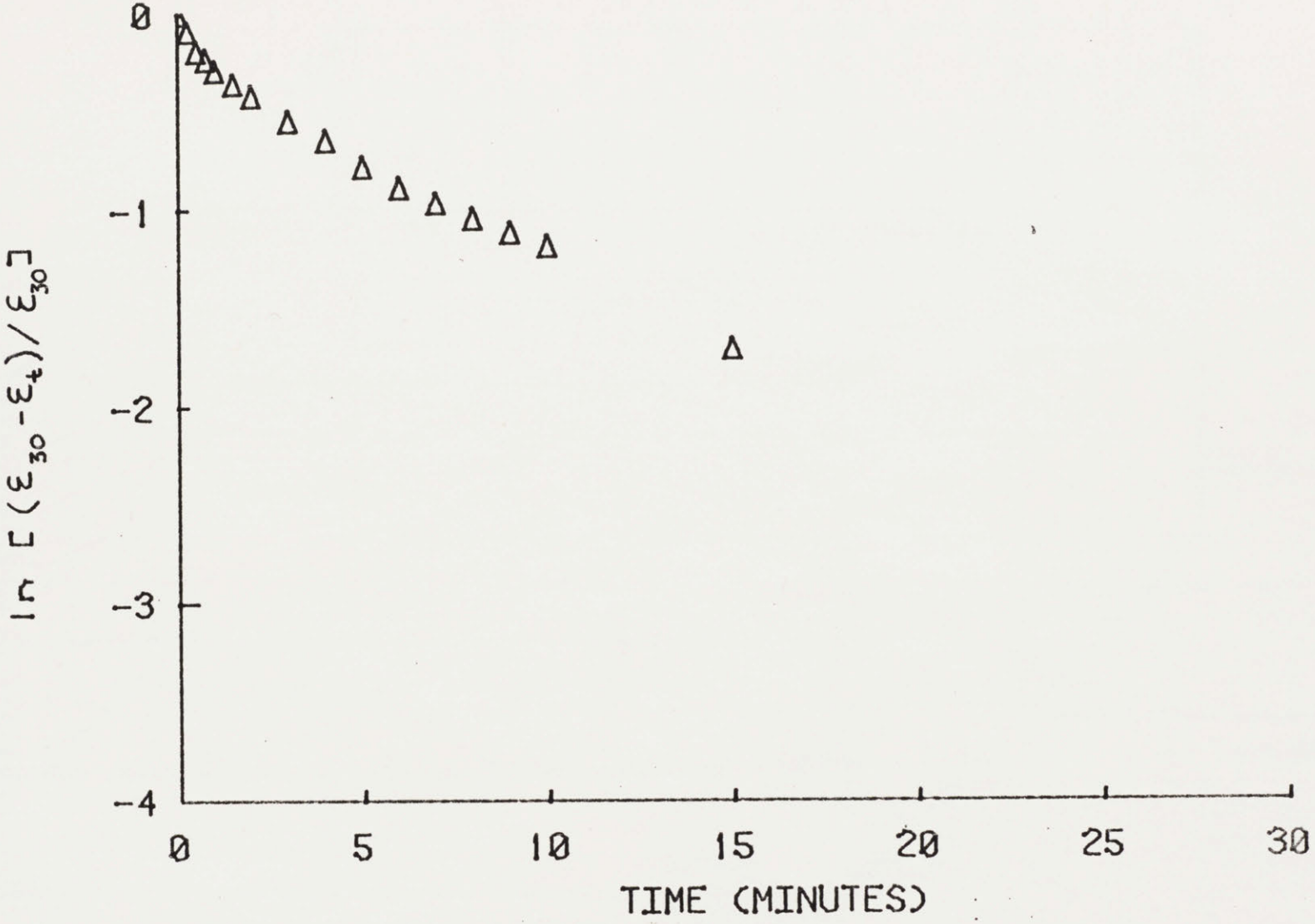

Figure 20

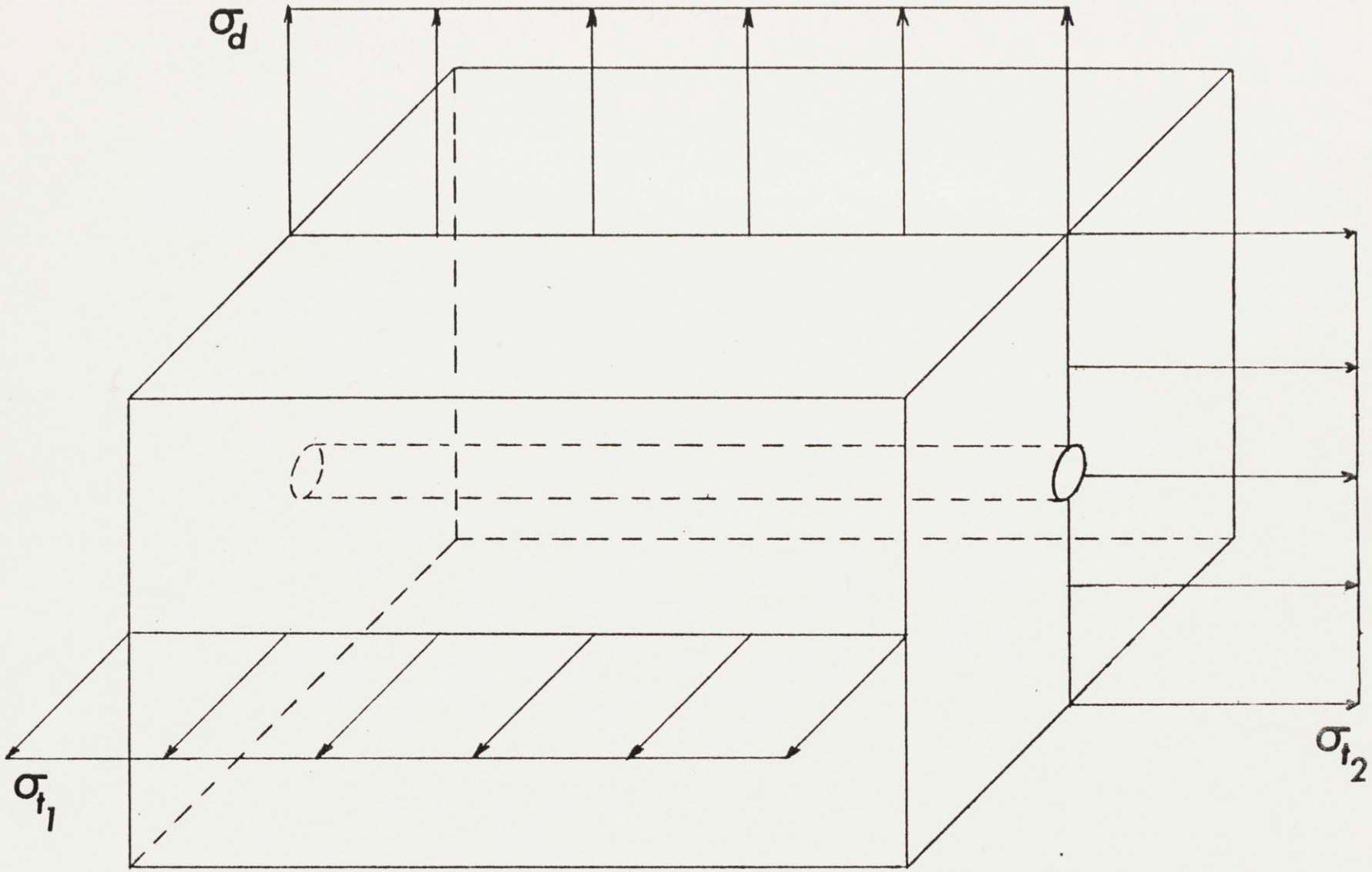

Figure 21

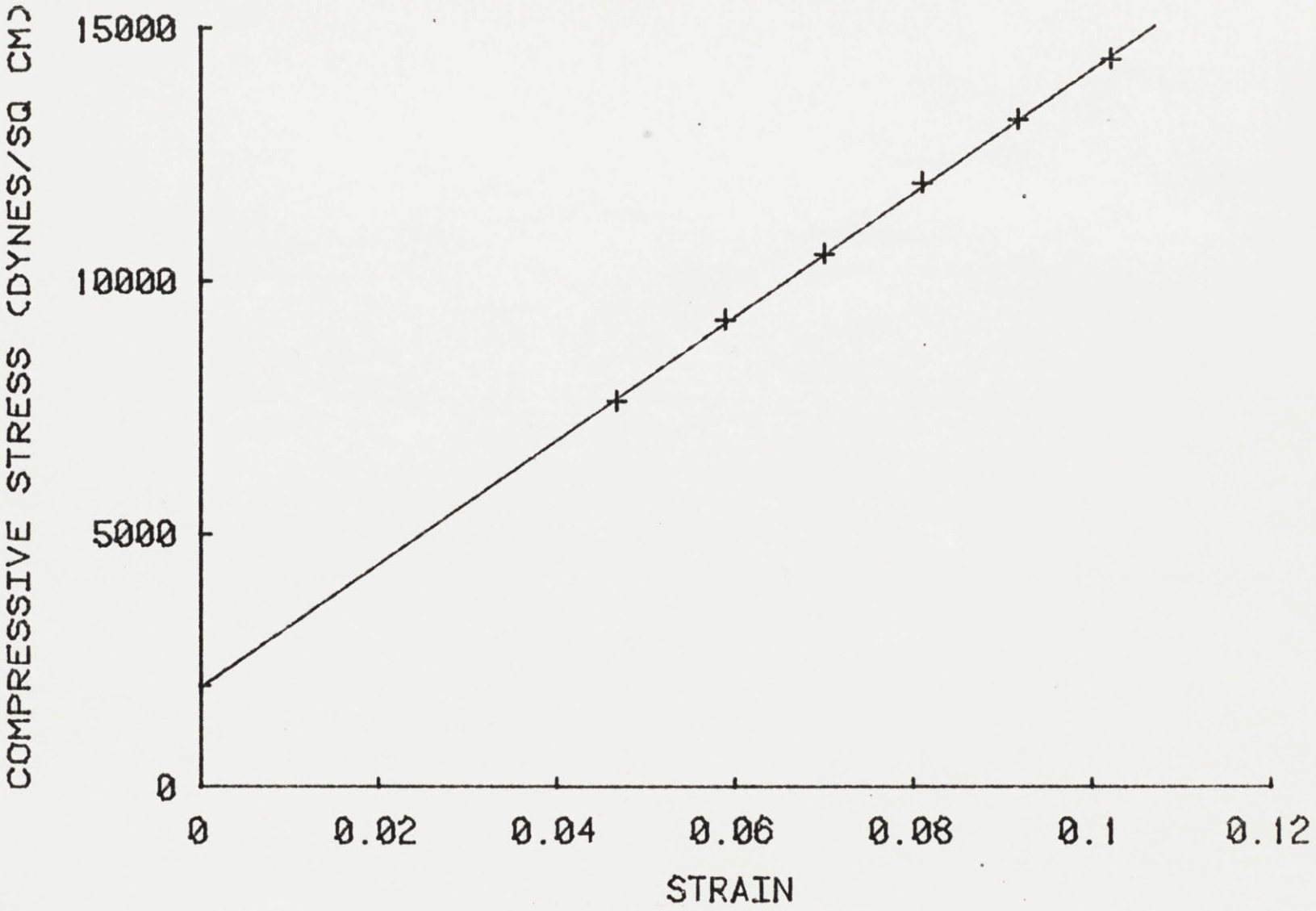
COMPRESSIVE STRESS (DYNES/SQ CM)
15000
10000
5000
0
0
0.02
0.04
0.06
0.08
0.1
0.12
STRAIN

Figure 22

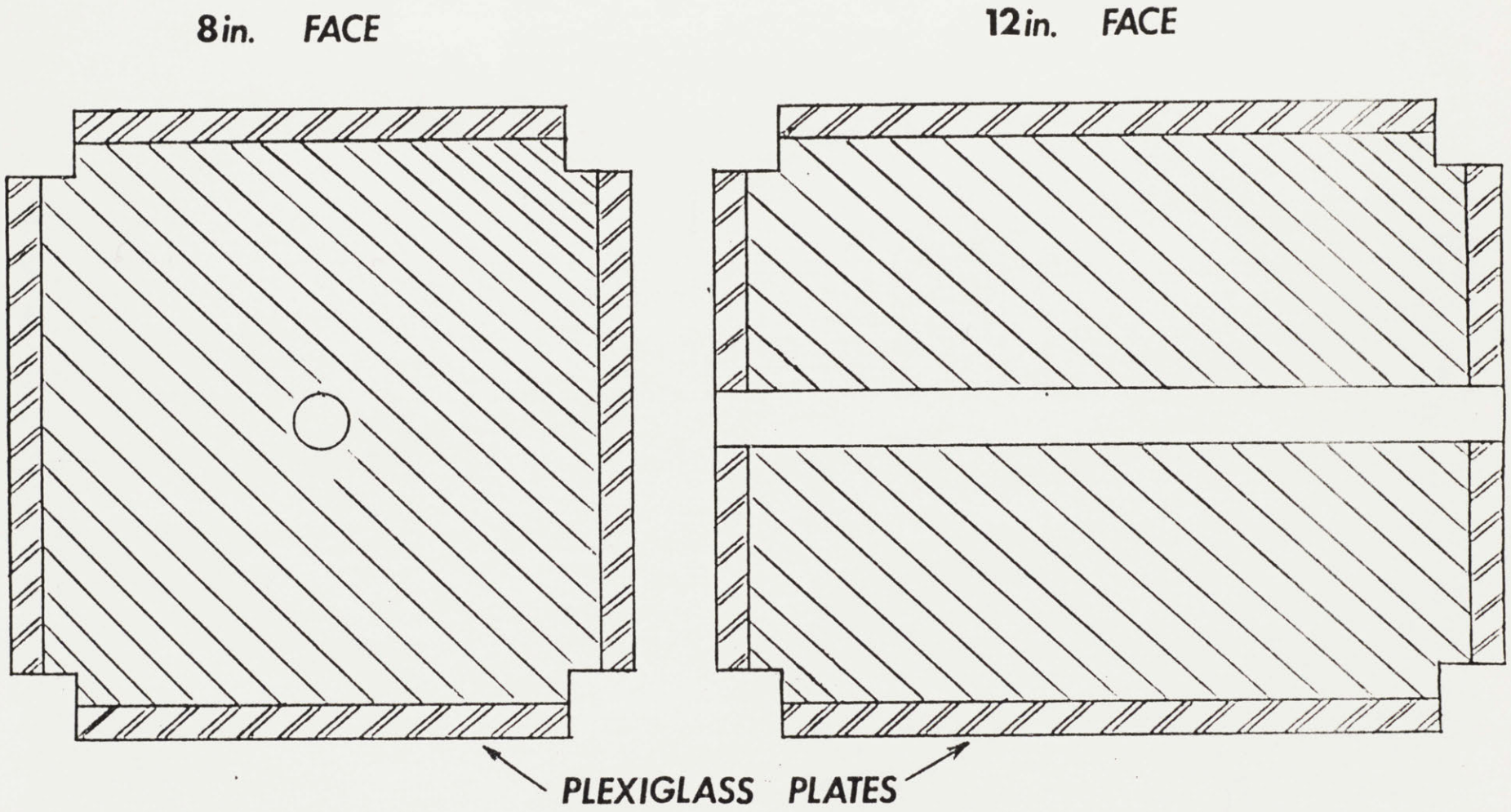

Figure 23

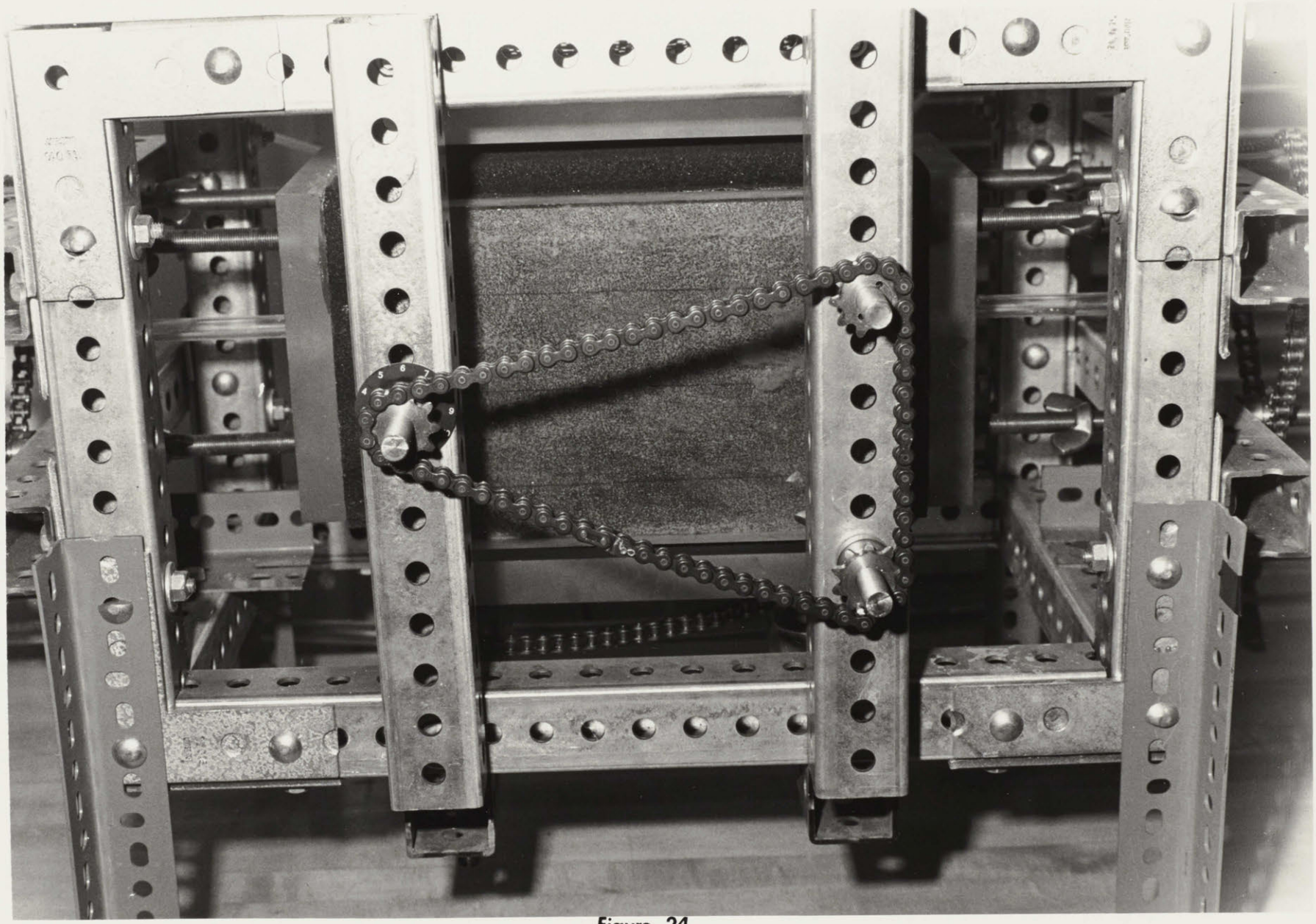

Figure 24

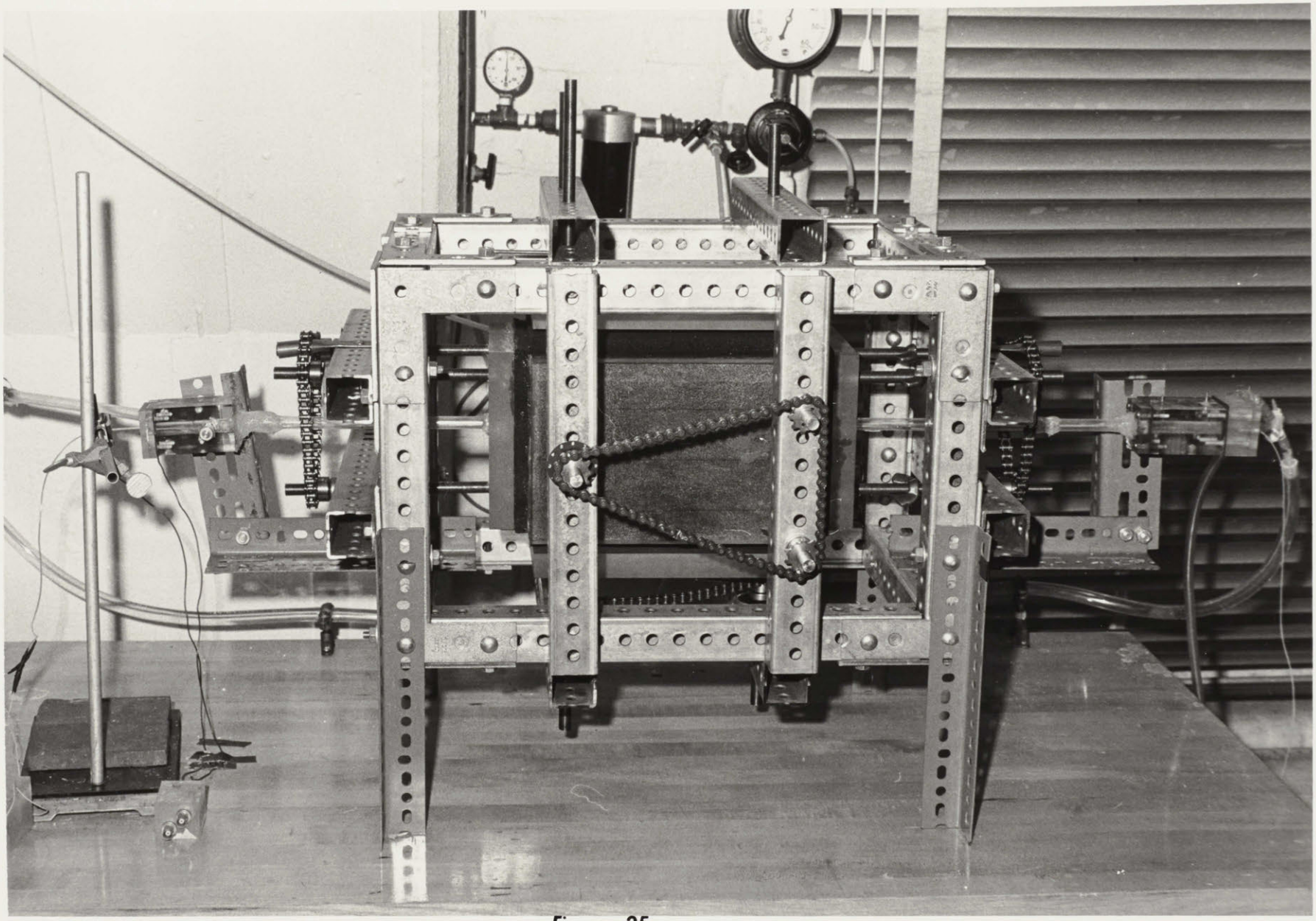

Figure 25

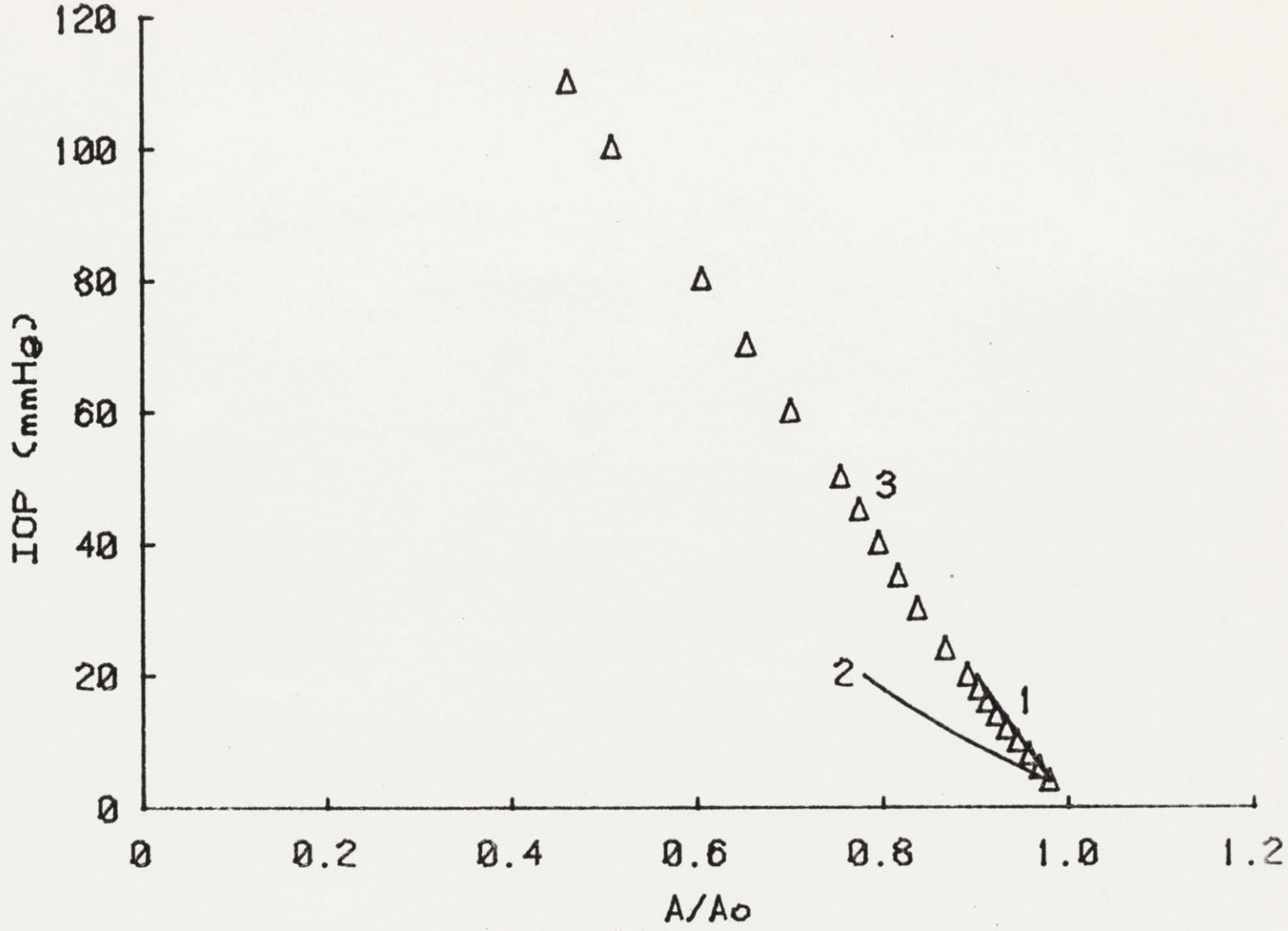

Figure 26

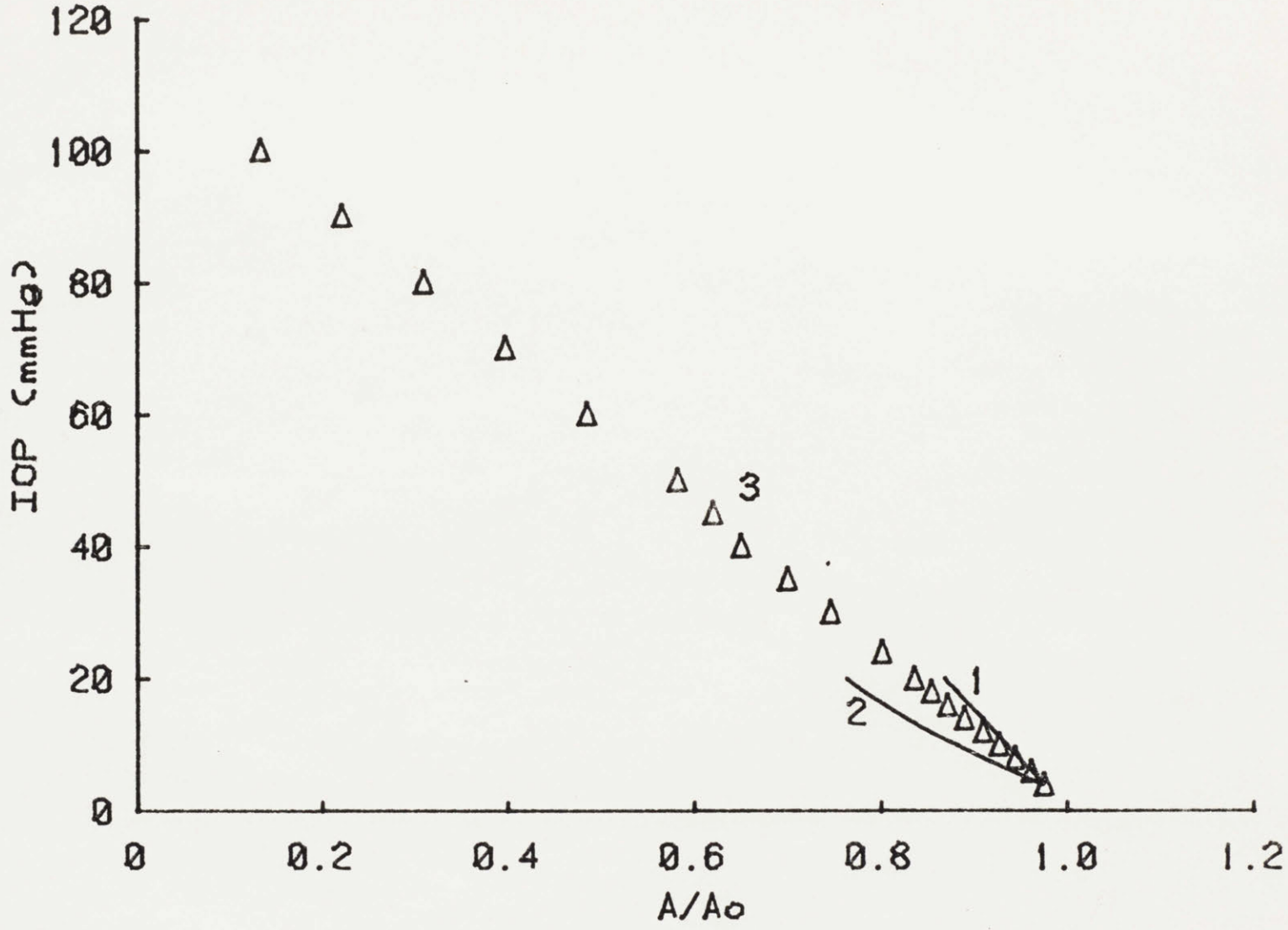

Figure 27

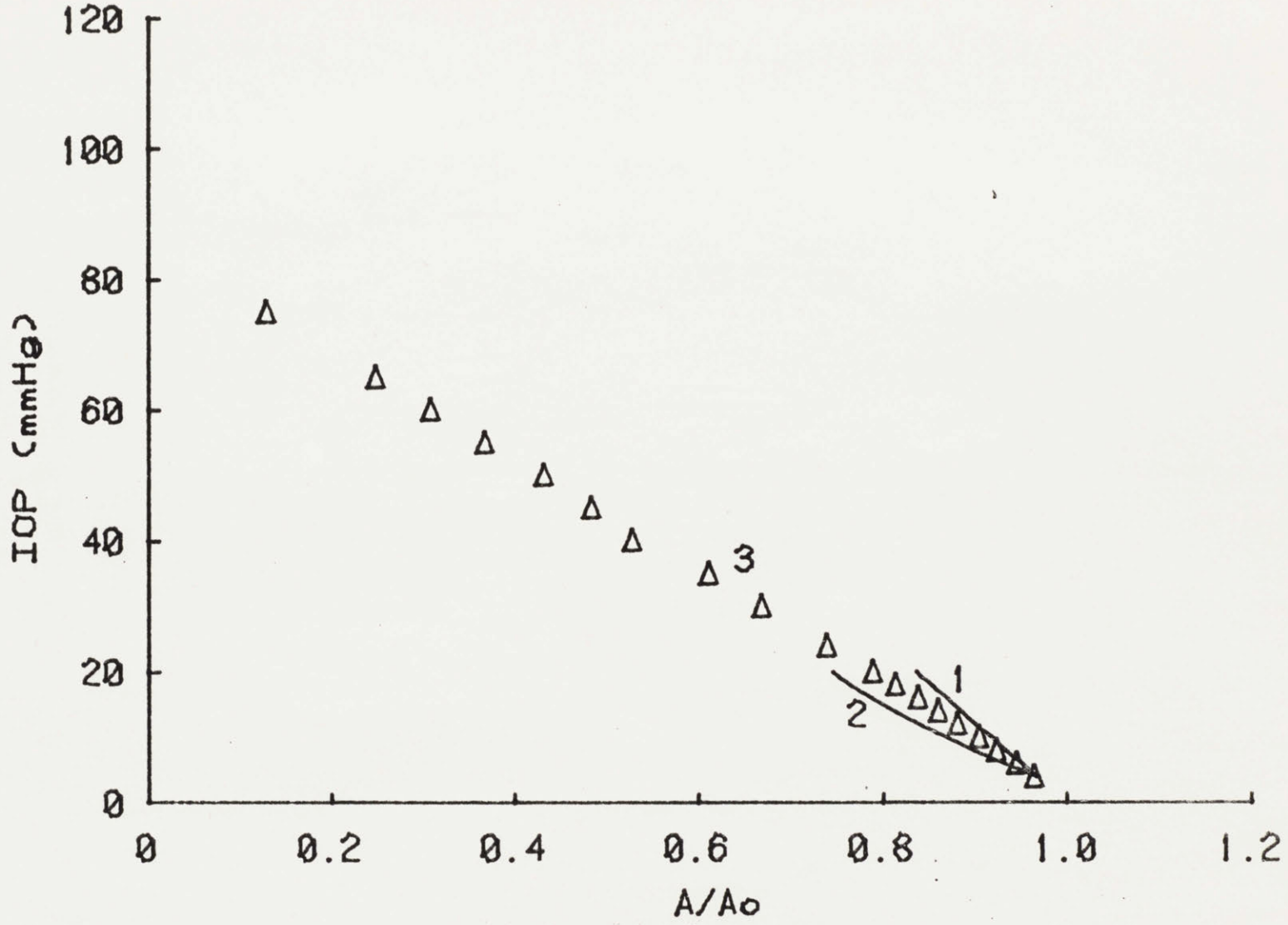

Figure 28

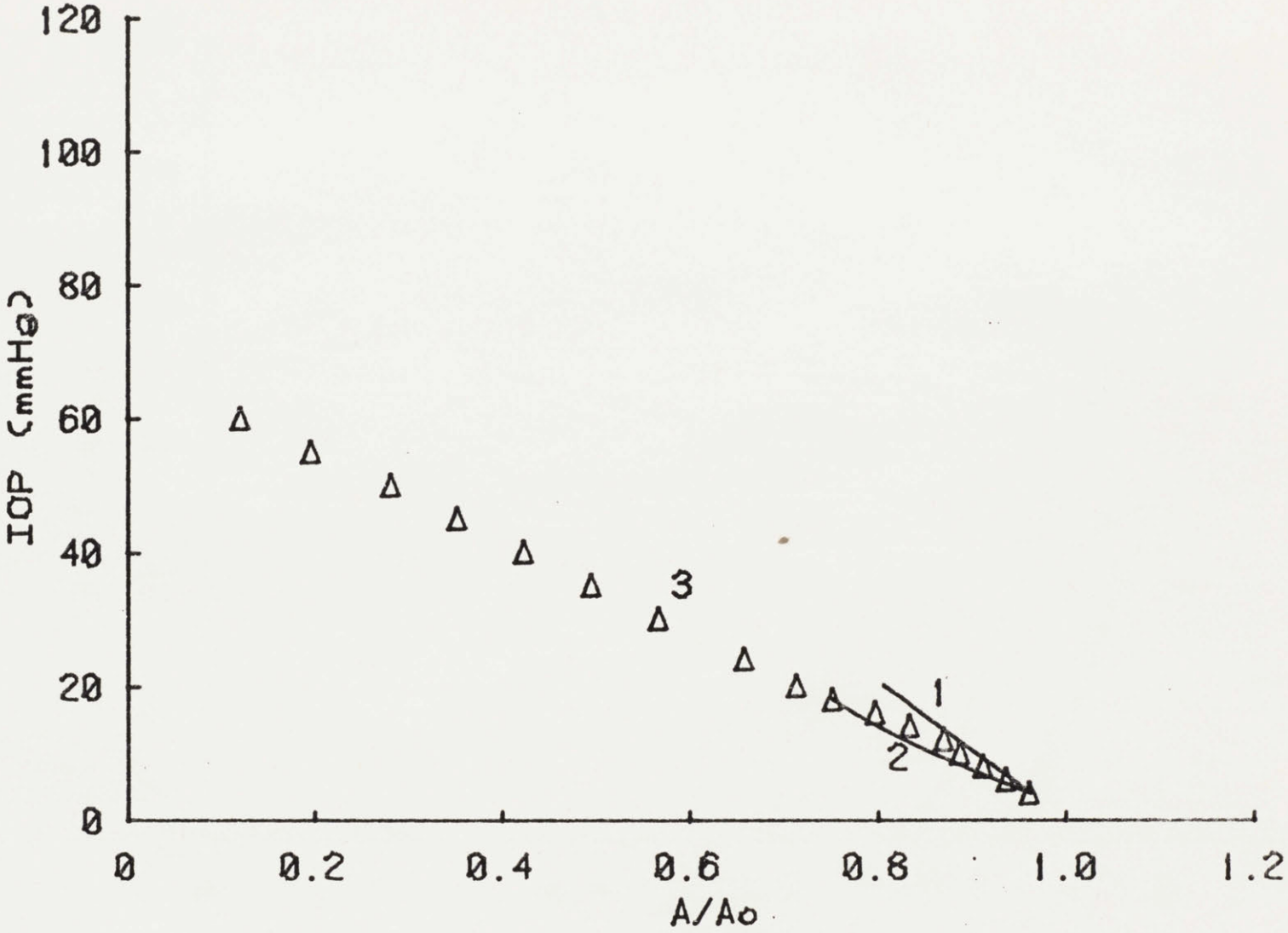

Figure 29

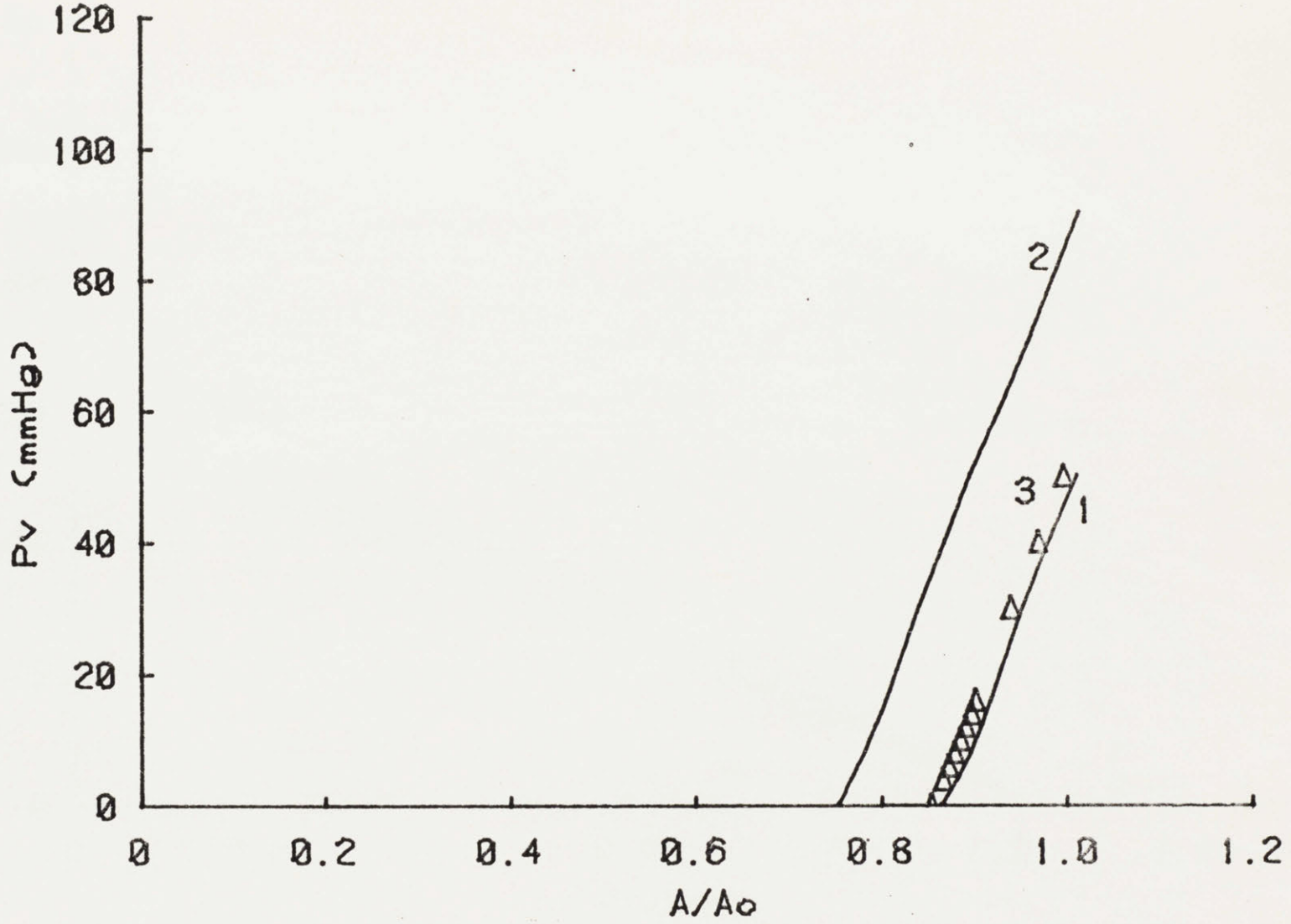

Figure 30

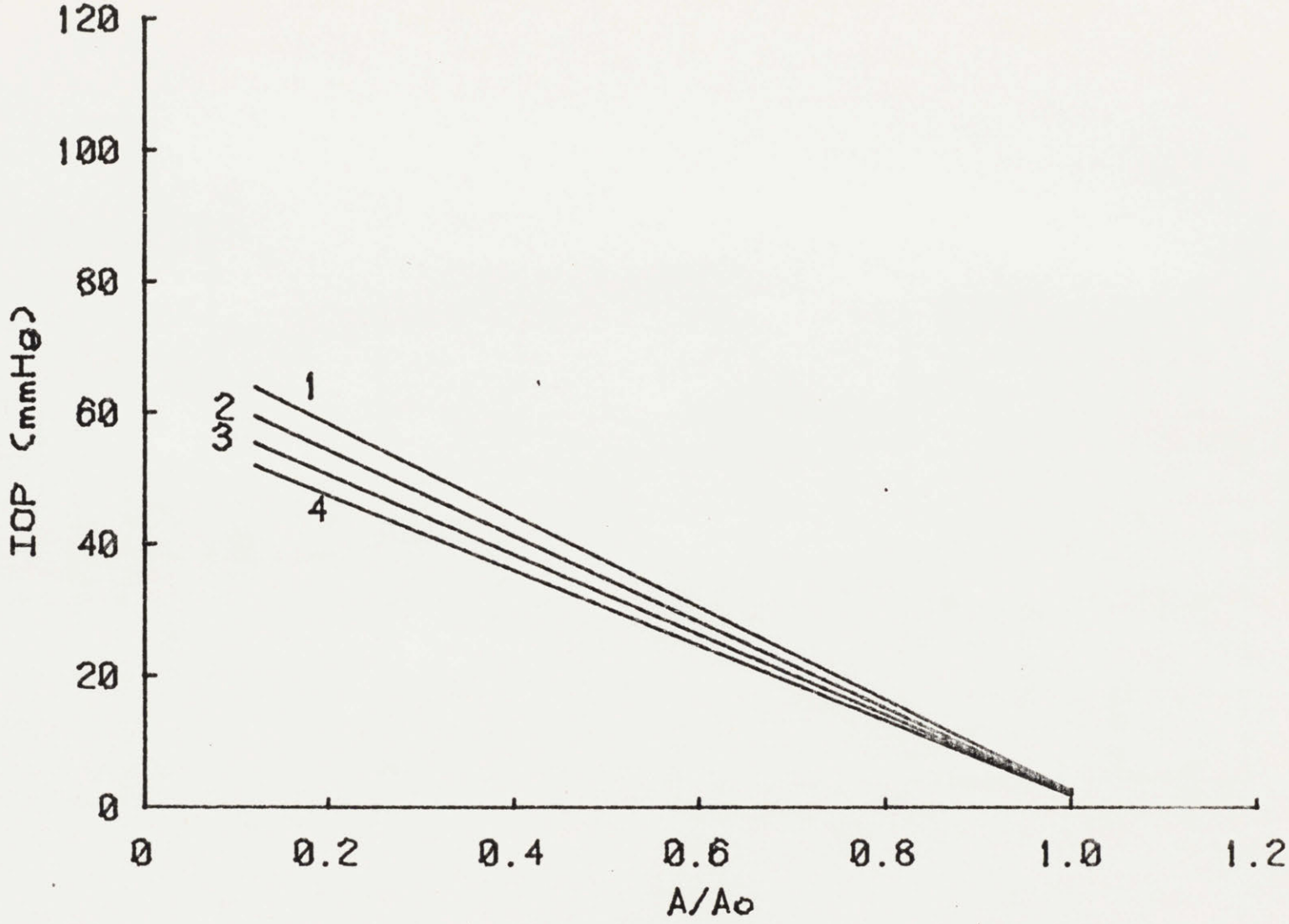

Figure 31

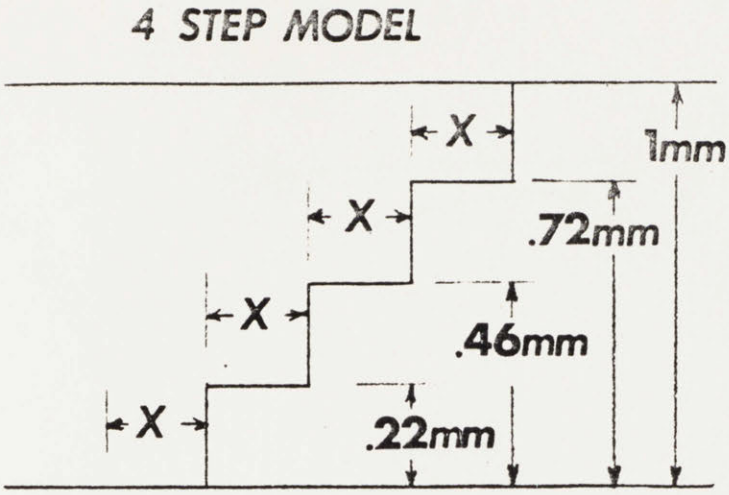

Figure 32a

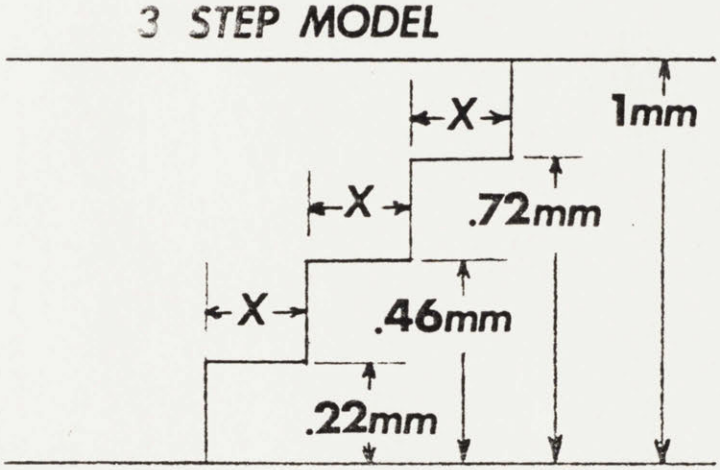

Figure 32b

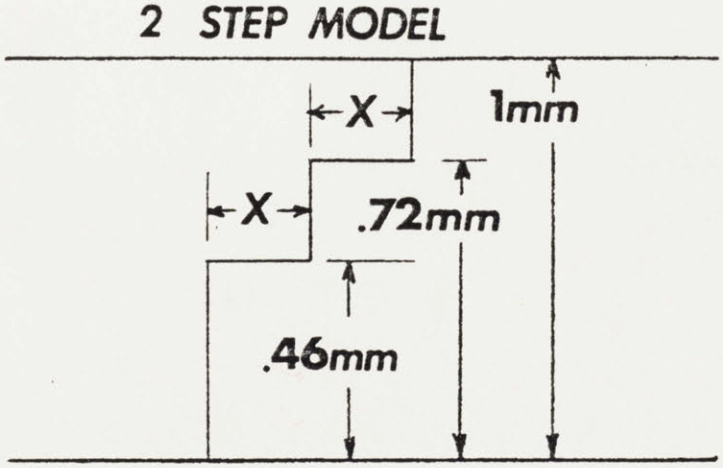

Figure 32c

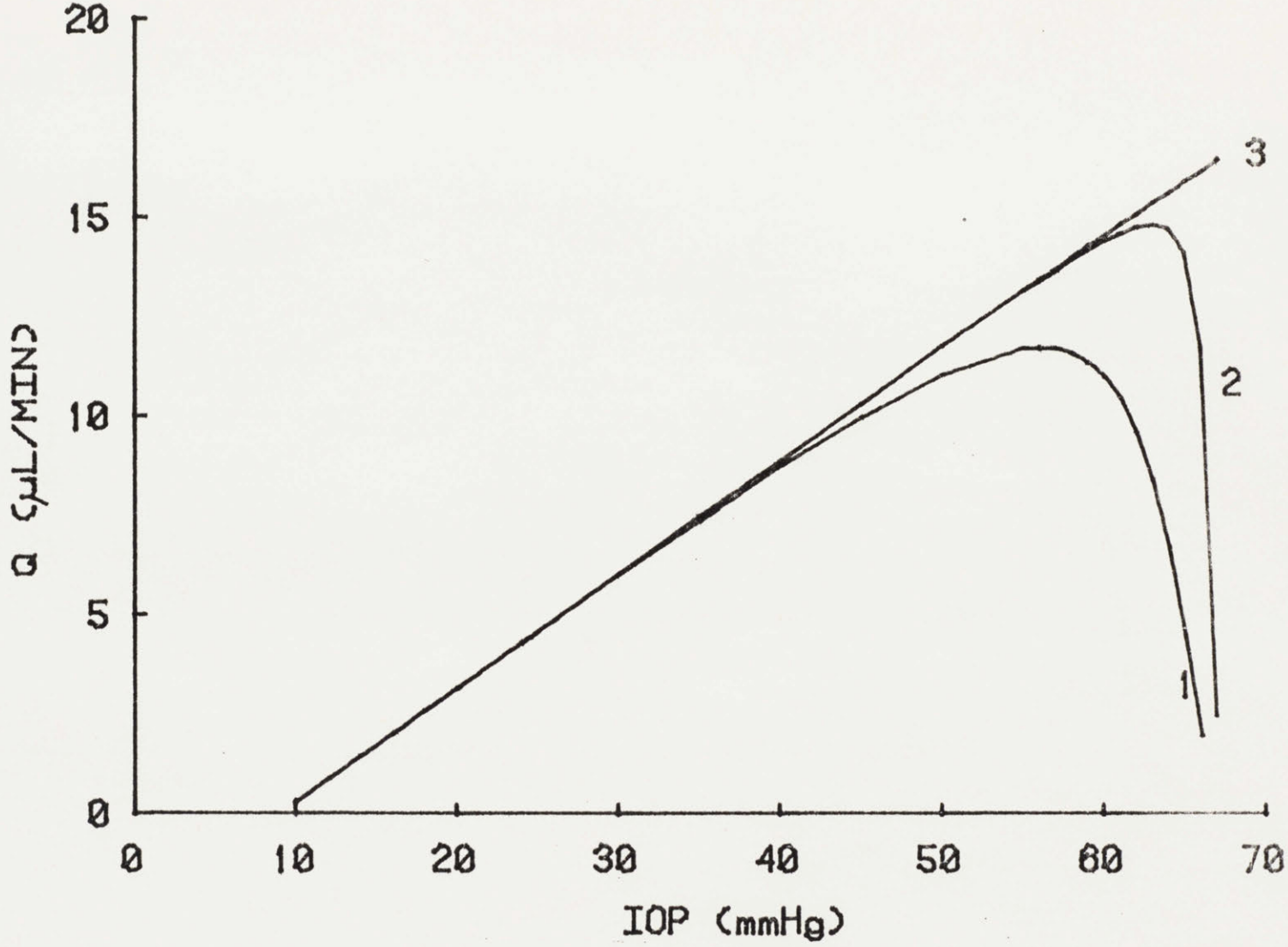

Figure 33

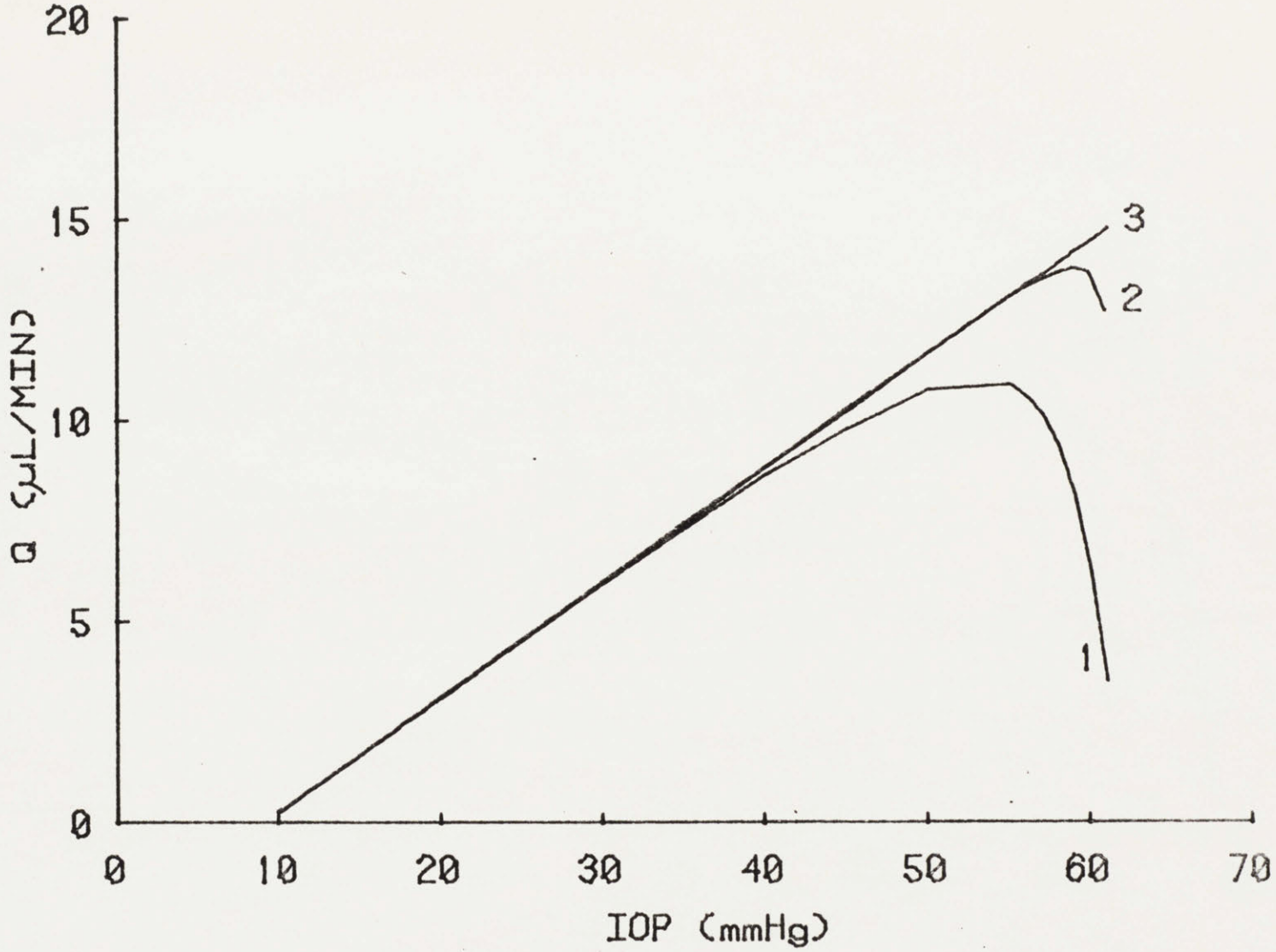

Figure 34

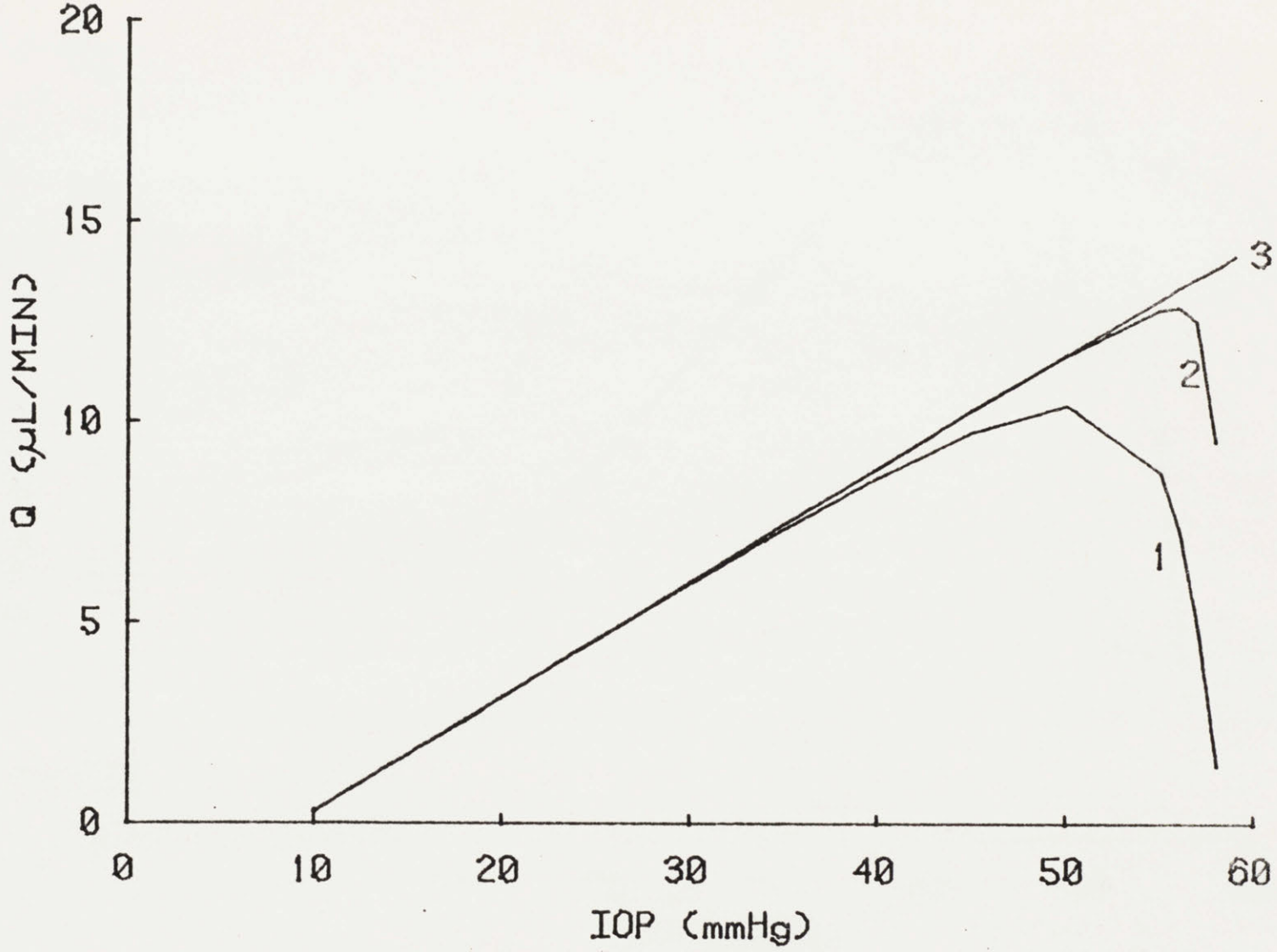

Figure 35

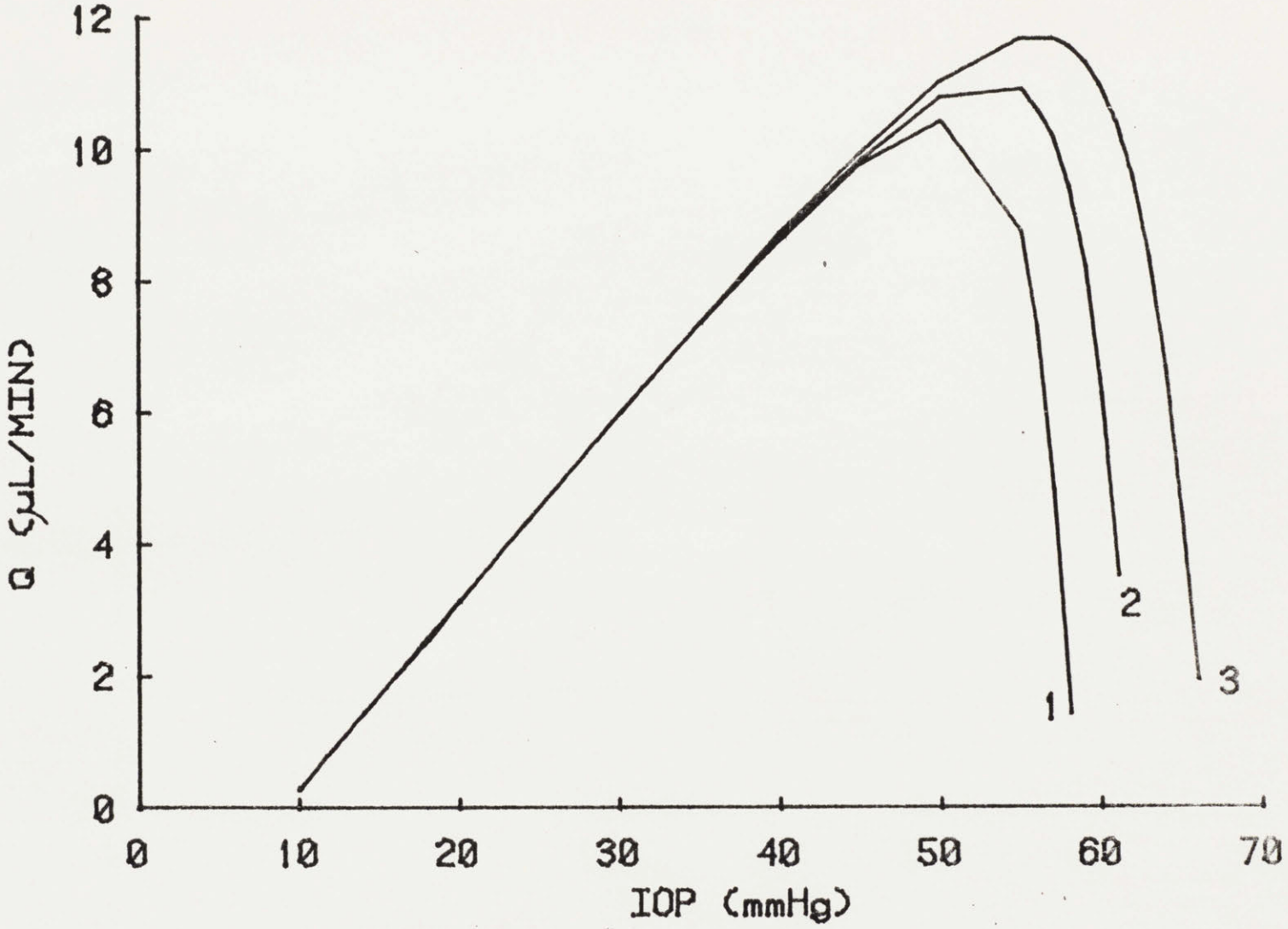

Figure 36

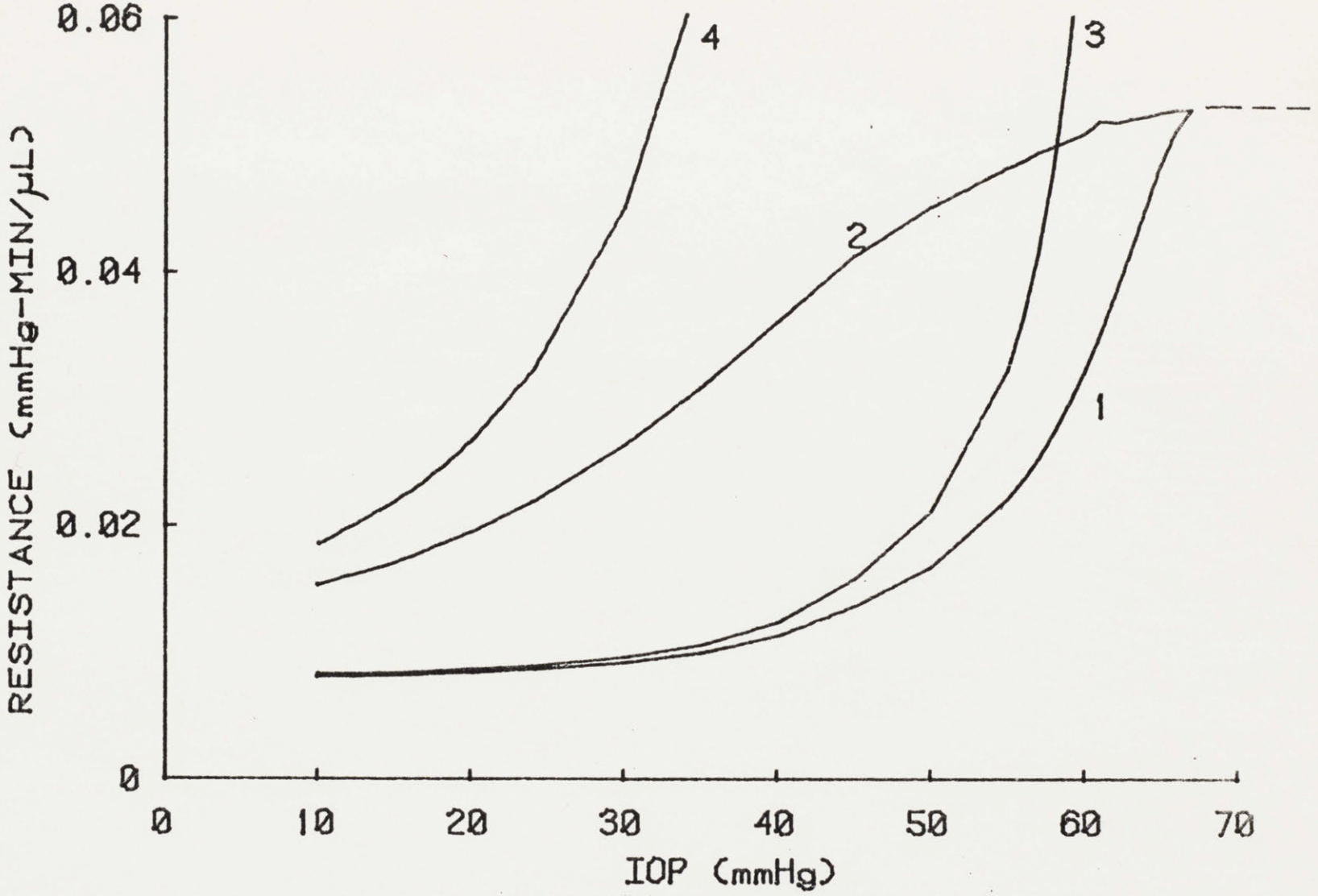
0.06
0.04
0.02
0
RESISTANCE (mmHg-MIN/μL)
4
3
2
1
0
10
20
30
40
50
60
70
IOP (mmHg)

Figure 37

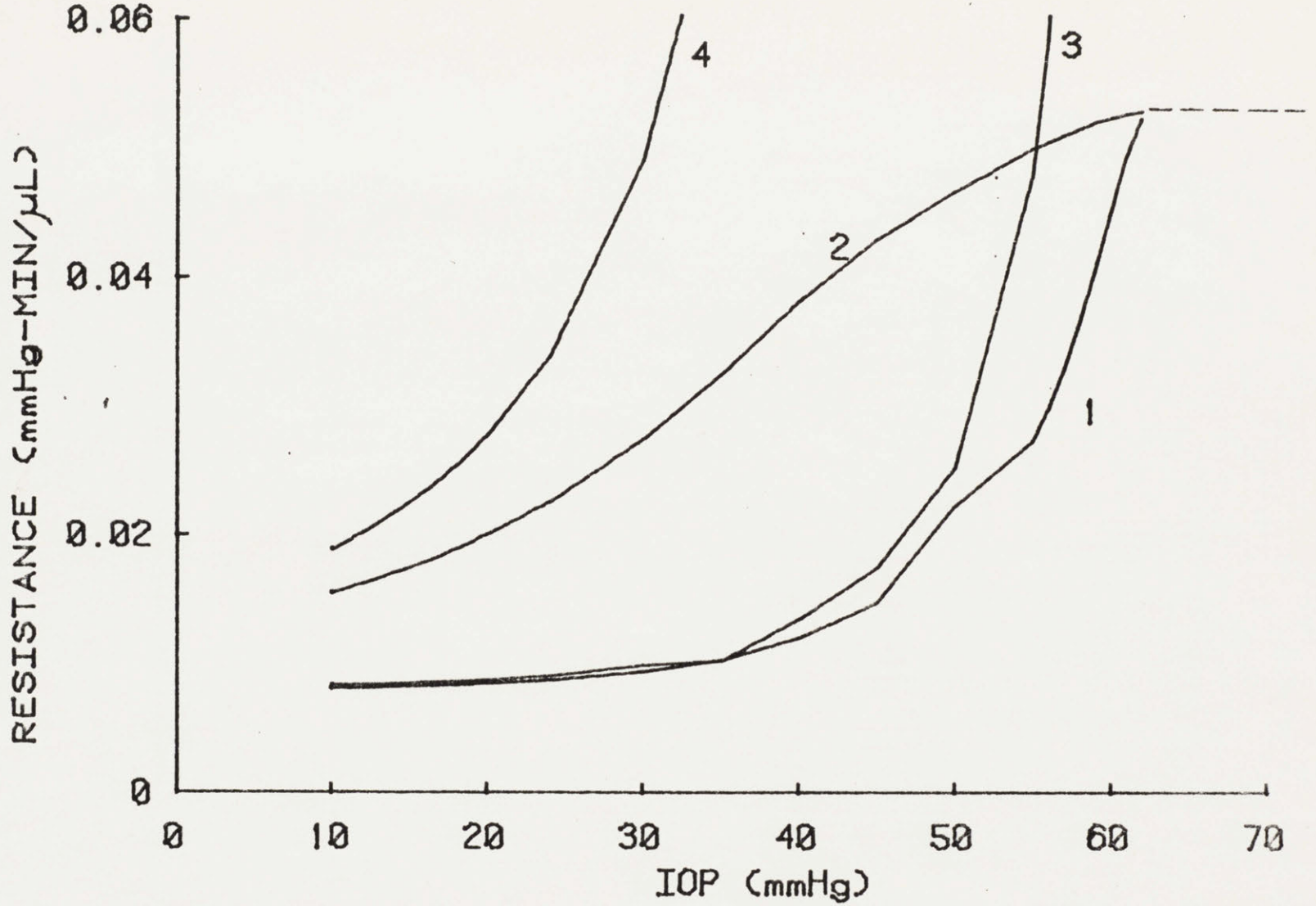
0.06
0.04
0.02
0
RESISTANCE (mmHg-MIN/μL)
4
3
2
1
0
10
20
30
40
50
60
70
IOP (mmHg)

Figure 38

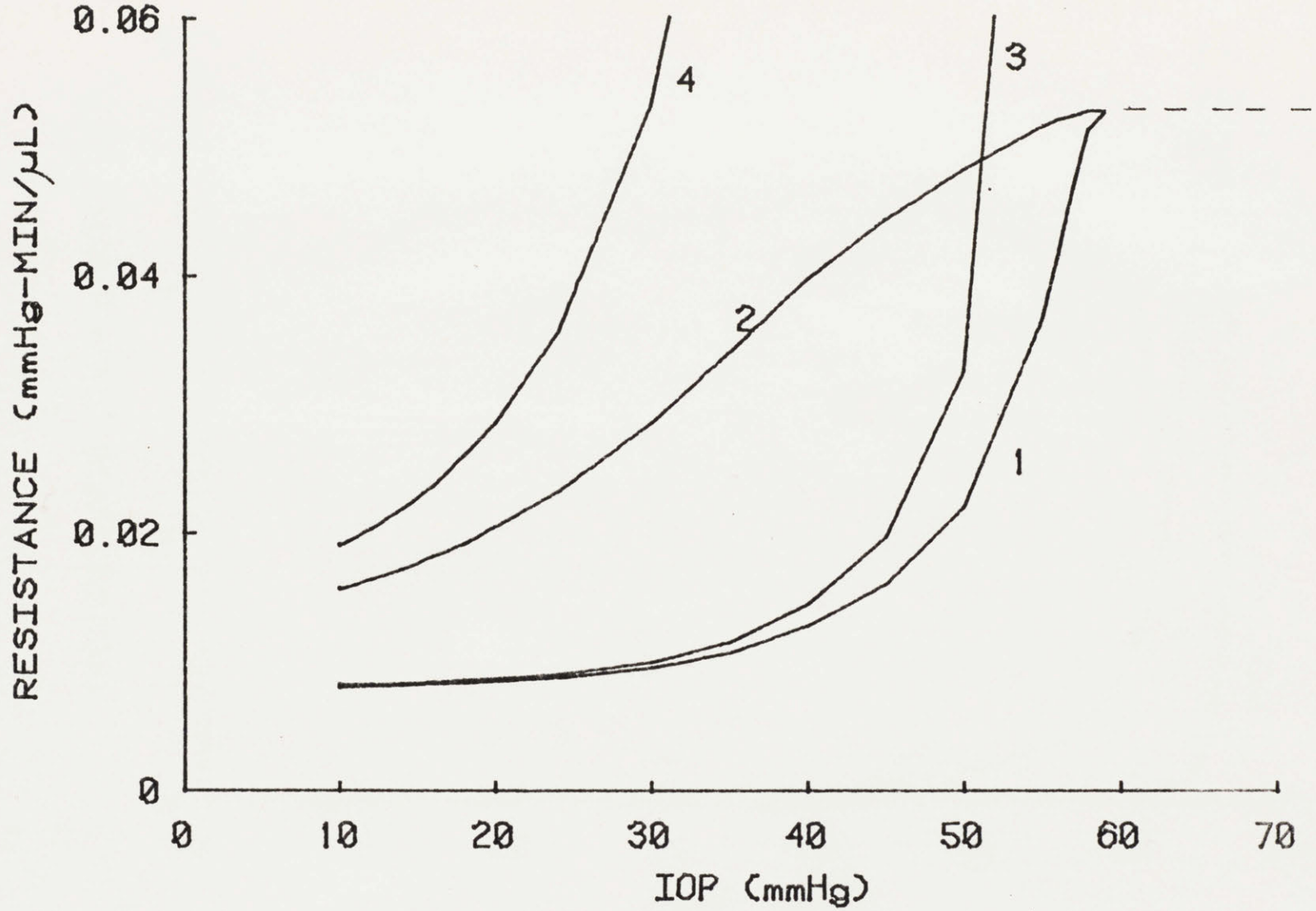
0.06
0.04
0.02
0
RESISTANCE (mmHg-MIN/μL)
4
3
2
1
0
10
20
30
40
50
60
70
IOP (mmHg)

Figure 39

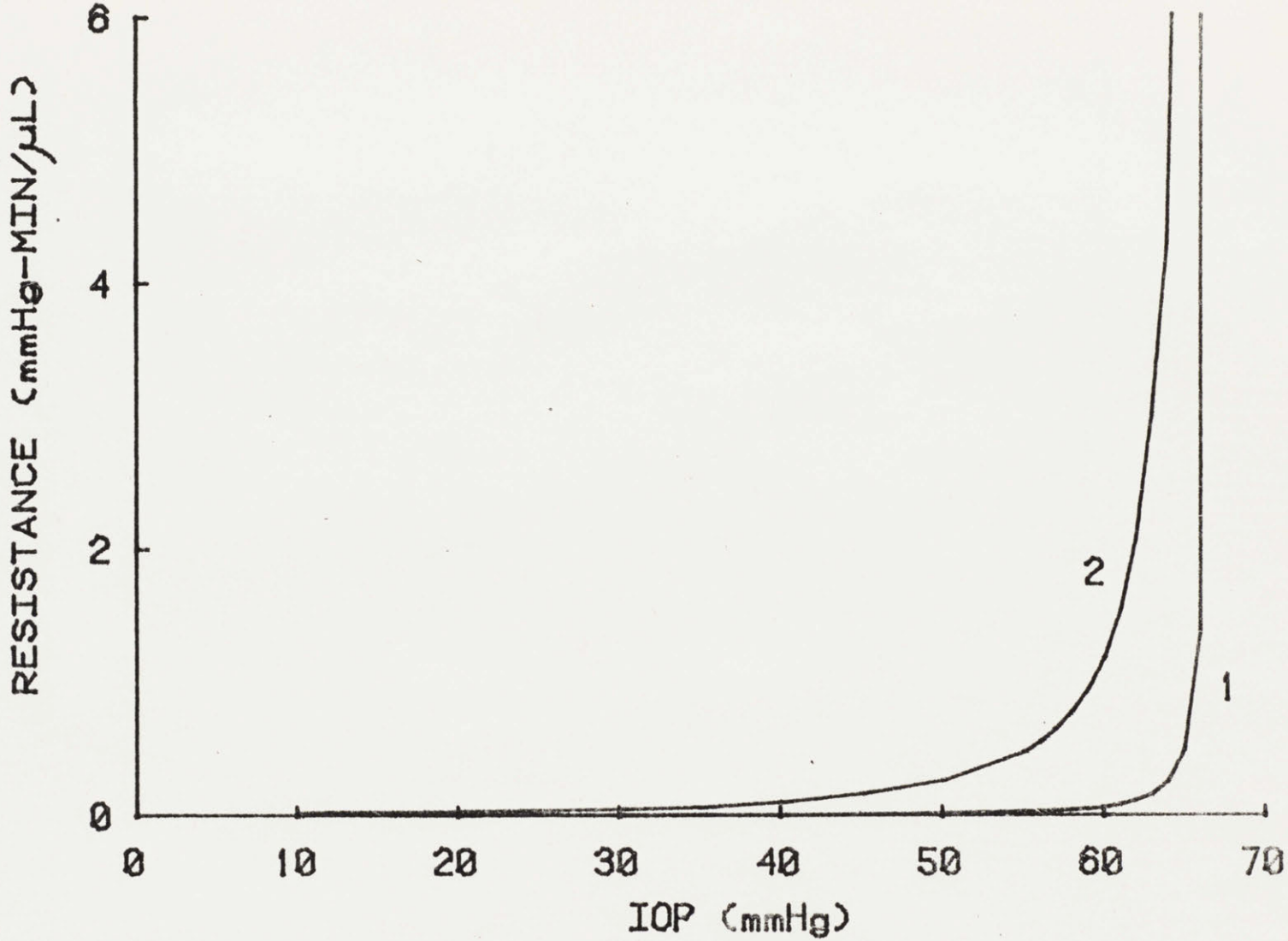

Figure 40

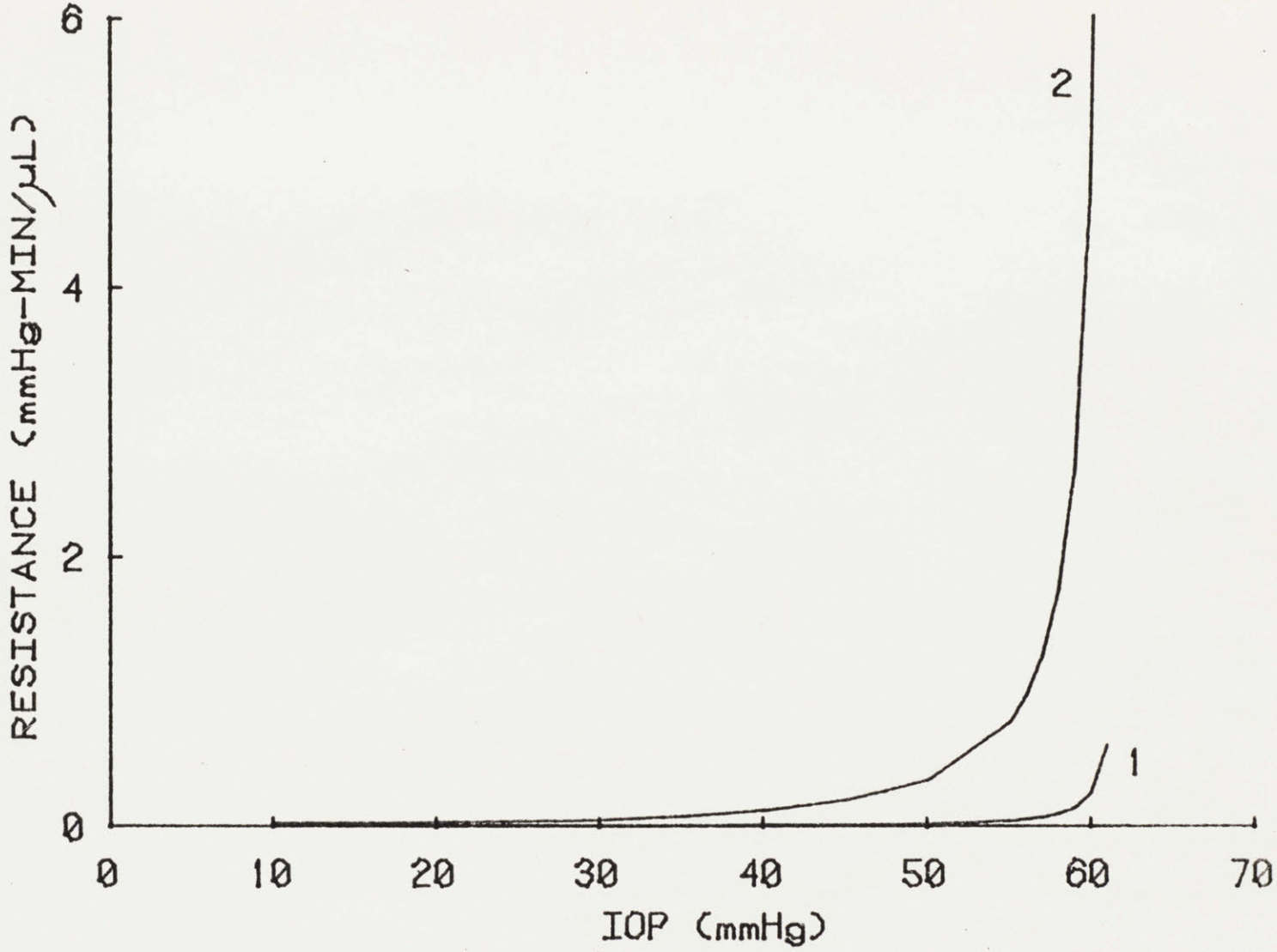

Figure 41

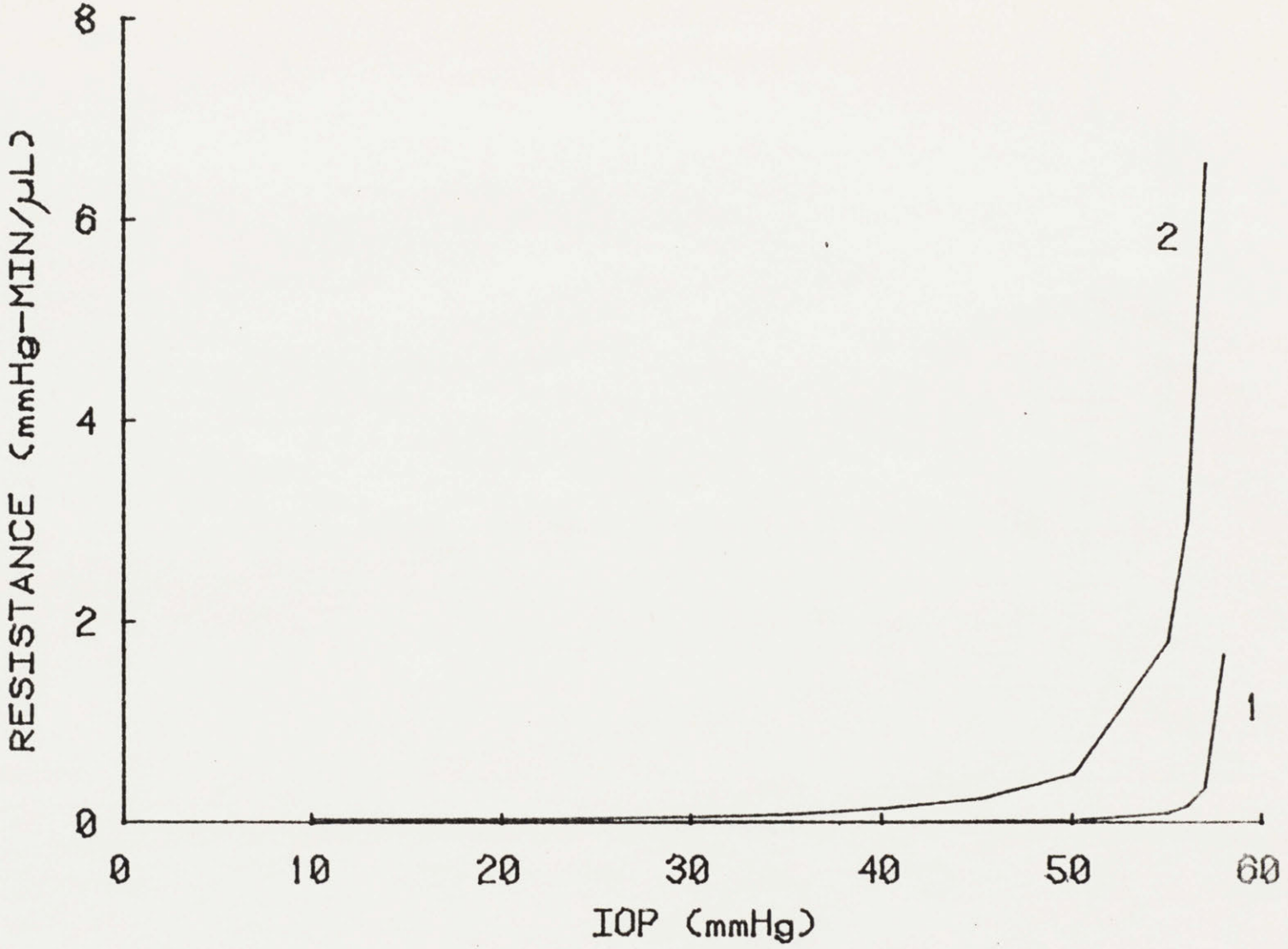

Figure 42

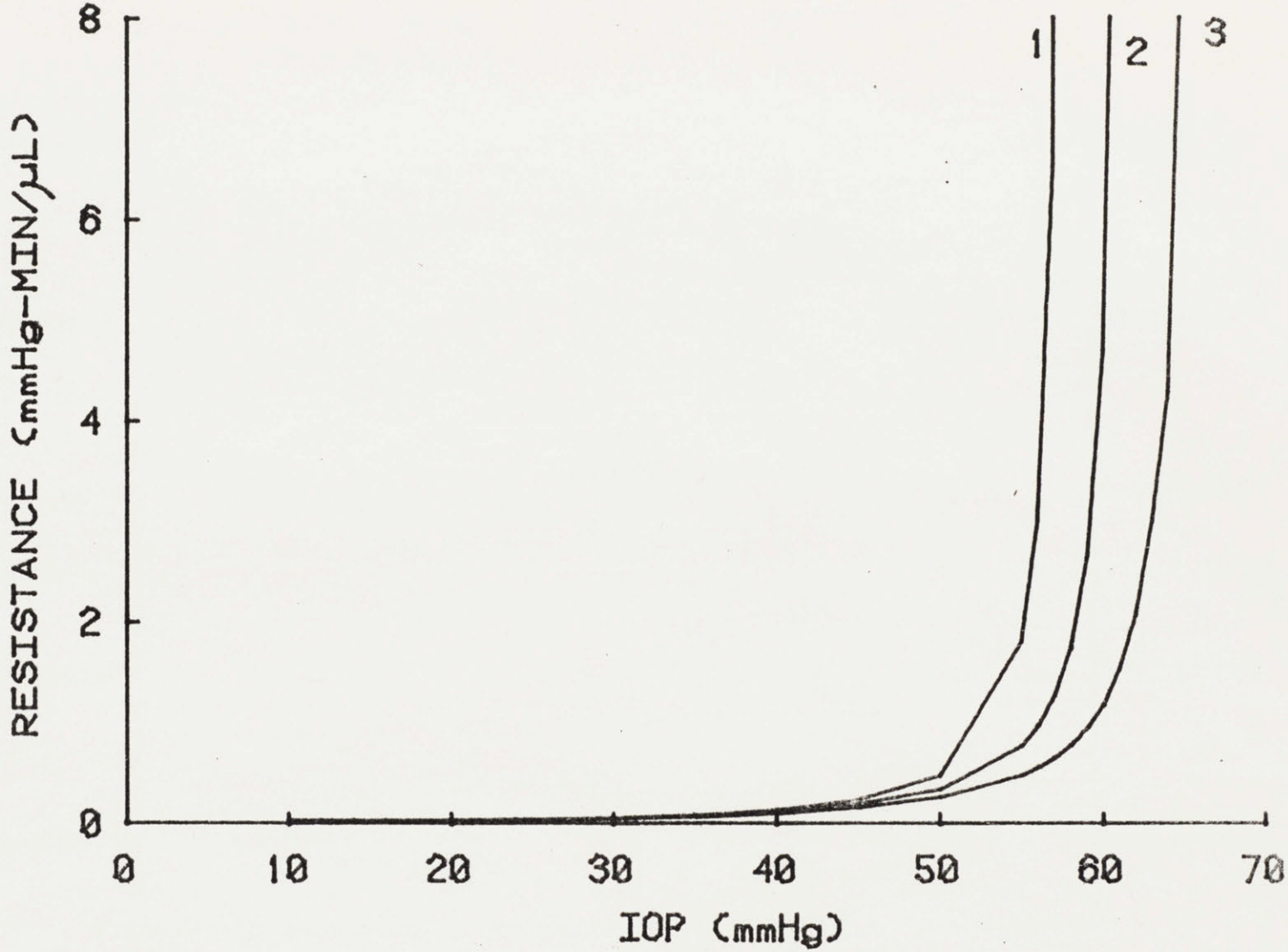

Figure 43

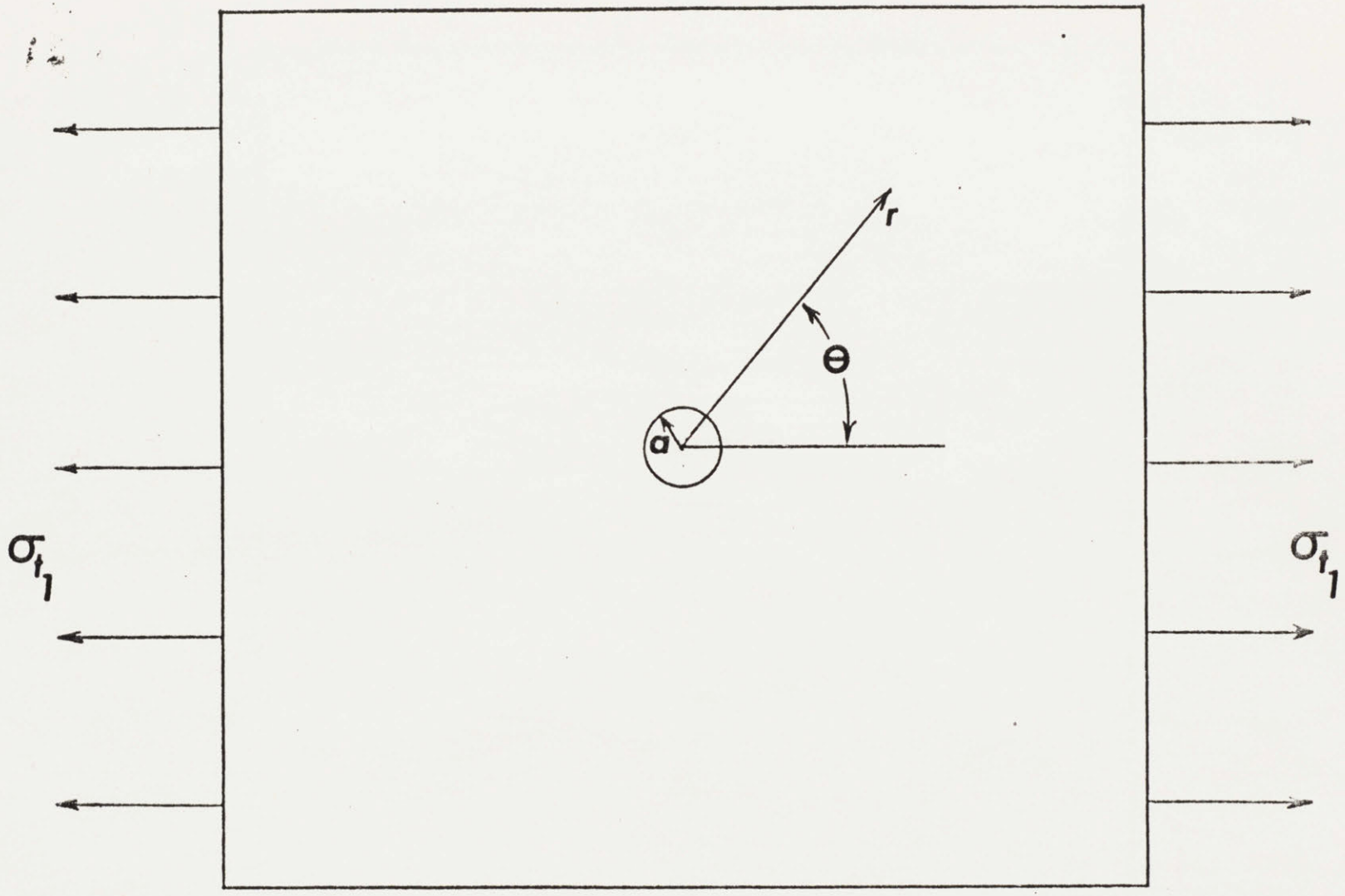

Figure A-1

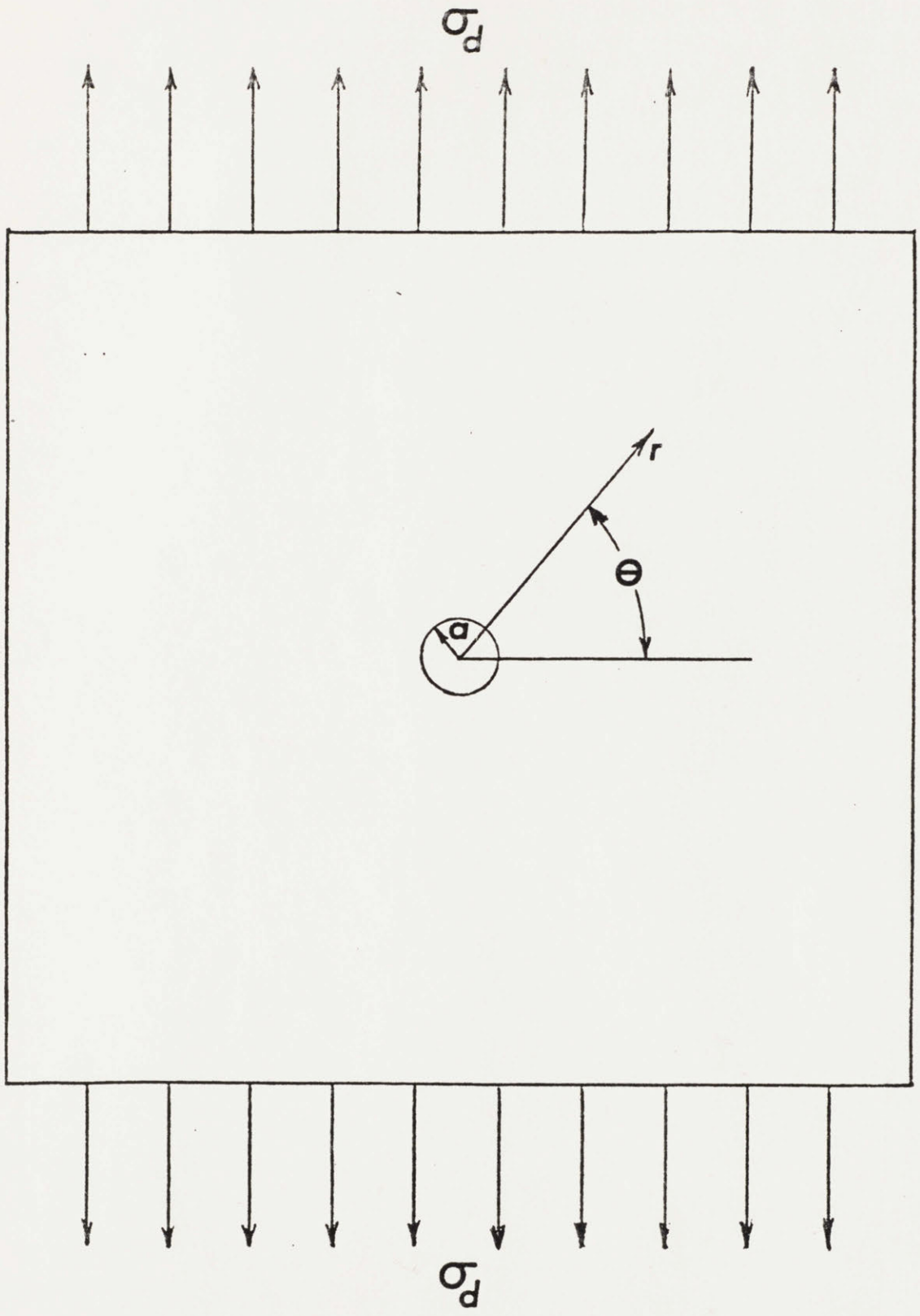

Figure A-2